The University Of Sheffield.

Modelling Cargo Transport and Deformation by Molecular Motors along Cytoskeletal Filaments

By:
Naruemon Rueangkham

A thesis submitted in partial fulfilment of the requirements for the degree of Doctor of Philosophy

The University of Sheffield
Faculty of Science
Department of Physics and Astronomy

Submission Date
14/7/2020

Acknowledgements

I would like to express my sincere gratitude and the deepest appreciation to my supervisor, Dr. Rhoda Hawkins, for her encouragements and suggestions throughout my Ph.D. Without her expert guidance and help, this thesis could not have been completed. I am thankful to my colleagues for providing feedback in my thesis. I specially thank to Development and Promotion of Science and Technology Talents Project (Royal Government of Thailand scholarship) for educational and financial support. I also thank Department of physics and astronomy, University of Sheffield, for providing me facilities. Finally, I sincerely thank to my family for supporting and giving me a spirit in every step of my life.

Abstract

In this thesis, we present a study of cargo transport or behaviors in a cell by clusters of molecular motors on a single and many parallel or anti-parallel microtubules. Molecular motors can be processive motors or non-processive motors which can bind on and off and switch between microtubules (lanes). Our study includes analytical theory, simulations and a detailed comparison with experiments. We extend the analytic expressions for the non-processive motors to the case of finite binding sites on a single lane and multiple lanes, as presented in chapter of one-lane and many-lane model, respectively. We performed Monte Carlo latticed based stochastic simulations to validate the corresponding system. The simulations also include simple exclusion process and sequence preservation of motors. Our results show that the limiting number of binding sites along the lanes and sequence preservation reduce the probability of non-processive motors binding, but has a relatively small effect on the velocity. Multiple-lane transport can enhance the velocity and averaged run length and reduce the delivery time. We also study cargo behaviour using a tug-of-war model in which the lanes on which motors step are oriented in anti-parallel arrays between right and left ends of the cargo, as presented in chapter of cargo deformation. This mechanism generates motor pulling force onto the cargo which results in changing its shape and position. The cargo can be any cargoes acting as a spring and the nucleus is the example of cargo that we are interested in. This model provides new insights of nuclear deformation and displacement caused by the motor pulling force. Our simulations show that the deformation and displacement can be induced by the increasing number of microtubules. This corresponds with the experimental results of Susana Godinho's group.

CONTENTS

LIST OF FIGURES

LIST OF TABLES

1. INTRODUCTION

1.1 Biological background

1.1.1 Intracellular transport

Intracellular transport is the movement of organelles, vesicles and substances in cells. Generally speaking there are two main types of intracellular transport which are passive diffusion and motor-driven active transport [11]. Diffusive transport can be found in some phases of the movement of microscopic particles in cells. However, active transport requires chemical energy in the movement of biomolecules. In eukaryotic cells, active transport is necessary for the movement of intracellular cargoes becausediffusion is too slow for many biological processes. The cargoes are transported to target sites by attaching to molecular motor proteins that move along filaments of cytoskeleton. Cargo transport driven molecular motors along cytoskeletal filaments can be found in neurons, cilia and flagella and many diverse cell types.

1.1.2 Cytoskeletal filaments

The cytoskeleton is present in both eukaryotic and prokaryotic cells. The function of the cytoskeleton varies and depends on organism and cell type. In prokaryotes, the cytoskeleton plays important roles in cell division, cell polarity and cell shape regulation[87, 47]. In eukaryotes, the cytoskeleton linking from the nucleus to the plasma membrane throughout the cytoplasm performs a veriety of functions because of the more complex intracellular structure. For example, it determines the cell shape and its spatial organization. Also, it allows either the cell to migrate or forms special structures for cell motility, such as flagella and cilia [27]. Moreover, it is crucial for intracellular transport involving the movement of vesicles and organelles which are absent in prokaryotes. In this case, the cytoskeleton acts as "roads" for "vehicles" represented by molecular motors carrying intracellular cargos like vesicles and organells. The complex network of cytoskeleton in all eukaryotes consists of three fundamental types of filaments: microtubules (MTs), actin filaments and intermediate filaments. We begin by describing the three main types of filaments in cells which are microtubules, actin filaments and intermediate

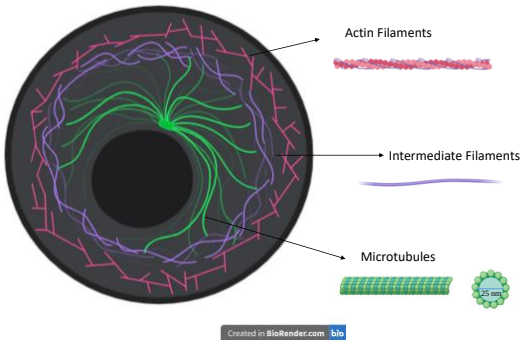

Fig. 1.1: Cytoskeletal network

filaments in general concepts, as depicted in Figure 1.1.

Microtubules

Microtubules are major components of the cytoskeleton and cn be found in all eukaryotic cells. They are related in mitosis, cell motility, intracellular transport and cell shape. They are long, hollow cylinders composed of alpha- and beta-tubulin subunits assembled into protofilaments. A single microtubule consists of 10 to 15 protofilaments to form a cylinder with a diameter of 25 nm and the length of around 50 μm. This basic knowledge is important in chapter 3. They are more rigid structures than actin filaments. One end of each microtubule are attached to a microtubule organizing centre (MTOC) called a centrosome which is positioned close to the nucleus. This is the basic of our model in chapter 4.

Actin filaments

Actin filaments or microfilaments are two-stranded helical polymers of the protein actin. They are thin filaments with a diameter of 5-9 nm that are beneath the plasma membrane. They mainly maintain cell shape and allow cell movement.

Intermediate filaments

Intermediate filaments are fibers with a diameter of around 10 nm. Mostly, they can be found just beneath the inner nuclear membrane and across the cytoplasm. The intermediate filaments mainly give the cell mechanical strength.

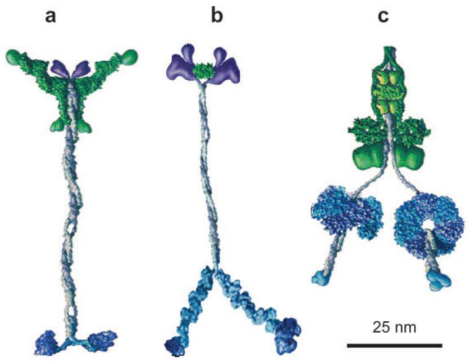

Fig. 1.2: The head domains (bottom) and the tail domains (top) of (a) kinesin, (b) myosin V and (c) dynein [49], with the approximate scale bar of 25 nm.

1.1.3 Motor proteins

Molecular motors are molecular machines that are the essential agents of transport in living cell called motor proteins. These remarkable proteins bind to cytoskeletal filaments and use the energy of ATP hydrolysis to move along the cytoskeleton [49]. Molecular motors' biological functions are specified by their domain structures as depicted in Figure 1.2. The most important parts are the motor domains called heads which bind to the filaments and perform a cycle of ATP hydrolysis. The tail domains are connected to cellular cargo such as membrane-enclosed organelles like mitochondria, Golgi stacks, or secretary vesicles in cells. The cargo domain binds to specified organelles or vesicles that depend on the biological function of individual motor proteins. Many motors carry enclosed organelles such as mitrochondria or specified vesicles whereas other motors are responsible for muscle contraction, ciliary beating and cell division. Moreover, they differ in the type of filaments they bind to and the direction they move along. Typically, the types of track and the direction of movement along it are determined by the motor heads. We classify motor proteins based on the cytoskeletal filaments that they interact with and differentiate their processivity as follows.

Cytoskeletal motors

MT-based motor proteins The two most important protein families moving along the microtubules are kinesins and dyneins. Both families are processive motors which rarely unbind from filaments on which they are moving [12]. Nonprocessive motors in contrast unbind from the filaments more frequently and they are a stronger team in larger groups which will be demonstrated in chapter 2. kinesins

and dyneins walk in different directions which are determined by the polarity of the two ends of MTs.

Kinesins Most kinesins move towards the plus-ends of the MTs, known as the anterograde direction, which is directed from the cell centre or nucleus to the cell periphery. In general, kinesins without load have a unidirectional motion, an absence of back-stepping [2, 5]. However, if the motor binds with a cargo, the cargo causes a load force which affects the motor's stepping. Back-stepping becomes more dominant depending on the size of force exerted by the cargo onto the motors. The relation between force and stepping velocity is thus an interesting issue to study and is one of our research problems.

The stepping of kinesins is triggered by the hydrolysis of ATP. There are two main states of motor heads during ATP hydrolysis: an ATP-bound head bound strongly to the track and an ADP-bound head unbound from the track. The ADP-bound head is brought to the front. After that, the ATP of the other head is hydrolyzed to ADP and inorganic phosphate that makes the binding weaker. This head thus detaches from the filament and is brought to the front as soon as the other head changes from ADP to ATP. The stepping cycle of kinesin is shown in Figure 1.3. The kinesin motors can mostly perform a large number of steps before detaching as a processive motor. In contrast, some kinesins unbind from the filament frequently as a nonprocessive motor. In this thesis, we focus on studying kinesin family which is kinesin-1 and kinesin-14 (Ncd) as a representative of processive and nonprocessive motor, respectively.

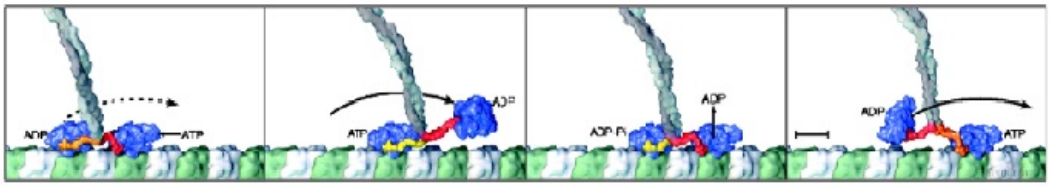

Fig. 1.3: The stepping cycle of kinesin. From left to right: an ATP-bound head induces a conformational change which brings the ADP-bound head to the front. The ATP of the now rear head then hydrolyzes to ADP and inorganic phosphate. After that, the rear head unbinds from the filament and is brought to the front. In the meantime, the other head exchanges its ADP by ATP [2].

Dyneins Most cytoplasmic dyneins move towards the minus-ends of MTs that are in the opposite direction compared to transport with the kinesin motor proteins. Dyneins have more complicated structure and more weight than kinesins.

They have two heads to bind to the MTs but each head has a ring shape as shown in Figure 1.2 which is different from kinesins. The cargo is bound to the domain at the other end (tail). The stepping cycle of dyneins differs from that of kinesins. The dynein head detaches from the MTs when it is bound with an ATP whereas the kinesin head detaches when an ADP is bound. However, it was reported from experiment that dyneins are processive motors which is similar to kinesins [103].

Dyneins and Kinesins can simultaneously attach to the same cargos and this will lead to bidirectional transport because both motors move in opposite directions. Bidirectional transport is an interesting situation of motors stepping behaviour and has been broadly studied in experiment and theory [41, 48, 58, 20]. This mechanism is also refered to as "tug of war" which will be discussed in section 1.5.

Actin-based motor proteins

Myosins Myosins are the cytoskeletal motor proteins moving along actin filaments which are an example of nonprocessive motors. There are many different subclasses of myosins which function differently. For example, myosin II has force generating machinery for muscle contraction due to pulling on actin filaments. Myosin II is a kind of non-processive motor which often unbinds from the filament. Myosin V is typically responsible for vesicle and organelle transport. Myosin V is able to interact along the track for a long period of time like processive motors which are similar to kinesins. All myosins move towards the plus-end of actin filaments, except myosin V, which moves towards the minus end. However, myosin is not elucidated in this work because our examples are based on microtubules.

1.2 Monte Carlo methods

Monte Carlo simulation is a broad class of computational algorithms with random sampling to obtain numerical results. It is often used in physical, chemical and mathematical problems and is substantially useful for the problems which cannot mathematically solve to find exact solutions. Monte Carlo methods are usually used for optimization, numerical integration, and generating draws from a probability distribution.

It might be difficult to talk about Monte Carlo methods in abstract terms. However, it can be described by the principle of a random walk model which will be used in our model simulating motors' stepping. As a general description of our model, we use the principle of Monte Carlo simulation through a random walk model and simple exclusion process.

The random walk Monte Carlo method is a class of algorithms for sampling from a probability distribution on constructing a Markov process in which the probability satisfies its equilibrium distribution. One of the generally used random walk Monte Carlo algorithms was proposed by Metropolis [63]. This method generates a random walk as a random number for accepting some of the proposed direction if the random number is under a probability density and rejecting if it is out of the probability density. The Metropolis algorithm can be basically constructed as the following scheme [28].

1. Select a particle at random, and calculate its energy $U(r^N)$.

2. Give the particle a random displacement; $r' = r + \triangle$, and calculate its new energy $U(r'^N)$.

3. Accept the move from r^N to r'^N with probability $\exp(-\beta[U(r'^N) - U(r^N)])$, where β is $1/(k_B T)$ where k_B is the Boltzmann constant and T is the temperature.

Furthermore, we also use simple exclusion process which is an interacting particle system of the Markov process. This process was introduced in 1970 by Frank Spitzer [90]. It has been widely used in stochastic modelling for transport phenomena which will be discussed in more detail below.

1.2.1 Simple Exclusion Process (SEP)

Stochastic modelling of the intracellular processes has been generally carried out by lattice based model which is discrete in space [2, 96]. In a lattice based model, a particle can occupy on one site of the lattice and then hop stochastically to another site with its own intrinsic rate called hopping rate. The particles move forward and backward according to the hopping forward and backward rates, respectively. It is accepted to move forward and backward if a generated random number is under the probability of hopping either forward or backward in order to mimic the stochastic motion of the system.

The stochastic lattice based model is an appropriate choice for the intracellular transport, especially motor-driven transport, because the hopping of particles on the lattice can be directly compared with the stepping of motors along the filament. That is because the stepping cycles exchanging between ATP and ADP can be summarized by a hopping rate [2].

The simple exclusion process is a model of stochastic transport to study interacting particle systems [37]. The model is performed on a one-dimensional lattice with discrete sites. One site can either be occupied or empty and the site can be occupied by one particle at most [76]. The particle hops forward with the forward rate, p_μ, and hops backward with the backward rate, q_μ, as shown

$$\begin{aligned} \mu 0 &\rightarrow 0\mu, \text{ with rate } p_\mu \\ 0\mu &\rightarrow \mu 0, \text{ with rate } q_\mu. \end{aligned} \tag{1.1}$$

where μ represents a particle. According to the exclusion process, hopping only succeeds if the target site is vacant. The motors cannot overtake, thus the motor sequence is preserved. By this reason, the particles based on simple exclusion process are interacted as short-range repulsion.

1.3 Mathematical description of transport by collective processive motors

Over the past decade theoretical investigations of transport by multiple molecular motors under a load force have resulted in two widely used theoretical models for how force affects the motors, namely a mean-field theory [48] and a leading motor model [12]. However which of these two models is more appropriate in particular applications remains ambiguous. Below we clarify the difference between these models and the assumptions made by them.

Mean-field theory

[48] proposed a mathematical model for a cargo transported by n molecular motors along a filament, assuming that the external load force F, is applied equally to the n bound motors, such that an individual motor experiences a force F/n (see Figure 1.4). A single motor can move along the filament with a certain average velocity v, which depends on the load force. The velocity decreases when the load force increases. [48] assume the velocity is a linear function of force and later Kunwar et al [51] extended the linear force-velocity relation to a more general nonlinear form with an exponent w, namely;

$$V_n(F) = v\left(1 - \left(\frac{F}{F_s n}\right)^w\right), \tag{1.2}$$

where v is the velocity when no load is applied and F_s is the stall force of a single motor (the force for which the cargo stops) and w is the exponent that characterises the force-velocity relation. If $w = 1$ the force-velocity relation is *linear*. For $w < 1$ the force-velocity relation is *sub-linear*, while $w > 1$ corresponds to a *super-linear* force-velocity relation [51].

This theoretical model is suitable to apply to experiments in which the external force is exerted in such a way that all the motors share it equally. However, in many scenarios, such as in a cell, motor transport is resisted by an internal viscous drag force on the cargo from a fluid medium such as the cytoplasm. Such a force may be all experienced by the leading motor with motors following behind force free. Optical trap force measurements on kinesin-1 by [32] using a polystyrene bead stuck to the motor assembly imply that one kinesin bears all the load. In the

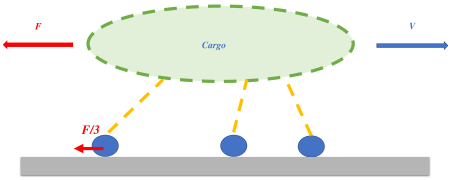

Fig. 1.4: Sketch showing three motors (blue circles) attached to a cargo. The cargo moves with velocity v and the force F is shared equally by all three motors [51].

next section we therefore review the leading motor model developed by [12] which is more appropriate for such scenarios.

The Leading motor model

An asymmetric simple exclusion process (ASEP) transport model was pioneered theoretically by Evans, et al [25] and then developed for molecular motors by Campas, et al [12] which was explained in section 1.2.1. In this model, they explain the dynamics of a cargo driven by processive motors by motor hopping rates. As illustrated in Figure 1.5, each motor is able to move stochastically in either direction along the filament track with specified forward, p, and backward, q, rates, similar to classical Brownian ratchet models [1, 73, 75]. If interactions between motors are included the rates are modified to v forwards and u backwards for nearest neighbour interactions, i.e. if a particle is next to an occupied site. This assumes the interactions are short ranged over one step length. Neutral interaction corresponds to $v = p$ and $u = q$. It is worth noting that neutral interactions between motors in the presence of simple exclusion process can be described as short range repulsive interaction because motors cannot occupy in the same site. Attractive interactions are modeled by $v < p, u < q$, whereas repulsive interactions are given by $v > p, u > q$. The hopping rates for the leading motor ($\mu = 1$) are dependent on the force, by a Boltzmann weighting; $p_1 = pe^{-f\delta}$, $q_1 = qe^{f(1-\delta)}$ and $v_1 = ve^{-f\delta}$, $u_1 = ue^{f(1-\delta)}$ where f is the dimensionless force exerted by the cargo such that the load force $F = fk_BT/\mathrm{d}x$ where $\mathrm{d}x$ is the motor step size. The dimensionless parameter, δ, varies from 0 to 1 and determines how much the forward versus backwards stepping rates are affected by the load force. For $\delta = 0$, the forward stepping is not affected by the load force and vice versa for $\delta = 1$. The forward and backward rates of all the motors following the leading motor are equal and independent of force such that $p_\mu = p$, $v_\mu = v$ and $q_\mu = q$, $u_\mu = u$ [12, 25].

The average velocity of a single motor in this model is $V_1 = p_1 - q_1$. For two motors, their average velocities are equal. This is because, according to the simple exclusion process (SEP) the motors cannot overtake each other, their sequence is preserved and their average steady state velocities are equal due to the velocities

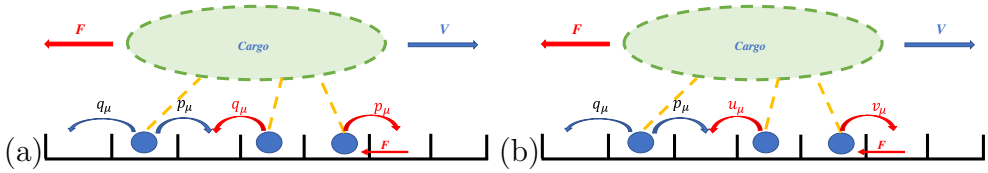

Fig. 1.5: Possible motor transitions and associated rates for (a) neutral and (b) attractive and repulsive interactions. The motor tails are attached to a cargo whereas the motor heads are attached on the filament. The boxes and balls represent lattice sites and motors, respectively [12].

of all motors being limited by that of the leading motor. Campas et al [12] express the average velocities of each of two motors in terms of v and u, referring to the cases of attractive and repulsive interactions, giving;

$$V_2 = \frac{v_1(p-q) + u(p_1 - q_1)}{(v_1 + u) + (p-q) - (p_1 - q_1)}. \tag{1.3}$$

For the general case with n motors following SEP, Campas et al [12] found an analytical expression for their average velocities in the neutral case where $v = p$ and $u = q$ given by;

$$V_n = p\frac{[1 - e^f(q/p)^n][1 - q/p]}{e^{f\delta}[1 - q/p] + e^f[q/p - (q/p)^n]}. \tag{1.4}$$

In the simple case of unidirectional motors for which $q = 0$, Eq. (1.4) reduces to $V_n = pe^{-f\delta}$. For small forces this can be expanded to reproduce the linear version of the mean-field theory in Eq. 1.2 with $\omega = 1$. We also note that a rough approximation of Eq. (1.4) can be obtained to describe the behaviour of multiple motors with a simpler model of a single motor with modified backwards stepping rates (see Appendix 2.7.5). However the validity of this approximation does not hold well for the parameter regions we are interested in. Campas et al.[12] also consider attractive and repulsive interactions between motors. Despite a small amount of evidence suggesting very weak attractive interactions [81], it is not yet clear what interactions are present experimentally. We therefore focus on the neutral case between motors according to the definition of Campas where we define as short range repulsion as a result of exclusion potentials in our work. As noted above, this model is suitable for situations for which the total force is experienced by the leading motor, for example the viscous drag force of the cargo *in vivo*. In addition this model can easily be extended to other forms of unequal loading. In this sense it is more general than the mean-field model, with the latter being a limiting case of the leading motor model. Kunwar et al.[53] present a

more detailed model of motors as springs which results in motors sharing the force equally when at the same position and the leading motor experiencing most of the force when it is ahead. In our model we consider simple exclusion and therefore do not allow multiple motors at the same site so the leading motor is the most appropriate model for us to use.

1.4 Stochastic simulations of cargo transport by molecular motors

S. Klumpp et al. developed the theoretical study of cargo transport pulled by several molecular motors [48]. They considered that each motor can unbind from the filament then can rebind to it again, so that the number of actively bound motors is not constant and can be vary between zero and N. They calculated the transport properties of cargoes pulled by several motors against an external load force in which the force-velocity relationships included the ability of detachment and attachment is presented. The average velocity is calculated by the distribution of number of bound motors, solved by master equation in an infinite system, multiplied with the velocity of bound motors which is based on mean-field theory (see more details in section 1.3). For this reason, it is worth noting that their theory is consistent with in *vitro* experiment and *vivo* experiment for small viscous force. Later, O. Campas et al. developed general solution of the force-velocity relationship for a cargo in *vivo* experiment transported by N motors not including attachment and detachment for general terms of viscous forces which are applied to the leading motor (see more details in section 1.3) [12]. They also considered motor-motor interaction and conducted lattice based simulations using Simple Exclusion Process (see more details in section 1.2.1). In their simulation, they presented results of force-velocity relation of transport by N fully processive motors with repulsive, attractive and neutral interactions. They also show the results of transport by a cluster of motors ($N = 100$) in the presence of detachment and attachment (nonprocessive motors) for neutral interaction in which the results behave a processsive motor when the cluster is large enough and there is no theory supporting in this case. Here, it is noticeable that there is a gap for theoretical study of general form of transport by nonprocessive motors for general terms of external force. There is also a big gap of the theoretical and simulation study of transport properties by a small team of nonprocessive motor which can be influenced by detachment and attachment. Thus there is motivation to develop the analytical solution and show more realistic stochastic simulation to fulfil the gap of understanding.

O. Campas et al. applied the leading motor model to explain the growth of membrane tubes pulled by molecular motors stepping along cytoskeletal filaments [13]. The motors moving along a microtubule can generate force to pull the mem-

brane tube. Generating this force is related to detachment of the leading motor. They conducted lattice based simulations in which a one-dimensional lattice represents a single protofilament and a motor can either bind or unbind on a lattice site. They observed how the unbinding rate depended on the force and compared these observations with experimental results. They revealed that motors clustering on a single protofilament is not enough to generate sufficient force to pull a membrane tube. It requires at least three protofilaments and a cluster of approximately nine molecular motors [13]. Meanwhile, A. Kunwar et al. investigated stochastic simulation of cargo transport by a multiple-motor system which is in the form of strain-gating where motors share load unevenly [53]. In this work, the motor dynamics are different and there are two phases. If the motors stay far away from each other, then the leading motor shares the high load while the rear motor is under low load, but if they stay close together then they share the load equally. Interestingly, they combined the leading motor model and mean-field theory together. However, the analytics relating to a cluster of nonprocessive motors have not been exposed. Later, they developed an algorithm using a combination of the stochastic model of motor dynamics and a Langevin equation for the motion of a spherical cargo along a microtubule [50]. The dynamics of motors include binding and unbinding and the Langevin equation includes the diffusive motion of cargo. They measured the velocity of a cargo pulled by a single motor in the comparison of experimental results and measured simulation results for the run length of cargoes transported by several motors against high viscous friction. Again, the analytical solution of velocity of transport by a cluster of nonprocessive motors has not been clearly proposed and the velocity is studied just the case of a single motor in this work.

A. Kunwar et al. has studied the mechanics of multiple motors including the ability of binding to and unbinding from the filaments to transport a cargo [51]. The average velocity of a cargo is then driven by the number of actually active motors that are bound to the filament because they can unbind from it. They expressed the probability of a number of bound motors by solving the stationary solution of the master equation proposed by S. Klumpp et al. [48]. The velocity of bound motors is expressed by using mean-field theory which assumes that motors share the force equally. However, we note that the probability obtained from the mater solution in [48] is assumed an infinite system which is not representative of a spherical cargo which has a limited space and is therefore bound by a limited number of motors.

After that, motor-motor interaction has been considered for the cargo transport by S. Bouzat et al. [9]. They studied the effects of excluded volume between motors on cargo transport. In this study, they also considered the dynamics of cargo following an approach similar to [50] by a continuum Langevin equation,

while the dynamics of motors follow a Monte Carlo algorithm including forward and backward stepping, and binding and unbinding events and under the theoretical framework proposed by A. Kunwar et al [51, 53]. They compared the Monte Carlo simulation results in the presence and in the absence of simple exclusion process on the dynamics of motors combining the Langevin dynamics of cargo. They found that the cargo driven by interacting motors moves slower than that by non-interacting motors. Moreover, they conducted simulations of interacting motors on multiple tracks which can either be protofilaments or parallel independent microtubules [9]. The increasing number of tracks can reduce the effect of interactions between motors for cargo transport. In this work, they mainly worked with Monte Carlo algorithms to study the effects of integrating cargo and motor dynamics, but they have not directly compared experimental results and analytical calculations.

Although the cargo transport by multiple motors have been studied in various models based on Monte Carlo algorithms in the literature, we note that there has been no comprehensive study of a number of motors bound to a cargo of finite size, rather than an infinite system. We can also develop stochastic models corresponding with our new insight and being more representative of the biological system in term of binding kinetics for transporting a cargo by several molecular motors including binding to, unbinding from and switching between cytokeletal filaments. This is the motivation for our work in Chapter 2 and Chapter 3. Meanwhile, another complex model for a cargo transport is proposed as tug-of-war model in which a cargo is mediated by different types of molecular motors, which will be discussed below. This model has been studied simultaneously with the development of our stochastic model of cargo transport mediated by multiple motors of the same type.

1.5 Tug-of-war

Intracellular transport can be carried out by either motor proteins kinesin or dynein which both move unidirectionally along microtubules, but in opposite directions. They can be attached simultaneously to a cargo which leads bidirectional transport. The bidirectional transport is caused by oppositely-directed motors attached to the same cargo which are plus-end directed kinesins and minus-end directed dyneins. Cargo transport can be achieved by unbalanced back-and-forth movements. Mostly, it can be found in neuronal transport [41, 68, 104, 72]. Understanding in motor behaviours underlying the bidirectional transport is important to their roles in neurodegenerative diseases, such as Alzheimer's disease, Huntington's disease and Parkinson's disease [41]. Bidirectional transport can be found in transport of larger organelles which is size of a few hundred nanometers on-

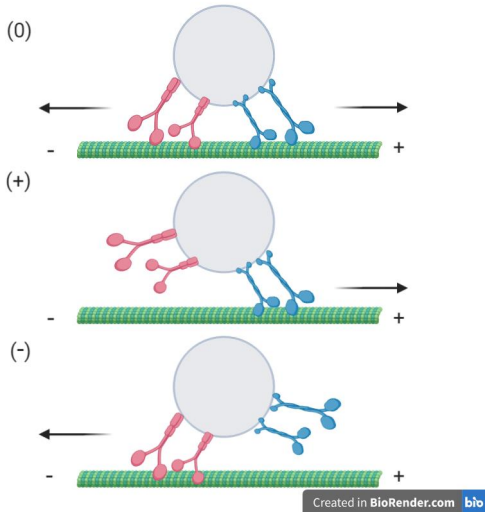

Fig. 1.6: Cartoon showing cargo transport by two kinesins directed to plus-end microtubule and two dyneins directed to minus-end microtubule. Three dominant configurations are no motion (0), fast plus motion (+) and fast minus motion (-).

wards [41]. For example, mitochondria, which are transported by kinesin-1 and dynein motors, move bidirectionally in axons. Melanosomes attach to kinesin-2 and dynein which will occasionally work together with myosin V. Furthermore, intraflagellar transport (IFT) is another category of bidirectional transport. It is the transport of proteins in cilia and flagella along axonemal microtubules[41]. Interestingly, this form of bidirectional transport is different from others that there is no directional switching during transport towards their cellular destination, so a change in direction can only occur at the end of the filament. [41].

The model used to describe bidirectional transport is tug-of war, known as a mechanical competition model between kinesin and dynein attached to the same cargo, which was originally formulated in [68, 67, 104] and published in 2008. Each motor species tries to move a cargo in its own direction, so the two motors are competing in a tug-of-war. An interesting question is how the two motor species achieve bidirectional transport. Cargo transport could be achieved by seven possible motility regimes in a tug-of-war model composed by three dominant regimes and their combinations [68]. The three configurations of the dominated regimes are (0), (+) and (-) which represent no motion, fast plus motion and fast minus motion of the cargo, respectively, as shown in Figure 1.6. The other motility states, (-,+), (-,0,+), (-,0) and (0,+), are the combination of the three dominant configurations which show switching. It is notable that the two regimes of (-,0,+) and (-,+) show bidirectional transport with and without pauses, respectively. The other two regimes of (-,0) and (0,+) show switching between one type of motors

active and two types of motors active at the same time which correspond to a pause state. The result is consistent with experiments which found a considerable amount of time spent in a pause state [21, 41, 30]. Another consistent feature found in experiment is elongated vesicles observed during directional switching of endosomes in Dictyostelium discoideum cells in vitro and deformation of mitochondria in vivo. This feature is consistent with the pulling of opposing motors during pause state in the tug-of-war model[89, 34, 52]. Here, we are interested in applying a tug-of-war model to study nuclear deformation surrounded by multiple microtubules in Chapter 4.

1.6 Nucleus

The nucleus is the largest organelle in eukaryotic cells which have a nucleus bound membrane, but this is not found in prokaryotic cells (e.g. bacteria) which have no membrane-bound organelles. It contains genetic materials which are the chromatin (cell's DNA) and associated proteins which are enclosed by a two concentric membranes, known as the nuclear envelope. However It can be connected with cytoplasm via nuclear pores through which most molecules are transported from the cytoskeleton via LINC (Linker of Nucleoskeleton and Cytoskeleton) complex by which mechanical interactions between nucleus and cytoskeleton are mediated . The nuclear membrane is supported by a network of intermediate filaments, known as lamina. This lamina, composed of lamina proteins (type A, B and C), are considered to be the primary source of the nucleus' strength [29].

The nucleus mainly contains DNA which maintains the genetic information of the cell for RNA transcription, DNA replication, and DNA repair/recombination [59]. However, DNA is a molecule that measures roughly two meters and can be complexed with proteins called chromatin. A subunit of chromatic is called nucleosome which is DNA complexed with histones [59]. The nucleosome appears as a bead and forms into a structure of long string like fibers. It is packaged and compacted into the small space of the cell nucleus within a viscous liquid called nucleoplasm, similar to cytoplasm found outside the nucleus. The chromatin functions as a memory device which stores and expresses the genetic information of cells [59].

Another prominent region found in the nucleus is the nucleolus. The nucleolus is the nuclear bodies which are not bound by membrane. Its function is to synthesize rRNA and assemble ribosomes. The main structure of the nucleus is displayed in Figure 1.7. Moreover, small structures in the nucleus include cajal bodies, promyelocytic leukemia bodies, nuclear speckles, etc. Although, the presence of these structure are important to the organization of the nucleus, but we don't know their functions clearly.

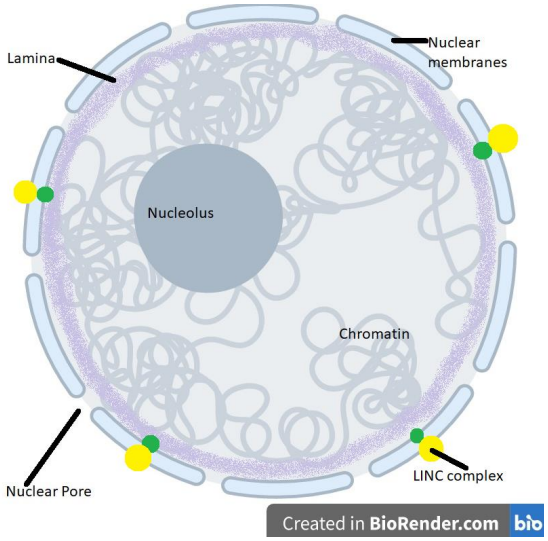

Fig. 1.7: Cartoon showing the components of the nucleus. The nuclear envelope (double bilayers) is punctured by the nuclear pores and LINC complex. The LINC connects between the lamina and the cytoskeleton (not shown in this figure). The chromatin containing DNA and nucleolus are inside the nucleus.

All of these components of the nucleus contribute to its mechanical properties. We are interested in is what provides the stiffness of nucleus because it is key to explain many processes such as nuclear deformation during cell migration. As mentioned above, we consider that its stiffness is mainly related by the lamina which is under the nuclear membrane and the chromatin which form strings inside the nucleus. In fact, the lamina has long been assumed to provide the nuclear rigidity [29, 38], but the impact of chromatin has recently been suggested [59, 93, 92].

The rigidity of nucleus

As mentioned previously, we assume that there are two main factors providing nuclear rigidity which are lamina and chromatin. The lamina structure underlying nuclear envelope plays an important role in its mechanical stiffness. The stiffness of the nuclear lamia was experimentally measured by micropipette aspiration of isolated Xenopus oocyte nuclei with and without the chromatin [17]. These results have revealed that the nucleus appears more deformable when it lacks Lamin A and C and a minor effect of Lamin B. Increased levels of lamin A lead to less deformable nuclei and reduced cell migration through small pores whereas nuclei with decreased levels of lamin A are more fragile [43, 18]. Therefore , it is obvious that the lamina play an important role in the nuclear rigidity with elastic

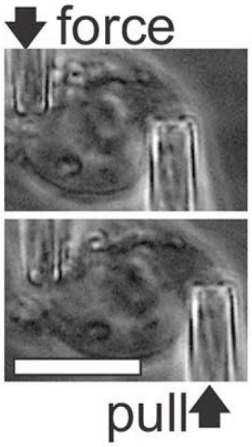

Stephens, *et al.*, 2018

Fig. 1.8: Experimental setup from [93] showing micromanipulation of a single isolated nucleus. It measures the extension of the whole nucleus by the movement of the 'pull' pipette and the deflection of the 'force' pipette. The force-extension plot provides its slope as a nuclear spring constant.

behaviour.

The effect of chromatin on nuclear stiffness has recently been studied [59, 92, 93, 88]. We know that the chromatin consists of nucleosomes complexed by DNA and histones (proteins). Apart from storing genetic messages, the chromatin has been suggested to support the nuclear structure. However, the involvement of chromatin contributing the nuclear rigidity is unknown.

There is a development for a force measurement microscopy setup with controlled biochemical manipulation of chromatin in human cell nuclei [59, 88]. They examined the rigidity of nuclei at different conditions of chromatin controlled by Mg^{2+} concentration. In the measurement, the isolated nuclei was captured by a pair of microneedles and they were then stretched apart. This showed the extension against force in the nuclei. It can be estimated as Hooke's law and its slope is its stiffness. This implied the nuclear rigidity in the relation of the resisting force and resultant deformation for condensed ($5mMMg^{2+}$) and decondensed chromatin ($0mMMg^{2+}$), respectively, and the results were different. They found that the nuclear rigidity clearly depended on Mg^{2+} concentration which influenced the chromatin compaction. The nuclear rigidity at decondensed chromatin was 10-fold lower than the value at highly condensed chromatin [59, 88].

It confirmed that the chromatin contributes to the stiffness of the nucleus, not only the lamina. Both the chromatin and lamin A/C provide nuclear stiffness and

they function as a spring [93, 92]. Stephens et al. also developed the same method of micromanipulation assay with a novel single-nucleus isolation to measure the whole nucleus-extensional spring constant [93]. Nuclei are isolated from single living cells and attached to two micropipettes. One is to extend the nucleus called the 'pull' pipette and another is to measure force called the 'force' pipette, as depicted in Figure 1.8. Nuclear spring constant can be calculated by the slope of force-extension plot which is $k = 0.52$ nN/μm [93]. At this point, this leads to the assumption of developed models in Chapter 4. We then assumed that a nucleus behaves like a spring by using empirical parameters of spring constant in normal conditions (see more in Chapter 4).

2. ONE-LANE MODEL

2.1 Abstract

Molecular motors are responsible for intracellular transport of a variety of biological cargo. We consider the collective behaviour of a finite number of motors attached on a cargo. We extend previous analytical work on processive motors to the case of non-processive motors, which stochastically bind on and off cytoskeletal filaments with a limited number of binding sites available. In agreement with others we find a Binomial distribution solution to our master equation for the distribution of bound motors assuming an unlimited number of binding sites along the filament.

However, physically motors attached to a cargo cannot bind anywhere along the filaments, so the number of accessible binding sites on the filament should be limited. Thus, we analytically study the distribution and the velocity of a cluster of non-processive motors bound on the cargo with limited number of binding sites in steady state. To validate our analytical results and to go beyond the level of detail possible analytically we perform Monte Carlo latticed based stochastic simulations. In particular in our simulation model we include sequence preservation of motors performing stepping and binding obeying a simple exclusion process. Using our simulations we compare alternative models for limiting the number of binding sites along a filament. We find that limiting the number of binding sites reduces the probability of non-processive motors binding but has a relatively small effect on force-velocity relations. Our analytical and stochastic simulation results compare well to published data from *in vitro* and *in vivo* experiments.

2.2 Introduction

Molecular motors that move cargoes such as vesicles, lipid droplets or mitochondria facilitate intracellular transport [12, 68, 48, 45]. Motors bound to cargo can work either alone or cooperatively. However, *in vivo*, transport is usually performed by several motors, as is experimentally observed by electron microscopy and by tracking of cargoes with optical methods [101, 32, 48, 60]. Many studies have demonstrated that the number of molecular motors influences cargo transport, af-

fecting the velocity, direction and persistence of cargoes due to the processivity of motors [32, 68, 44, 105, 55].

In general, molecular motors can be classified according to their processivity, which refers to the distance that they can move along a filament before detaching [12, 2]. Processive motors can individually interact with a filament for long time and so perform a large number of steps before detaching, i.e. they rarely unbind from the filament during their motion. Examples of processive motors include kinesin, which move toward to the plus-ends of microtubules (anterograde direction) and dyenin, which move toward to the minus-ends of microtubules (retrograde direction) [2]. By contrast, nonprocessive motors will often unbind[12], remaining on a filament for only a short time and moving only a short distance. An example of a nonprocessive motors is myosin, which moves along actin filaments. In experimental biology the distinction between processive and nonprocessive is between rare and common unbinding. However, in this work we use a purer definition of processive and nonprocessive motors to align with the qualitative difference between theoretical models. We assume "processive" motors never unbind during the timeframe under study whereas "nonprocessive" motors are able to unbind and rebind to a filament within the timeframe of the study.

Motors pull a cargo against a force which affects their velocity. The force may be just the drag force caused by the cargo moving through the viscous medium or there may be additional external forces. For example, *in vitro* experiments can exert an external force on the cargo using optical tweezers or a magnetic field [32]. Various mathematical models have been introduced to explain collective motor dynamics from different perspectives [51, 12, 10, 48, 39, 15]. In particular, two different models for processive motors published in [12] and [51] have both have been widely cited but confusion exists in the literature in applying these models. The former, [12], introduced the leading motor model in which all the load force from the cargo is exerted on the leading motor. In contrast, the latter, [51], used a mean-field theory, assuming that all motors share the force equally, to analytically calculate the velocity of a cluster of motors moving along a cytoskeletal filament.

In this work, we model molecular motors moving along cytoskeleton filaments by using Monte Carlo simulations. We compare our simulation results with mathematical models for a fixed number of motors on a single track. Campas et al [12] derived the analytical result for the velocity against force for a cluster of such processive motors. We extend this model to obtain an analytical expression for the case of nonprocessive motors. In addition we compare our analytical and simulation results to published experimental data [32, 78].

2.3 Processive motors

2.3.1 Mathematic Description for processive motors

[12] developed an asymmetric simple exclusion process (ASEP) [91, 19, 25, 94] for cargo dynamics driven by processive molecular motors. The Simple Exclusion Process (SEP) is explained in details in section 1.2.1. As illustrated in Figure 2.1, each motor is able to move stochastically with specified forward, p, and backward, q, rates, similar to classical Brownian ratchet models [1, 73, 75]

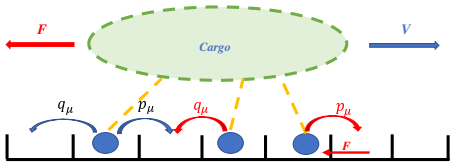

Fig. 2.1: Possible motor transitions and associated rates. Motor tails are attached to a cargo whereas motor heads (blue circles) are attached to a filament. The boxes represent a one dimensional lattice of binding sites on the filament [12].

The hopping rates for the leading motor are dependent on the force, [80], by a Boltzmann weighting; $p_1 = pe^{-f\delta}$ and $q_1 = qe^{f(1-\delta)}$ where f is the dimensionless force exerted by the cargo such that the load force $F = fk_BT/\mathrm{d}x$ where $\mathrm{d}x$ is the motor step size. The dimensionless parameter, δ, varies from 0 to 1 and determines how much the forward versus backwards stepping rates are affected by the load force. This is explained in more details of SEP with leading motor model in section 1.3 .

$$V_n = p\frac{(1-e^f(q/p)^n)(1-q/p)}{e^{f\delta}(1-q/p)+e^f(q/p-(q/p)^n)}. \tag{2.1}$$

Therefore, in order to consider the collective behaviour of multiple processive motors in intracellular transport, we use this leading motor model in which the leading motor experiences all the force and the following motors none of the force in section 2.3. We then extend this model to include motor attachment and detachment to study in the case of non-processive motors. Campas et al [13] studied this extension to non-processive motors using simulations but did not do the analytical extension which we do in section 2.4.

2.3.2 Simulations of processive motors

We first simulate the model of N processive motors which do not unbind from the filament. We model the filament as an one-dimensional lattice with lattice

spacing equal to the motor step size, dx. We initialise the simulation by randomly placing N motors within the width of cargo. We choose the initial cargo width to be 10 lattice sites for $N < 10$ and $(N + 10)$ lattice sites for $N \geq 10$. To check this choice of initial conditions does not influence our results, we varied the width of the cargo between 10 and 100 and found that our results are insensitive to the chosen initial cargo width.

The simple exclusion rule dictates that each site may be either occupied or empty but cannot be occupied by more than one motor. Motors can thus move to a neighbouring site only if the new site is unoccupied. In the simulation, an individual motor moves forward with a rate p_μ and backward with a rate, q_μ, where the subscript represents the motor μ (see Figure 2.1).

For consistency throughout this work we present results from our simulations using a discretized fixed time step Monte Carlo method. However since continuous-time discrete-state Markov processes such as the ones we study here are often stochastically simulated with the well-known event-driven approach of Gillespie [22], we checked our method against this. We validate the model by using Gillespie method in section 2.7.1. We found that our results using the fixed time step and Gillespie algorithm methods are equivalent within the error bars (see results presented in section 2.7.1. We use our fixed time step method for our full study since it is ten times faster than the Gillespie algorithm for our non-processive motors case. In our fixed time step method, at each time step, dt, forward and backward steps are attempted with the probabilities $P_f = p_\mu \, \mathrm{d}t$ and $P_b = q_\mu \, \mathrm{d}t$, respectively. If motor μ meets the condition for moving to a neighbouring site, the position of the motor x_μ is updated to $x_\mu \pm \mathrm{d}x$ for motion forwards(+) or backwards(-) along the track, where dx is the motor step size.

Processive motors based on Simple Exclusion Process (SEP) are considered as short-range repulsive interacting species, as explained in section 1.2.1. The parameters are defined by the following equation.

$$\begin{aligned} p_\mu &= p, q_\mu = q \\ v_\mu &= v, u_\mu = u \end{aligned} \tag{2.2}$$

for $\mu \geq 2$, whereas the rates of the leading motor ($\mu = 1$) depend on the external force at the following equation.

$$\begin{aligned} p_1 &= pe^{-f\delta} \\ q_1 &= qe^{f(1-\delta)} \end{aligned} \tag{2.3}$$

The procedures to simulate collective transport of multiple motors included the exclusion principle are following these steps.

1. Initially, we place all N motors randomly positioned within a length given by the cargo width, then all N motors are occupied at position x_i where $i = 1$ to N at $t = 0$.

2. For each time step, we visit each of the N motors and calculate their tentative steps and positions as described in step 2 and 3 of the single motor's procedure. In this case, only the stepping rates of the leading motor are dependent on force as shown in Eq. 2.3, but that of the other motors are independent with force as shown in Eq. 2.2. If the each motor's step is approved, then we set $x_i(t+\Delta t) = x_i(t)+1$ or $x_i(t+\Delta t) = x_i(t)-1$ or $x_i(t+\Delta t) = x_i(t)$ depending on the tentative states of each motor's stepping at each time step.

3. To compare with the theoretical perspective in Eq. 2.1, we calculate velocity from similation results, $\bar{V} = (x_i(T)-x_i(0))/(T-0)$ where T is the total simulation time.

2.3.3 Results of processive motors

Here we present our results for fully processive motors, which do not unbind from the track and may move bidirectionally with the rates p and q. The case of unidirectional motors is easily obtained by setting $q = 0$. Our models can be applied to a variety of different molecular motors. The simulation results we show here are for parameter values $p = 100\ s^{-1}$ and $q = 10\ s^{-1}$ corresponding to experimental values for processive kinesin-1 [14, 32] and the assumption that the ratio of forward to backward rates is ten [64, 16].

To compare with the analytical solution, Eq. (2.1), we calculate the steady state velocity of the leading motor from our simulation results, $V_{sim} = \frac{x_1(T)-x_1(t_s)}{T-t_s}$ where $x_1(t)$ is the position of the leading motor at time t, T is the total simulation time and t_s is the time we start measuring from once the system has reached steady state. We find that running our simulations for $T = 5 \times 10^6$ time steps of $\mathrm{d}t = 1.0 \times 10^{-3}s$ is long enough to ensure that the results are not dependent on specific initial conditions chosen. We choose $t_s = 1000$ steps by which time all cases have reached steady state (checked by plotting trajectories, not shown). We ran each simulation 100 times and plot the standard deviation as error bars in the results graphs.

The leading motor's velocity for different numbers, N, of bound motors is shown in Figure 2.2 using our fixed time step Monte Carlo method. It is clear that the velocities for different number of motors N decrease rapidly with force as also seen in [12]. The force at which the velocity reaches zero (hits the x-axis in Figure 2.2) is known as the stall force. For large N and dimensionless force, f, the motors form a dense cluster which moves very slowly. Furthermore, these results imply that the force-velocity curves for multiple motors ($N > 5$) are almost

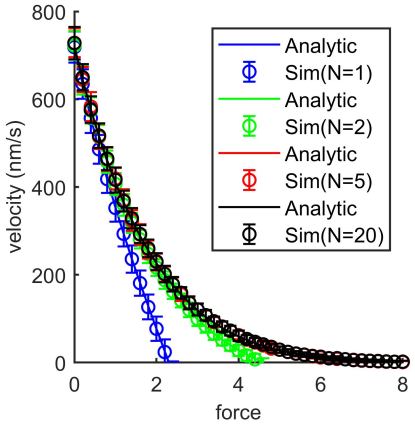

Fig. 2.2: Force-velocity curves of processive motors from Monte Carlo simulations (symbols) for different number of motors $N = 1$ (blue), 2 (green), 5 (red) and 20 (black) compared with the analytical solution (lines) given by Eq. 2.1 with parameters $p = 100s^{-1}$, $q = 10s^{-1}$, $\delta = 0.5$ [14, 32, 12].The force on the x-axis is the dimensionless force $f = F\mathrm{d}x/k_BT$ where F is the physical force and $\mathrm{d}x = 8nm$ is the step size.

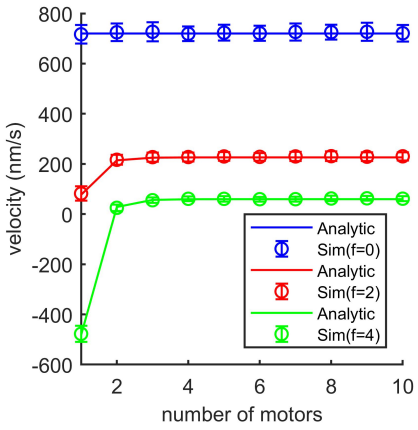

Fig. 2.3: Velocity against number of processive motors under different loads (blue $f = 0$, red $f = 2$ and green $f = 4$) from our fixed time Monte Carlo simulations (symbols) compared with the analytical solution (lines) given by Eq. (2.1) with $p = 100\ s^{-1}$, $q = 10\ s^{-1}$ and $\delta = 0.5$ [14, 32, 12].

indistinguishable.

To clarify the effect of number of motors N on the velocity of the collection of motors, we plot the velocity against the number of processive motors under different loads in Figure 2.3. The figure shows the leading motor's velocity versus

different total numbers of motors N from 1 to 10 for different loads (various values of dimensionless force $f = 0, 2$ and 4). The results in this figure confirm that the velocities of collections of $N > 1$ motors pulling the same force, f, are almost independent of the exact number of motors N. However, for $N \sim 1$ and finite force the velocity is dependent on the number of motors and for large forces the velocity may be backwards (negative).

2.4 Nonprocessive motors

We now extend the theory and simulations described above to the case of non-processive motors. We allow motors to bind on and off the filament with rates k_{on} and k_{off}, respectively, as illustrated in Figure 2.4. Including the dynamics of motor binding and unbinding means that, unlike the processive motor case, the number of motors bound to a filament changes over time.

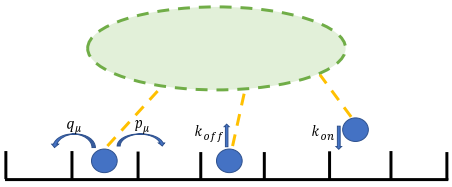

Fig. 2.4: Cartoon showing motors bind to and unbind from a filament with rates k_{on} and k_{off}, respectively.

2.4.1 Mathematic Description for non-processive motors

Since including stochastic binding and unbinding of motors (with rates k_{on} and k_{off}) means the number of bound motors changes over time, we need to know the probability distribution of the number of bound motors. The average velocity of a cluster of motors capable of binding and unbinding can be calculated in terms of the probability, P_n of having n motors bound [48];

$$\bar{V} = \sum_{n=1}^{N} \frac{P_n V_n}{1 - P_0} \tag{2.4}$$

where V_n is the velocity when there are n motors bound given by (2.1) and N is the total number of motors in the system. In using this equation we assume that each cluster of n motors travels with its steady state velocity V_n. This assumption is valid as long as stepping is fast enough compared to (un)binding. In our work, we use Eq. (2.4), to calculate the average velocity of a cluster of non-processive motors and we calculate the probability distribution, P_n, as detailed in the following. Eq.

(2.4) relies on the steady state assumption. Note that if this assumption is broken then the analytical solution gives an over estimate since the steady state SEP cluster has reduced backwards stepping rates leading to faster forwards velocities compared to non-steady-state.

Initially we assume that the number of binding sites available is unlimited such that the binding rate of a single motor, k_{on}, is constant. We write down a discrete master equation for the probability, P_n, that there are n motors bound at time t; Initially we assume that the number of binding sites available is unlimited such that the binding rate of a single motor, k_{on}, is constant. We write down a discrete master equation for the probability, P_n, that there are n motors bound at time t;

$$\begin{aligned}\frac{\partial P_n}{\partial t} =&(N-n+1)k_{\text{on}}P_{n-1} + (n+1)k_{\text{off}}P_{n+1} \\ &- (N-n)k_{\text{on}}P_n - nk_{\text{off}}P_n,\end{aligned} \tag{2.5}$$

where N is the total number of motors in the system (bound plus unbound motors). This master equation is equivalent to that used by [48]. At steady state, $\frac{\partial P_n}{\partial t} = 0$, we obtain the detailed balance condition that the binding and unbinding processes occur with equal probability such that;

$$(N-n+1)k_{\text{on}}P_{n-1} = nk_{\text{off}}P_n. \tag{2.6}$$

The probability, P_n, of being in a state with n bound motors can therefore be written in terms of the binding rates k_{on} and k_{off} and the total number of motors, N. Using Eq. (2.6) and the normalisation $\sum_{n=0}^{N} P_n(N) = 1$, we obtain;

$$P_n(N) = \frac{N!}{n!(N-n)!}\left(\frac{k_{\text{on}}}{k_{\text{off}}}\right)^n P_0 \tag{2.7}$$

where P_0 is the normalisation constant. If $k_{\text{on}} < k_{\text{off}}$ this can be written as a convergent series, $P_0 = (1 + \frac{k_{\text{on}}}{k_{\text{off}}})^{-N}$, and the maximum number of bound motors, N, can be infinitely large. The opposite case of $k_{\text{on}} > k_{\text{off}}$ will become incompatible with the initial assumption of constant k_{on} as this will break down as the filament becomes saturated with motors. For that case the finite number of binding sites available needs to be addressed by limiting the binding sites, as addressed in the next paragraph. The distribution (2.7) is the Binomial distribution used by [84, 83] and understood from considering the stochastic binding and unbinding of each motor when the maximum number of motors that can bind is N. Considering the case of multiple motors attached to the same cargo we expect the number of filament binding sites accessible to those motors to be limited by the size of the motors and cargo. We therefore study the effects of limiting the number of binding sites. However we do this without going into the level of detail of modelling

motors as springs as some authors have done [53, 51]. Instead we simply limit the binding sites accessible to the motors. If the number of binding sites on the filament is limited to M, which can be considered as the width of cargo, then $k_{\text{on}}(M,n) = (M-n)k^s_{\text{on}}$ where the superscript s refers to the binding rate per site, obtained by dividing the unlimited binding rate by M, i.e. $k^s_{\text{on}} = k_{\text{on}}/M$. Eq.2.5 can be extended by including the limited number of binding sites, M as follows;

$$\begin{aligned}\frac{\partial P_n}{\partial t} =&(N-n+1)(M-n+1){k^s}_{\text{on}}P_{n-1} + (n+1)k_{\text{off}}P_{n+1}\\ &-(N-n)(M-n){k^s}_{\text{on}}P_n - nk_{\text{off}}P_n,\end{aligned} \tag{2.8}$$

The distribution of bound motors in this case is given by

$$P_n(N,M) = \frac{N!M!}{n!(N-n)!(M-n)!}\left(\frac{k^s_{\text{on}}}{k_{\text{off}}}\right)^n P_0 \tag{2.9}$$

where P_0 is the normalisation constant given by $\sum_{n=0}^{N} P_n(N,M) = 1$.

The average velocity of N non-processive motors is then obtained by substituting Eq. (2.1) and (2.7) into Eq. (2.4) for unlimited binding sites giving;

$$\bar{V} = \sum_{n=1}^{N}\frac{N!}{n!(N-n)!}\frac{P_0}{1-P_0}\left(\frac{k_{\text{on}}}{k_{\text{off}}}\right)^n\left(p\frac{(1-e^f(\frac{q}{p})^n)(1-\frac{q}{p})}{e^{f\delta}(1-\frac{q}{p})+e^f(\frac{q}{p}-(\frac{q}{p})^n)}\right). \tag{2.10}$$

For the case of limited binding sites the equivalent expression is obtained by substituting Eq. (2.1) and (2.9) into Eq. (2.4).

2.4.2 Simulations of non-processive motors

We extend the fixed time step Monte Carlo algorithm we used for processive motors (described in section 2.3.2) to the system of N non-processive motors (drawn in Figure 2.4) and validate the results and efficiency against a Gillespie algorithm as shown in Appendix 2.7.2. We consider N motors attached to a cargo, thus the number, n, of motors bound on the filament at time t varies between zero and N. We choose an initial condition with all the motors unbound from the filament. Then, at subsequent time steps, each motor is allowed to attach to the filament track with the attachment probability $P_{\text{on}} = k_{\text{on}}\,\mathrm{d}t$.

In each time step of the simulation, we visit each of the N motors to consider their possible states and positions. Each motor is allowed to either bind to and unbind from the track according to the relevant probability, $P_{\text{on}} = k_{\text{on}}\,\mathrm{d}t$ or $P_{\text{off}} = k_{\text{off}}\,\mathrm{d}t$, respectively. After that the bound motors are allowed to move along the track with the forward/backwards stepping probabilities and the constraints of the

simple exclusion process in the same way as for the simulation of processive motors described in section 2.3.2. Therefore, the motors cannot overtake each other when stepping along the track. We describe our procedure for simulating non-processive motors in the following steps and summarize in a schematic in Figure 2.5.

1. First, we have maximum number of motors, N, in the system. At initial time $t = 0$, all motors are dissociated from the track.

2. We visit each detached motor and calculate the attachment probability for the present time step, $P_{on} = k_{on}dt$ with a generated number r_1 .

- If $r_1 \leq P_{on}$, then the motor is attached to the track and calculate the motor's position x_i. The binding position is randomly positioned within a length limited by either the (moved) fore and back motors' positions because they cannot overtake each other or the (moved) cargo width if no prevented motors at each time step. The attached motor then performs stepping in the next step.

- If not, the motor is still detached.

Meanwhile, attached motors from a previous step are allowed to detach from the track with a probability $P_{off} = k_{off}dt$.

3. For each attached motor, it performs stepping. Stepping occurs with the probability as the same with the case of multiple motors in the absence of binding/unbinding as mentioned in step 2. The i^{th} motor's position will be $x_i(t + dt) = x_i(t) + 1$ or $x_i(t + dt) = x_i(t) - 1$ or $x_i(t + dt) = x_i(t)$.

4. Calculate the leading motor's velocity by recording the initial bound position $x_i(t_1)$ at time t_1 and final bound position $x_i(t_2)$ at time t_2 on the track, thus the velocity is obtained by $\bar{V} = (x_i(t_2) - x_i(t_1))/(t_2 - t_1)$.

2.4.3 Results of non-processive motors

We now present the results of our fixed time step Monte Carlo simulations for the stepping of a cluster of N motors including the ability of binding on and off the filaments (k_{on} and k_{off}). Since we are interested in motor clusters we study strongly binding molecular motors for which the binding rate, k_{on}, is higher than the unbinding rate, k_{off} [48, 32, 8, 31]. We choose Ncd (kinesin-14) as an example of a non-processive motor which unbinds often [32, 77]. In our simulation, we use $k_{\text{off}} = 10\,\text{s}^{-1}$ as measured experimentally [32, 86, 77]. k_{on} is more difficult to measure experimentally but, since we are interested in the case $k_{\text{on}} > k_{\text{off}}$, we choose $k_{\text{on}} = 20\,\text{s}^{-1}$. We run our simulations for 5×10^7 time steps with a time step of $1.0 \times 10^{-3}\,\text{s}$. This is longer than required for processive motors because non-processive motors take longer to reach steady state due to the binding dynamics. For non-processive motors we set $t_s = 2500$ steps and $t_s = 25000$ steps by which

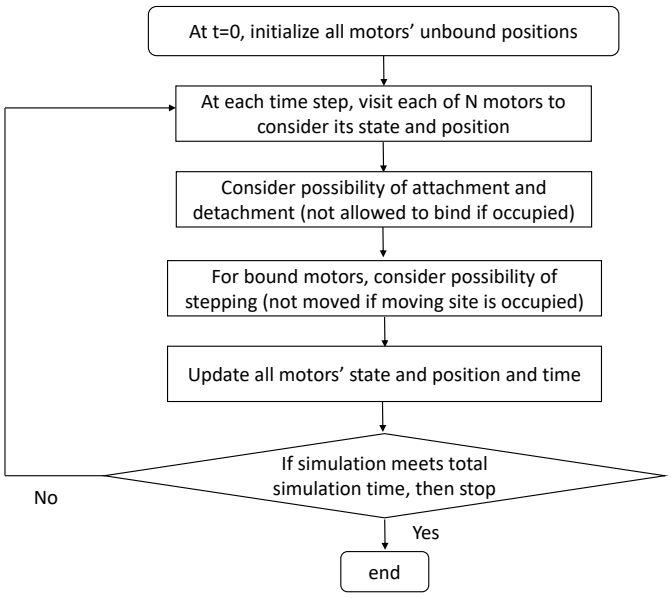

Fig. 2.5: Flow chart of our fixed time step Monte Carlo simulations for nonprocessive motors.

time all cases have reached steady state for $N \leq 10$ and $N = 100$, respectively. In the following, we first present the distribution of the number of bound motors and then the average velocity, stall force and run length.

Probability Distribution of bound motors

We consider the effect of number of binding sites in two scenarios. First, the number of binding sites is fixed in scenario A. Second, the number of binding sites is variable in scenario B and the sequence of motors is preserved on binding.

Scenario A: Fixed number of binding sites. We first assume that the number of binding sites accessible by the motors is fixed to M lattice sites as illustrated in Figure 2.6(a). In this scenario, the motors are only able to bind within these M sites, which can be considered to correspond to the cargo width. In this scenario we allow an unbound motor to bind onto any of the unoccupied sites within the M sites. This means that the sequence of motors may change during rebinding. In other words, in the simulation of this scenario motors are allowed to swap positions on rebinding.

In Figure 2.6(b), we plot the probability distribution of bound motors, $P_n(N, M)$ for $N = 10$ and various different number of binding sites M. We choose $N = 10$

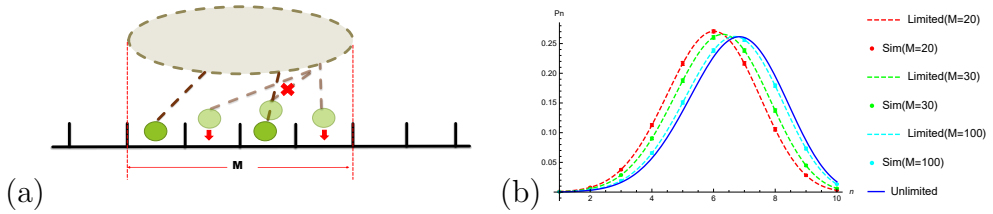

Fig. 2.6: (a) Cartoon showing scenario A in which motors may bind only to unoccupied sites within a fixed limited number M of binding sites but they may swap positions on rebinding. (b) Probability distribution of non-processive motors attached on the same cargo for various fixed number of binding sites ($M = 20, 30, 100$ for red, green, blue respectively) from simulation results (points) and Eq. 2.7 (dark blue line) and Eq. 2.9 (dashed lines). The parameter values are $k_{\text{on}} = 20\,\text{s}^{-1}$, $k_{\text{off}} = 10\,\text{s}^{-1}$ [32, 86, 77], $p = 22\,\text{s}^{-1}$ [32], $q = 2.2\,\text{s}^{-1}$, $\delta = 0.5$, $f = 0$ and $N = 10$.

here to highlight the differences between limited and unlimited Binomial distributions which are smaller for $N \leq 10$. The dark blue solid line is the analytical distribution for unlimited binding sites (Eq. 2.7) and the dashed lines are the analytical distributions for the number of binding sites limited to M (Eq. 2.9) where the different colours represent different values of M. The coloured points are results from Monte Carlo simulations of scenario A (fixed M binding sites) allowing the motors to swap positions on rebinding. The simulation results match the relevant analytical expressions (Eq. 2.9) within the error bars. For $M \gg N$ the simulations and analytical distribution for the limited case (Eq. 2.9) approach that of the unlimited case (Eq. 2.7) as expected. Consequently, if the cargo size as defined by M is large enough then we can describe the probability distribution of bound motors by the unlimited Binomial distribution.

However, *in vivo*, due to steric hindrance, the molecular motors may preserve their sequence on rebinding. In this case the number of accessible binding sites would change over time according to the positions of the leading and last motors. We consider this scenario in the following.

Scenario B: Variable number of binding sites with sequence preservation. Here we present a second, more realistic, scenario in which the motor sequence is preserved on rebinding and the number of binding sites M is no longer fixed. To preserve the sequence a motor can only bind to unoccupied sites between its neighbouring motors. The number of accessible binding sites changes over time following the first and last motors' positions. Additionally, we allow one more site in front/behind the position of the leading/back motors to be accessible to stepping and binding. This latter accommodation allows for a motor to stretch to reach the adjacent site.

At the end of each time step, after motors have had the chance to bind and move, the number of binding sites M is changed following the bound/moved leading and last motor positions. In the case that all motors are detached, M is determined from the positions of leading/back motors when they were last attached. The number of binding sites $M(t)$ in this scenario is thus updated each time step. In this case, M is limited to the steady state cluster size plus 2.

The simulation results for $P(n)$ shown in Figure 2.7 fit better with limited Binomial distribution, Eq. 2.9, than unlimited Binomial distribution (Eq. 2.7). However the simulation results are shifted slightly lower than the analytical distribution because of the sequence preservation on motor rebinding in the simulation which is not included in the analytical expression. Figure 2.17 in Appendix 2.7.2 shows that the results of this variable number of binding sites case without sequence preservation on rebinding do coincide with the analytical limited Binomial distribution.

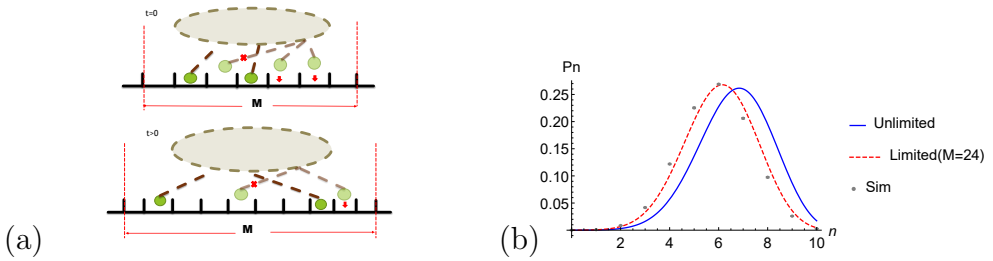

Fig. 2.7: (a) Cartoon showing scenario B (variable number of binding sites and sequence preservation) in which motors may bind only to unoccupied sites between neighbouring motors such that the sequence is preserved. (b) Probability distribution of non-processive motors with no exerted force and variable number of binding sites, $M(t)$, from simulation results (points) comparing with Eq. 2.7 (blue line) and Eq. 2.9 (dashed line) with the value of M being the average calculated over the whole simulation. The parameter values used are $k_{\text{on}} = 20\,\text{s}^{-1}$, $k_{\text{off}} = 10\,\text{s}^{-1}$ [32, 86, 77], $p = 22\,\text{s}^{-1}$ [32], $q = 2.2\,\text{s}^{-1}$, $\delta = 0.5$, $f = 0$ and $N = 10$.

To date there is no clear experimental evidence showing whether motors swap position or preserve their sequence during rebinding. However, most literature models use the assumption that the sequence of motors is preserved on binding [61, 12, 48]. Also, many of these studies do not support the assumption that motors are restricted to bind within a fixed determined space as is the case in our scenario A. We suggest that our scenario B (variable number of binding sites with sequence preservation) is more realistic for intracellular transport. We therefore choose scenario B to further study further the velocity of a cluster of non-processive motors in the following section.

Average Velocity

We compute the velocity of the motor cluster from the simulation by averaging the leading motor's velocity when at least one motor is bound on the track. The average velocity is then calculated by $V_{sim} = \langle \frac{x(t_2)-x(t_1)}{t_2-t_1} \rangle$ where $x(t_1)$ is the leading motor's position on binding and $x(t_2)$ is the motor's position when it unbinds from the track. During the course of the simulation which motor is the leading motor will change according to the binding and unbinding of motors. The leading motor is the bound motor with the forward most position at that point in time, i.e. the largest $x_\mu(t)$. We calculate the velocity over the time that an individual motor acts as the leading motor ($t = t_1$ to t_2) and then calculate the velocity of the next motor that acts as the leading motor. We then average over all these velocities.

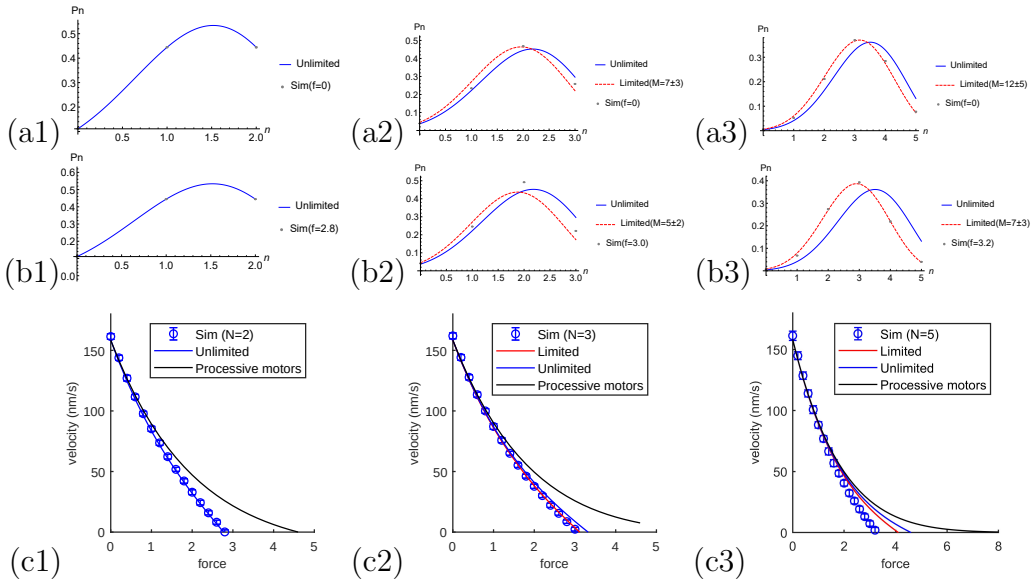

Fig. 2.8: (a1-b3) Probability distribution of n bound motors with maximum number of motors $N = 2, 3$ and 5 under (a1-a3) no force, $f = 0$ and (b1-b3) stall force, $f = f_s$, from simulations (symbols) compared with $P(n)$ given by Eq. 2.9 by averaging M sites (dashed red) and Eq. 2.7 (solid blue). (c1-c3) Velocity of clusters of $N = 2, 3$ and 5 from simulation results (symbols) compared with the analytical solution Eq. (2.10) for limited (red) and unlimited (blue) binding sites. Note that, for $N = 2$, there are always available sites to bind, so it is not compared with limited Binomial distribution. The solid black lines are the velocities of having $N = 2, 3$ and 5 bound processive motors without (un)binding, given by Eq 2.1. The other parameter values are those for Ncd i.e. the same as in Figure 2.7, namely $k_{\text{on}} = 20\,\text{s}^{-1}$, $k_{\text{off}} = 10\,\text{s}^{-1}$, $p = 22\,\text{s}^{-1}$, $q = 2.2\,\text{s}^{-1}$, $\delta = 0.5$ and $\text{d}x = 8\,\text{nm}$. For the processive case (black lines) $k_{\text{on}} = k_{\text{off}} = 0$.

In order to obtain the force-velocity relation for non-processive motors, we first consider the appropriate steady state probability distribution for the number of bound motors $P(n)$ at different forces and then consider the velocity at different forces. Figure 2.8 shows $P(n)$ from simulations and analytical expressions (Eq. 2.7 and 2.9) for (a) zero force, $f = 0$, and (b) the stall force, $f = f_s$ (the force for which the velocity is zero) for small numbers of total motors $N = 2$, 3, and 5. We choose values $k_{\text{on}} = 20\ \text{s}^{-1}$, $k_{\text{off}} = 10\ \text{s}^{-1}$, such that $k_{\text{on}} > k_{\text{off}}$ to study motor clusters. As discussed in the previous section the analytical expression for the distribution of bound motors with limited number of binding sites, Eq 2.9, is a better approximation to the simulation results than the unlimited Binomial distribution, particularly at larger force. This is because the leading motor is more likely to move backwards at larger force, further reducing the number of accessible binding sites. Consequently the probability distribution of motors bound on the track is shifted to smaller numbers of motors than the case assuming unlimited binding sites (Eq. 2.7), as is evident in Figure 2.8 (b2) and (b3). The case of $N = 2$, shown in Figure 2.8 (a1) and (b1), is well described by the unlimited binding sites expression (Eq. 2.7). This is because our model allows binding to one site in front/behind the leading/back motor which means for $N = 2$ there are always available sites to bind. For $N = 3$, Figure 2.8(a2), the simulation points are between that of the limited and unlimited curves due to the extra freedom provided by the end sites. However by $N = 5$, Figure 2.8(a3) we see a good agreement with the limited analytical expression. Note for $N = 10$ in Figure 2.7(b) the simulation points are shifted to smaller n than the limited analytical expression. This is caused by the restrictions imposed in the simulations to ensure sequence preservation which is not captured by the analytical expressions (see more discussion in Appendix 2.7.3).

Figure 2.8(c1-c3) shows the velocity as a function of force calculated from simulations and analytical calculations (Eq. 2.4) for small numbers of total non-processive motors $N = 2$, 3, and 5. The processive motor case, Eq. 2.1, is plotted on the same graph for comparison. The parameter values used are those for Ncd for the non-processive case and $k_{\text{on}} = k_{\text{off}} = 0$ for the processive case (black line). See Figure 2.8 caption for the full list of parameters.

As expected from our studies of the probability distributions for the number of bound motors (Figure 2.8(a) and (b)), the velocity for the case of limited number of binding sites is a closer approximation than that of unlimited binding sites. However the effect on the velocity of limiting the number of binding sites is slight for small number of motors up to $N = 3$ (Figure 2.8(c2)) with both analytical cases falling within the error bars of the simulations for almost the entire range of forces $f = 0$ to $f = f_s$. However clear discrepancies develop for the $N = 5$ case (Figure 2.8(c3)) at larger forces. Although the limited number of binding sites case is closer

to the simulation results even this is outside of the error bars for $N = 5$ at larger forces. This may be partly due to the larger forces decreasing the stepping rate such that the validity of steady state assumption of Eq. 2.4 is weakened resulting in the analytical solution overestimating the velocity. The discrepancy seen in Figure 2.8(c3) also reflects the influence of sequence preservation that is included in the simulations but not in the analytical results. This effect is more pronounced for larger clusters of motors and larger forces (see Figure 2.9 and Appendix 2.7.2).

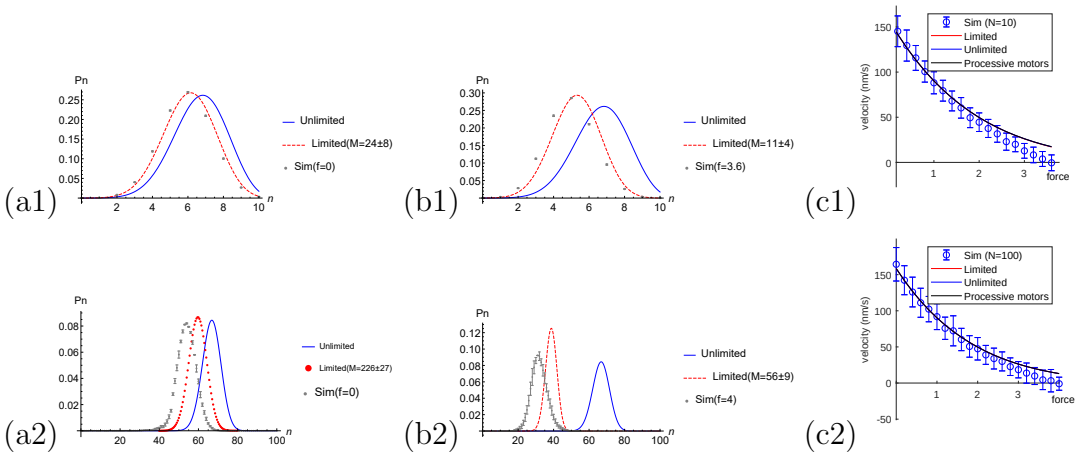

Fig. 2.9: Probability distribution of n bound motors with maximum number of motors $N = 10$ under (a1) no force, $f = 0$, and (b1) stall force, $f = f_s$ and $N = 100$ (a2) $f = 0$ and (b2) $f = f_s$, from simulation (symbols) compared with Eq. 2.9 by averaging M sites (dashed red) and Eq. 2.7 (solid blue). (c1-c2) Velocity of large clusters of motors (c1) $N = 10$ and (c2) $N = 100$ are plotted and the analytical velocity of having N bound processive motors without (un)binding (solid black) is also shown, given by Eq 2.1. The other parameter values are the same as in Figure 2.7, namely $k_{\text{on}} = 20\,\text{s}^{-1}$, $k_{\text{off}} = 10\,\text{s}^{-1}$, $p = 22\,\text{s}^{-1}$, $q = 2.2\,\text{s}^{-1}$, $\delta = 0.5$ and $\mathrm{d}x = 8\,\text{nm}$. For the processive case (black lines) $k_{\text{on}} = k_{\text{off}} = 0$.

Figure 2.9(a1) and (b1) shows the probability distribution of bound motors, $P(n)$, at no force, $f = 0$, and the stall force, $f = f_s$, for a larger motor cluster of $N = 10$. As expected, we see that the case of limited binding sites fits better than for unlimited binding sites for both extremes of the force range. In Figure 2.9 (b1) we can see that the simulation points are shifted towards smaller number of bound motors compared to the analytical limited binding sites case. This is even more pronounced for the $N = 100$ case shown in Figure 2.9(a2) and (b2). This is due to the effect of sequence preservation which has a greater impact for larger clusters and larger forces. Figure 2.17 in Appendix 2.7.2 shows that without sequence preservation on rebinding the probability distributions of the number of

bound motors follow that of the analytical expression for limited binding sites.

In Figure 2.9 (c1) we show the velocity of a cluster of $N = 10$ non-processive motors with parameters for Ncd. We compare our simulation results against the analytical results for the cases of unlimited and limited binding sites as well as the case of 10 processive motors with $k_{\text{on}} = k_{\text{off}} = 0$. As can be seen in Figure 2.9 (c1) all three analytical curves collapse onto that of the processive motor case for $N = 10$ indicating that for $N = 10$ there are enough motors in the cluster that they behave as processive motors. This processive behaviour of large clusters of non-processive motors can be justified analytically. Consider approximating the average velocity given by Eq. 2.4 by the velocity for the number of bound motors at the peak of the probability distribution for the number of bound motors. For unlimited number of binding sites the peak of the relevant Binomial distribution is at $n = \frac{Nk_{\text{on}}}{k_{\text{on}}+k_{\text{off}}}$. We see from Figure 2.3 that for large number of motors the velocity is independent from the number of motors. Therefore if $\frac{Nk_{\text{on}}}{k_{\text{on}}+k_{\text{off}}} \gg 1$ then $\bar{V} \approx V_{\frac{Nk_{\text{on}}}{k_{\text{on}}+k_{\text{off}}}} \approx V_N$. Approximating the average velocity by that for the peak of the distribution for the number of bound motors is valid as long as the bulk of the probability distribution is for $n \gg 1$ bound motors since V_n is independent of n for $n \gg 1$. Figure 2.9(a1) shows that this is already the case for $N = 10$. For $N = 100$ Figure 2.9 (c2) shows that within the errors the velocity of $N = 100$ non-processive motors is as fast as that of processive motors. This is because for $N = 100$ there is almost always at least one motor bound so, since the velocity of a cluster is limited by the leading motor, the effect of detachment is negligible. Therefore, we can approximate the velocity of a cluster of large enough numbers of non-processive motors as equivalent to the velocity of processive motors with the same number of motors.

In summary our simulation results show that it is better to approximate the distribution of number of bound motors with Eq. 2.9 including the limited number of binding sites. This expression does not fit exactly because the simulation includes sequence preservation which is not included in the analytical theory. However, when we calculate the velocity of a cluster of $N < 10$ motors, both limited and unlimited analytical distributions can similarly approximate the velocity of a simulated motor cluster, see Figure 2.8(c1-3). Therefore, when investigating the velocity, it is not crucial which distribution we use for small N. The distribution with unlimited number of binding sites has the advantage that it requires fewer parameters such that we only need to know the total number of motors N and we do not need to know the size of the cargo nor number of binding sites M. This case of small $N < 10$ motor clusters bound to a single cargo has been shown to be relevant *in vivo* [4, 62]. For large motor clusters $N > 10$ however, the distribution with unlimited number of binding sites is not a good approximation for the probability distribution of bound motors due to sequence preservation. However, since

large clusters of $N > 10$ rarely have all motors unbound they behave like processive motors and the force-velocity curve can be described by that for processive motors.

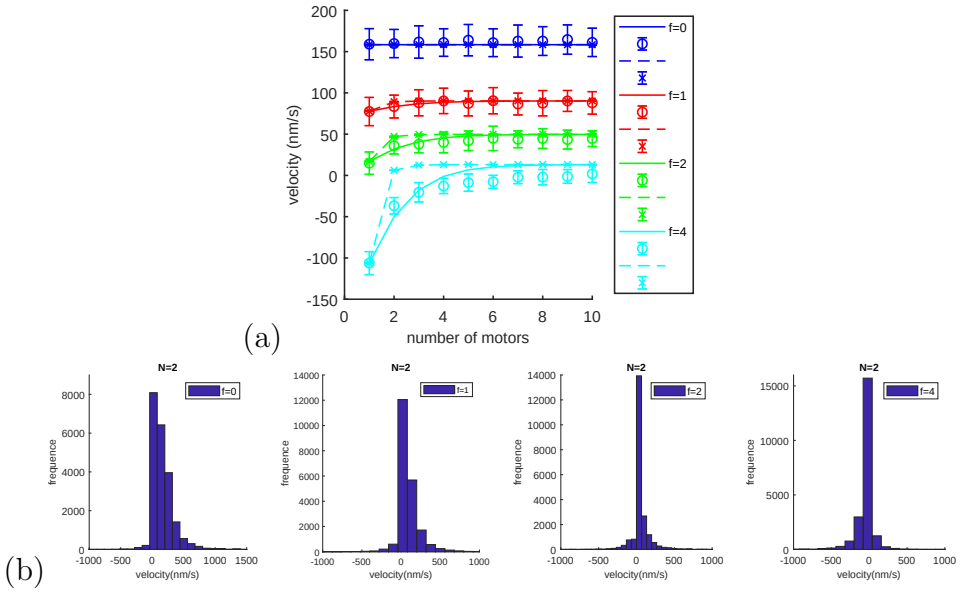

Fig. 2.10: (a) Velocity against number of non-processive motors pulling a load with dimensionless force $f = 0, 1, 2$ and 4 (dark blue, red, green, light blue respectively) from Monte Carlo simulations (circle symbols) and analytical expression using unlimited Binomial distribution, Eq.2.10 (solid lines). We also plot the case of processive motors (with $k_{\text{on}} = 0\,\text{s}^{-1}$, $k_{\text{off}} = 0\,\text{s}^{-1}$ simulation (cross symbols) and analytical expression, Eq. 2.1 (dashed lines). (b)The distribution of velocities in panel (a) for $N = 2$ with $f = 0, 1, 2$ and 4 (left to right). The other parameter values are the same as in Figure 2.7, namely $k_{\text{on}} = 20\,\text{s}^{-1}$, $k_{\text{off}} = 10\,\text{s}^{-1}$, $p = 22\,\text{s}^{-1}$, $q = 2.2\,\text{s}^{-1}$, $\delta = 0.5$ and $\mathrm{d}x = 8\,\text{nm}$.

For completeness, in Figure 2.10 (a), we plot the velocity against the number of non-processive motors from simulations and analytical calculations using the unlimited binomial distribution. This is the non-processive motor equivalent of Figure 2.3 which is for processive motors. Note that the values for the velocities are different for these cases due to the different forward and backward stepping rates used to mimic the molecular motors kinesin and Ncd. For comparison we therefore also plot the case of processive motors (with $k_{\text{on}} = 0\,\text{s}^{-1}$, $k_{\text{off}} = 0\,\text{s}^{-1}$) and other parameters for NcD on Figure 2.10 (a) for simulation (cross symbols) and analytical expression, Eq. 2.1 (dashed lines). This comparison clearly supports the point that non-processive motors behave as processive motors for larger $N = 10$, consistent with Figure 2.9 (c1). Figure 2.10(a) shows the velocity increases with

the maximum number of motors, N, but tends to a plateau for $N > 5$ suggesting that for $N > 5$ the binding of additional motors makes little difference to the velocity. This is similar to the case for processive motors (Figure 2.3) except that for those the plateau is reached for $N > 1$. We also plot the distribution of these velocities for $N = 2$ with different forces in Figure 2.10 (b). Discrepancies between the simulation and analytical results can be seen for the larger force $f = 4$, shown in light blue in Figure 2.10(a). This is due to sequence preservation included in the simulation but not in the analytical results. As expected sequence preservation has a larger effect at larger forces. This can be seen by comparing Figure 2.9(a1) and (b1) with Figure 2.17 in Appendix 2.7.2 for $N = 10$ at $f = 0$ and $f = f_s$ with and without sequence preservation on rebinding.

Stall force against number of motors

The stall force is the force at which the cargo stops moving because the team of motors is no longer able to pull it against the load force. We can calculate the stall force, F_s, by substituting $V = 0$ into Eq. (2.1) for processive motors. For non-processive motors, we calculate the stall force from the force-velocity relations by setting Eq. (2.4) to zero using the unlimited Binomial distribution and limited Binomial distribution.

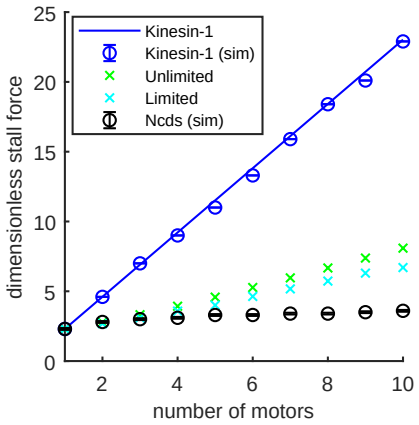

Fig. 2.11: Dimensionless stall force against number of motors, N. For processive kinesin-1 motors we calculate this analytically by setting Eq. (2.1 to zero (solid blue line). For non-processive Ncd motors we set Eq. (2.4) to zero and solve numerically using the distribution of bound motors with limited (Eq.2.9, light blue crosses) and unlimited (Eq. 2.7 green crosses) binding sites. Simulation results are shown with circle symbols for parameter values $p = 100\,\mathrm{s}^{-1}$ and $q = 10\,\mathrm{s}^{-1}$ for kinesin-1 processive motors (blue circles) and $p = 22\,\mathrm{s}^{-1}$ $q = 2.2\,\mathrm{s}^{-1}$, $k_{\mathrm{on}} = 20\,\mathrm{s}^{-1}$ and $k_{\mathrm{off}} = 10\,\mathrm{s}^{-1}$ for Ncd non-processive motors (black circles).

For processive motors, Eq. (2.1) can be solved analytically for the stall force giving $F_s(N) = NF_s(1)$ where $F_s(1)$ is the stall force of a single motor, i.e. for processive motors the stall force increases linearly with the number of motors. In dimensionless form the stall force for a single motor is given by $f_s(1) = \ln(p/q)$ and is the same for both kinesin-1 and Ncd with the parameters we use for these different motors. We plot this in Figure 2.11 along with the stall force for kinesin-1 extracted from our simulations displayed in Figure 2.2. We use a threshold of $|\frac{V_{fs}}{V_{f_0}}| \leq 10^{-5}$ to determine the stall force from our simulations.

For non-processive motors N is the maximum number of motors that can attach to the filament, so the number of attached motors at a particular time can vary from zero to N. Consequently, our numerical calculation of the stall force from the analytical result Eq. (2.4) for the stall force in the case of non-processive Ncd motors is lower than that of processive motors at the total number of motors N, as shown in Figure 2.11. The numerical result for non-processive motors with unlimited number of binding sites increases linearly for large number of motors ($N > 10$) with the same gradient as that for processive motors (see Appendix 2.7.4). This is also the case for binding sites limited to the average found in simulations. This is to be expected from our observations that clusters of N non-processive motors behave like processive motors for large N. In other words, once the number of motors is large enough, the stochasticity is effectively averaged out and no longer significantly affects the strength of the motor cluster. We therefore conclude that the larger the number of motors, N, bound to a cargo the larger the load forces that can be overcome by the motors to transport a cargo for both processive and non-processive motors. Note that the stall force scales with the number of motors for cargoes such as beads [32] or filaments in motility assays [56, 66] but that for fluid like cargo such as vesicles [105] or membrane tubes [13, 86] it does not since these cargo do not experience tangential forces [13].

Figure 2.11 shows that for small number of motors the stall forces for non-processive Ncds extracted from our simulations (black circles) correspond well with those those numerically calculated from the analytical solutions with the number of binding sites unlimited (green crosses) and limited (light blue crosses). However for $N > 3$ the results from our simulations are are lower than those obtained from the analytical expressions. This is due to the sequence preservation included in the simulations but not in the analytical results, as discussed in section 2.4.3 and Appendix 2.7.2.

Run Length

We also examine the run length defined as the distance that the cargo moves until all the motors have detached from the filament. To find the average run length, we record the position, x_1, of the first motor to bind to the filament at

time t_1 and the position, x_2, where the last remaining motor unbinds at time t_2. The difference between these positions gives the run length of the cargo. We take the average over all the periods when the cargo is bound to the filament. Mathematically we calculate this by $\langle x \rangle = \langle x_2(t_2) - x_1(t_1) \rangle$. We found from our simulations that the larger the team of motors pulling the cargo the longer the average run length before the cargo detaches from the filament, as shown in Figure 2.12 (a).

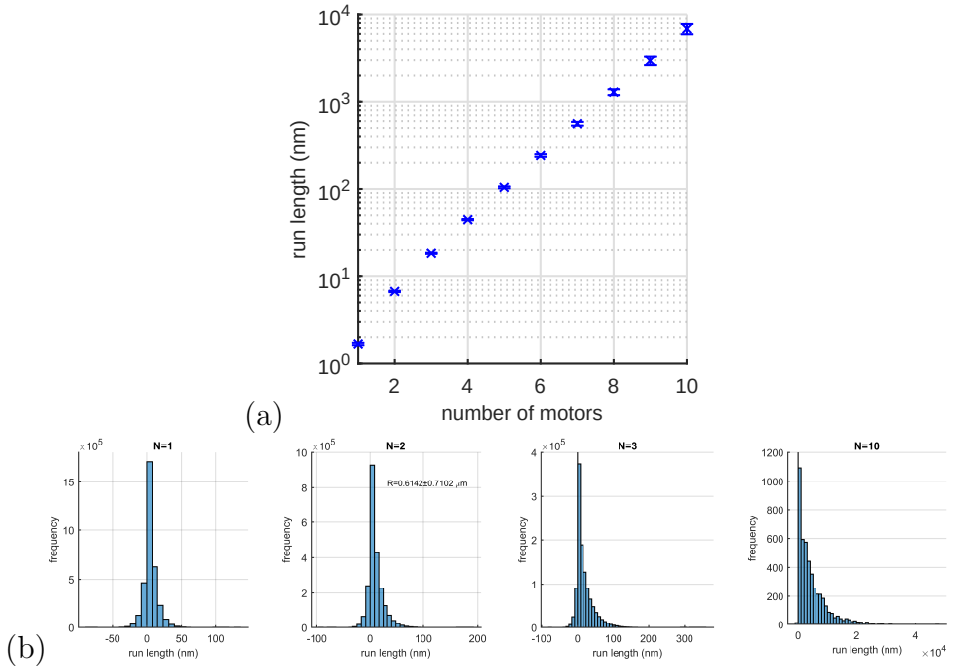

Fig. 2.12: (a) Average run lengths of $N = 1$ to $N = 10$ non-processive motors from 100 Monte Carlo simulation runs with $f = 2$. The other parameter values are $k_{\text{on}} = 20\,\text{s}^{-1}$, $k_{\text{off}} = 10\,\text{s}^{-1}$, $p = 22\,\text{s}^{-1}$, $q = 2.2\,\text{s}^{-1}$ and $\delta = 0.5$. (b) Histograms of the distributions of run lengths in (a) for $N = 1$, 2, 3, and $N = 10$. The total number of data is about 33000, 22000, 11000, and 100 per simulation for $N = 1, 2, 3$, and $N = 10$, respectively.

Moreover, we plot histograms of the distributions of run length for different values of N in Figure 2.12 (b). For a few motors $N = 1, 2$ and 3, we see that the cargo often moves backwards in addition to the preferred forwards direction whereas the cargo with $N = 10$ motors in Figure 2.12(b) almost always moves in the positive direction. For multiple motors the run length appears to be roughly exponential in the number of motors, which corresponds with the conclusion of [51, 48].

Recently [106] have reported that cargo diffusion shortens the run length for single kinesin-1 leading to a non monotonic relationship with increasing cargo viscous drag in simulations. This effect is due to load dependence of off rates such that at low viscous drag cargo diffusion can assist the motor direction whereas at high viscous drag the run length is shortened because of the viscous drag of the load. Assuming the viscosity in cytoplasm is more than 10 times that of water and the cargo size is more than 0.1μm this low viscosity cargo diffusion effect is not important. Another suggestion of non-monotonic run length is given by [102] who use first passage time calculations and Monte Carlo simulations to find the run length for two motors coupled by a spring. This spring coupling is a different scenario from what we study so not directly comparable.

2.5 Comparison with experimental results

In this section we compare our theoretical and computational results with literature experimental data from two different systems.

In vitro experiment First we compare our results with the *in vitro* experiments by Furuta et al [32] who measure collective transport by processive kinesin-1 and non-processive Ncd motors. They constructed DNA-motor assemblies with a set number of motors varying from 1 to 4. They linked the motors with defined spacing by their DNA scaffold. They track the movement of the assemblies along microtubules by observing a fluorescent dye attached to the DNA scaffold using total internal reflection fluorescence microscopy. In their system there is no cargo, apart from the DNA linking the motors together, and we therefore assume the load force, f, is zero. To compare their experimental results with our model we ran simulations using parameters for kinesin-1 and Ncd as observed in the experiment (see below for details). We also compared the results with the analytical solution of Eq. 2.1 and Eq. 2.10 for processive and non-processive motors, respectively.

For the processive motor kinesin-1, the step length is 8 nm and the forward minus backwards stepping rate is found from the measured velocity to be $p - q = 98 \pm 0.6\,\mathrm{s}^{-1}$ for one motor and $p - q = 89 \pm 0.8\,\mathrm{s}^{-1}$ for multiple motors [32]. For no load, $f = 0$, the velocity given by Eq. (2.1) is independent from the motor number N. However, the experimental results of the velocity kinesin-1 in [32] show a slight decrease in velocity with increased number of motors. Furuta et al [32] suggest that the motors in their assemblies slightly interfere with each other. The motors in their assemblies are coupled with DNA fragments so the motors are likely to experience attractive interactions at separations in which the elasticity of the linking DNA becomes important. This unknown interaction effect is not captured by our simple model. We therefore use different stepping rates for $N = 1$

and $N > 1$. Assuming $p = 10q$ [14] we use $p = 110\,\mathrm{s}^{-1}$ for $N = 1$ and $p = 100\,\mathrm{s}^{-1}$ for $N > 1$ in the plot in Figure 2.13.

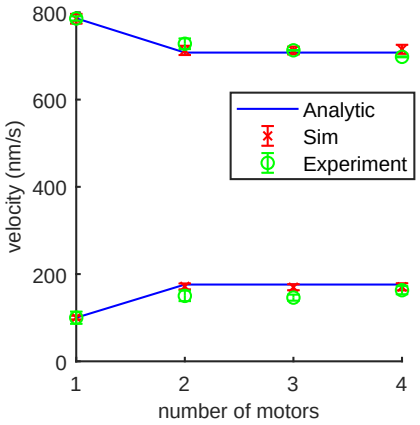

Fig. 2.13: Velocity against number of motors to compare experimental data [32], simulation and analytical solution (Eq. 2.1) for processive motor kinesin-1 (top) and Eq. 2.10 for non-processive motor Ncd (bottom), both with zero load, $f = 0$. For processive motors (top), parameters are $p = 110\,\mathrm{s}^{-1}$ for single kinesin-1 and $p = 100\,\mathrm{s}^{-1}$ for multiple kinesin-1. For non-processive motors (bottom), parameters are $p = 11\,\mathrm{s}^{-1}$ for single Ncd and $p = 22\,\mathrm{s}^{-1}$, $k_{\mathrm{on}} = 20\,\mathrm{s}^{-1}$ and $k_{\mathrm{off}} = 10\,\mathrm{s}^{-1}$ for multiple Ncds. $p = 10q$ for all cases.

For the non-processive motor Ncd, the step length is also 8 nm and the forward stepping rate is $12.6 \pm 2.0\,\mathrm{s}^{-1}$ or $18.75 \pm 1.5\,\mathrm{s}^{-1}$ from the measured value for the velocity of one motor or two coupled. The results for the velocity from simulations and the analytical solution are plotted in Figure 2.13 along with experimental data from [32] for both processive kinesin-1 and non-processive Ncd. Note that [32] suggest that single Ncd has a lower forward stepping rate than when it is linked to other Ncd motors due to the unbound motors being kept close to the microtubule in the latter case. Our simulated and analytical results using the leading motor model in Eq. 2.10 match (within error bars) with their experimental data.

In vivo Experiment A significant practical problem of any motor transport experiment *in vivo* is to identify the numbers and types of motor proteins on the cargo. Therefore comparing theoretical results with *in vivo* experimental data is more challenging because of the difficulty in determining the number of motors on the cargo, particularly in case of non-processive motors. Several studies have indicated that many cellular cargoes *in vivo* are moved by a moderate number of motors ranging between one to five and the force exerted by the kinesin and dynein motors are mostly reported as about 1 pN [95, 6, 23].

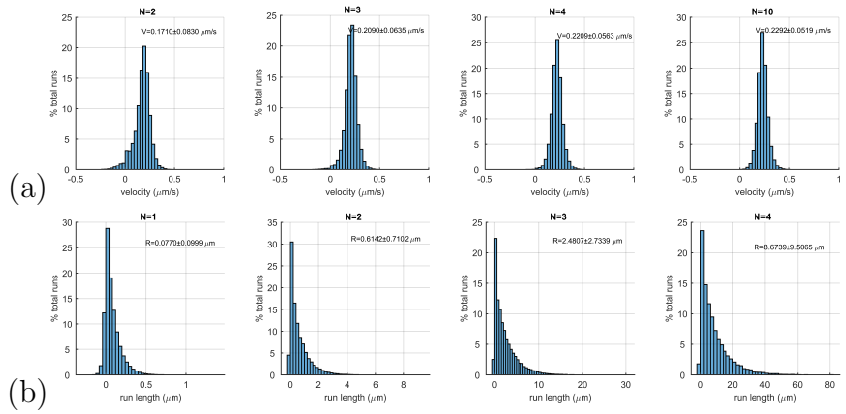

Fig. 2.14: From our simulation, (b) velocity distribution for 1, 2 3, 5 and 10 kinesin-1 and (c) run length distributions for 1, 2 and 3 kinesin-1. The parameters are $p = 100\,\mathrm{s}^{-1}$, $q = 10\,\mathrm{s}^{-1}$, $k_{\mathrm{on}} = 5\,\mathrm{s}^{-1}$ and $k_{\mathrm{off}} = 1\,\mathrm{s}^{-1}$ [48].

To compare our results with an *in vivo* experiment, we used data from Pilling et al [78] who tracked mitochondria in the axons of live Drosophila neurons. They tracked the movement of GFP labelled mitochondria using scanning confocal fluorescence microscopy. They report that the net velocity of anterograde mitochondria (assumed to be moved by kinesin-1) was $0.26 \pm 0.10\mu\mathrm{m\,s}^{-1}$. They found the mean $\pm$ standard deviation run length for anterograde mitochondria was $1.82 \pm 1.19\mu$m. It is difficult to know *in vivo* how many motors are attached to a cargo such as a mitochodrion. However using our model we can predict the expected number of kinesin-1 motors carrying the axonal mitrochondria. We use the same stepping rate parameters for kinesin-1 that we use in earlier parts of this chapter i.e. $p = 100\,\mathrm{s}^{-1}$ and $q = 10\,\mathrm{s}^{-1}$. However, as is seen in trajectories in [78], axonal kinesin-1 is slightly non-processive so we use $k_{\mathrm{on}} = 5\,\mathrm{s}^{-1}$ and $k_{\mathrm{off}} = 1\,\mathrm{s}^{-1}$ as proposed in [48]. We used $f = 2$ in our simulation corresponding to $F = \frac{fk_BT}{\mathrm{d}x} = 1.1\,\mathrm{pN}$. We calculate the distribution of velocity and run length from our model for different number of motors and compare with the histograms from experiment in [78]. Figure 2.14(a), shows that our simulations display almost always positive velocity when $N \geq 3$ (velocity $= 0.21 \pm 0.06\mu\mathrm{m\,s}^{-1}$, run length $= 2.48 \pm 2.73\mu$m). The histograms plotted in Figure 2.14 indicate that our model for $N = 3$ corresponds best with the experimental measurements [78] (velocity $= 0.26 \pm 0.10\mu\mathrm{m\,s}^{-1}$, run length $= 1.82 \pm 1.19\mu$m). Therefore, our simulation predicts that the expected number of motors carrying axonal mitochondria in [78] is three kinesin-1.

2.6 Conclusion

In this work we have shown by analytical modelling and stochastic simulations that the velocity of cargo pulled by a cluster of molecular motors is insensitive to the number of motors N bound to the cargo for $N > 1$ for processive motors and $N > 5$ for non-processive motors. Therefore a cell investing in more than a handful of molecular motors on a cargo will not result in faster cargo transport. However we find that the stall force is linear with the number of motors in the cluster for processive motors and also for large ($N > 10$) clusters of non-processive motors. Therefore, if a cargo is subjected to large forces, investing in more than a handful of molecular motors will enable a cell to overcome larger forces.

As expected, we find that the average velocity of cargoes pulled by small ($N < 5$) clusters of non-processive motors is significantly less than the velocity of the same number of processive motors. However, significantly, we show that for large number of motors, $N > 5$, clusters of non-processive motors approach the same velocity as those of clusters of processive motors (see Figure 2.10). For cargoes pulled by large, $N > 5$, clusters of non-processive motors the average velocity is insensitive to the detachment of motors since there is almost always at least one motor bound and therefore large non-processive motor clusters have the same velocity as for processive motors (see Figure 2.9). Therefore, according to our model and parameters used, a cluster of $N = 5$ non-processive motors is as fast at pulling a cargo as two processive motors. This is a clear indication of the effectiveness of non-processive motors for cellular transport.

A natural extension to our work would be to include force dependence in the unbinding rate k_{off} as has been done by [53, 13, 51] and recently by [97]. We would expect that including this effect would increase the force sensitivity, increase the time taken to reach steady state, decrease the stall force and decrease the mean velocity due to the zipper effect of successive leading motors experiencing the force dependent unbinding.

We have extended the analytical model to the novel case of non-processive motors with limited number of binding sites since for motors bound to a cargo the number binding sites they can access on a filament may be severely limited by the cargo size. Limiting the number of binding sites M decreases the number of non-processive motors bound to the filament. Our analytical expression for the probability distribution of number of bound motors with limited binding sites correctly reproduces that for unlimited binding sites for $M \gg N$. We find that if the number of binding sites are limited, despite the clear shift in the probability distribution to smaller number of bound motors, the velocity is insensitive to this difference in probability distributions for small N (see Figure 2.8). For large N, the velocity of a cluster of non-processive motors with limited binding sites approaches that of a cluster of processive motors. Our simulation results of the

distribution of number bound motors fit better with the analytical distribution for limited number of binding sites than that for unlimited binding sites. However, since for small clusters the effect of limiting number of binding sites makes only a small difference to the average velocity, the distribution with unlimited number of binding sites is sufficient for calculating the average velocity of small clusters of non-processive motors and it has the advantage of one fewer parameters.

Our run length studies show that for small N the cargo can move backwards as well as forwards but for $N \geq 10$ it almost always moves forwards. These findings may be of significant importance in interpreting *in vivo* experiments when assumptions are made about the identity of molecular motor types based on the observed direction of cargo. Enough data should be obtained to make a judgement based on statistically significant values given the stochasticity of the system.

Our simulations show the effect of sequence preservation which shifts the probability of bound motors to lower number of motors and decreases the stall force. This effect is larger for larger forces and larger clusters.

Finally our model fits well with *in vitro* experiments by Furuta et al [32] and predicts $N = 3$ as the most likely number of kinesin-1 motors bound to axonal mitochondria *in vivo* in the experiments by Pilling et al [78].

2.7 Appendix

2.7.1 Gillespie Algorithm for processive motors

The Gillespie algorithm is the method where the time until the next event dt is drawn from an exponential distribution with rate parameter given by the sum of the rates of all events possible from the current state. The main concept is that one, and only one, event happens each time step and that the duration of each time step changes. The leading motor can move forward and backward with rates p_1 and q_1 and the following motors with the rates p and q, respectively. Therefore, there are four possible events, however, due to the simple exclusion process, not all these events will be available in each time step. The time until the next event is calculated each time step as $\tau = \frac{1}{\alpha} \ln \frac{1}{r_1}$ where α is the total probability of all events possible in that time step and r_1 is a random number from a uniform distribution $(0, 1)$. Which event happens in that time step is determined by a second random number, r_2, drawn from the uniform distribution.

We perform the following four main steps simulating this method.

(1) Generate two random numbers uniformly distributes in (0,1), r_1 to compute the time step and r_2 to choose the happening events.

(2) Compute the total probability for all the events

$$\begin{aligned}
\alpha_1 &= a_1 * p_1 \\
\alpha_2 &= a_2 * q_1 \\
\alpha_3 &= a_3 * p \\
\alpha_4 &= a_4 * q \\
\alpha_0 &= \alpha_1 + \alpha_2 + \alpha_3 + \alpha_4
\end{aligned} \tag{2.11}$$

(3) Compute the time when the next event takes place as $t + \tau$ where

$$\tau = \frac{1}{\alpha_0} ln[\frac{1}{r_1}]. \tag{2.12}$$

(4) Compute the even happening at time $t + \tau$ by

$$\begin{aligned}
&state1 : x_1 = x_1 + 1 \quad if \quad r_2 \leq \frac{\alpha_1}{\alpha_0} \\
&state2 : x_1 = x_1 - 1 \quad if \quad \frac{\alpha_1}{\alpha_0} \leq r_2 \leq \frac{\alpha_1 + \alpha_2}{\alpha_0} \\
&state3 : x_\mu = x_\mu + 1 \quad if \quad \frac{\alpha_1 + \alpha_2}{\alpha_0} \leq r_2 \leq \frac{\alpha_1 + \alpha_2 + \alpha_3}{\alpha_0} \\
&state4 : x_\mu = x_\mu - 1 \quad if \quad \frac{\alpha_1 + \alpha_2 + \alpha_3}{\alpha_0} \leq r_2 \leq \frac{\alpha_1 + \alpha_2 + \alpha_3 + \alpha_4}{\alpha_0}
\end{aligned} \tag{2.13}$$

where state 1 and 2 are the stepping probability of the leading motor whereas state 3 and 4 are that of the following motor.

The leading motor's velocity for different number, N, of bound motors from our Gillespie simulations is shown in Figure 2.15 (a) and (b).

Our simulation results using the Gillespie algorithm match those using our fixed time step method within the error bars. The error bars for the Gillespie algorithm are so small as to be barely visible in Figure 2.15 since they lie inside those of our fixed time step method. Given the equivalence of our results using each method we are satisfied to use the faster fixed time step method to present our results in the main text.

2.7.2 Gillespie Algorithm for non-processive motors

We also adapt the Gillespie algorithm from processive motors to non-processive model drawn in Figure 2.4. Including the binding on and off the filament means we now have six possible events to include in the total probability α with the addition

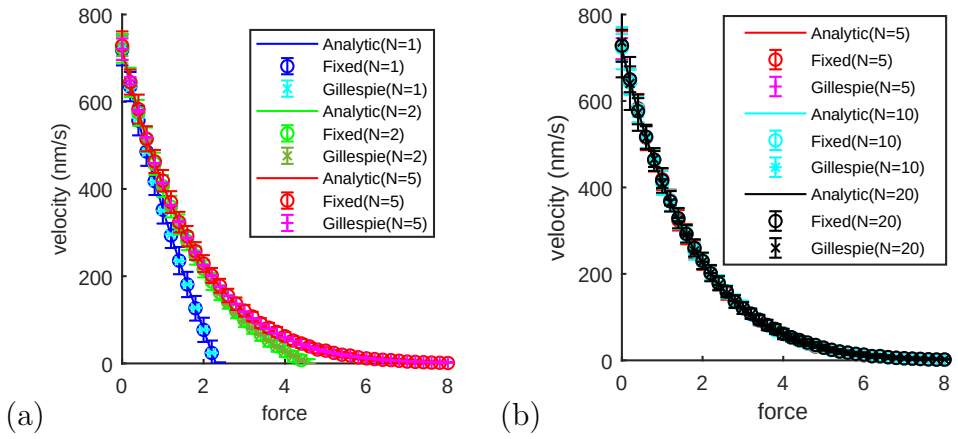

Fig. 2.15: Force-velocity curves of processive motors from simulations using the Gillespie algorithm (star symbols) compared to our fixed time step Monte Carlo algorithm (circles) for (a) a small motor number ($N = 1, 2$ and 5) and (b) for a large motor number ($N = 5, 10$ and 20) compared with the analytical solution (lines) given by Eq. (2.1) with parameters $p = 100s^{-1}$, $q = 10s^{-1}$, $\delta = 0.5$. The force on the x-axis is the dimensionless force $f = F\mathrm{d}x/k_BT$ where F is the physical force.

of nk_{off} and $(N-n)k_{\mathrm{on}}$ for the probabilities of binding off or on respectively. The rest of the algorithm is the same as that described in section 2.7.1.

We compare this algorithm with our results from our fixed time step Monte Carlo simulations described in in section 2.4.3 for scenario B (variable number of binding sites). We performed all the modelling details in the same way as for our fixed time step simulations. In scenario B, the number of accessible binding sites changes with time according to the positions of motors already bound in front or behind, as discussed in section 2.4.3. This preserves the sequence of the motors, preventing them from overtaking each other and reflects the idea that their sequence is determined by their attachments to the cargo. This sequence preservation feature is not captured in our mathematical expressions in section 2.4.1.

We perform the following four main steps simulating this method.

(1) Generate two random numbers uniformly distributes in (0,1), r_1 to compute the time step and r_2 to choose one happening event.

(2) Compute the total probability for all event

$$\begin{aligned}
\alpha_1 &= n * k_{off} \\
\alpha_2 &= (N - n) * k_{on} \\
\alpha_3 &= a_1 * p_1 \\
\alpha_4 &= a_2 * q_1 \\
\alpha_5 &= a_3 * p \\
\alpha_6 &= a_4 * q \\
\alpha_0 &= \alpha_1 + \alpha_2 + \alpha_3 + \alpha_4 + \alpha_5 + \alpha_6
\end{aligned} \tag{2.14}$$

(3) Compute the time when the next event takes place at $t + \tau$ by using r_1 when τ is given by

$$\tau = \frac{1}{\alpha_0} ln[\frac{1}{r_1}]. \tag{2.15}$$

(4) Compute the selected event at time by using r_2 $t + \tau$ by

$$\begin{aligned}
state1 : n = n - 1 \quad if \quad & r_2 \leq \frac{\alpha_1}{\alpha_0} \\
state2 : n = n + 1 \quad if \quad & \frac{\alpha_1}{\alpha_0} \leq r_2 \leq \frac{\alpha_1 + \alpha_2}{\alpha_0} \\
state3 : x_1 = x_1 + 1 \quad if \quad & \frac{\alpha_1 + \alpha_2}{\alpha_0} \leq r_2 \leq \frac{\alpha_1 + \alpha_2 + \alpha_3}{\alpha_0} \\
state4 : x_1 = x_1 - 1 \quad if \quad & \frac{\alpha_1 + \alpha_2 + \alpha_3}{\alpha_0} \leq r_2 \leq \frac{\alpha_1 + \alpha_2 + \alpha_3 + \alpha_4}{\alpha_0} \\
state5 : x = x + 1 \quad if \quad & \frac{\alpha_1 + \alpha_2 + \alpha_3 + \alpha_4}{\alpha_0} \leq r_2 \leq \frac{\alpha_1 + \alpha_2 + \alpha_3 + \alpha_4 + \alpha_5}{\alpha_0} \\
state6 : x = x - 1 \quad if \quad & \frac{\alpha_1 + \alpha_2 + \alpha_3 + \alpha_4 + \alpha_5}{\alpha_0} \leq r_2 \leq \frac{\alpha_1 + \alpha_2 + \alpha_3 + \alpha_4 + \alpha_5 + \alpha_6}{\alpha_0}
\end{aligned} \tag{2.16}$$

(5) Update the number of motors and bound motors' position based the event chosen.

We compare the velocity for scenario B (variable number of binding sites) simulated using our fixed time step Monte Carlo and Gillespie algorithm at different forces in Figure 2.16 The results for the velocity from our fixed time step Monte Carlo in Figure 2.16 are consistent with the Gillespie algorithm within the error bars. As expected the smaller error bars in Figure 2.16 show that the Gillespie algorithm is more accurate. However, in our case the Gillespie algorithm takes ten

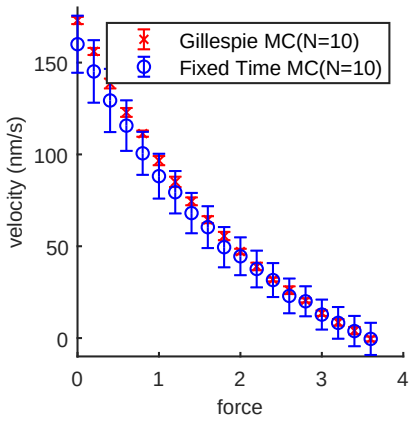

Fig. 2.16: Velocity of a cluster of $N = 10$ non-processive motors from our fixed time step (o) and Gillespie simulations (x) with error bars. The parameters we used are $k_{\text{on}} = 20\ \text{s}^{-1}$, $k_{\text{off}} = 10\ \text{s}^{-1}$, $p = 22\ \text{s}^{-1}$, $q = 2.2\ \text{s}^{-1}$ and $\delta = 0.5$.

times longer to run than our fixed time step Monte Carlo simulations. Therefore in the main text we present results using our fixed time step Monte Carlo simulations since they are more time efficient and sufficiently accurate for our purposes.

Sequence Preservation

In Figure 2.17 we present probability distributions for the case of variable number of binding sites (scenario B) but without sequence preservation for both extremes of force $f = 0$ and $f = f_s$. In the simulations presented in this section the simple exclusion process ensures sequence preservation for bound motors stepping but motors can swap positions by unbinding and rebinding. This is in contrast to the scenario B case in section 2.4.3 in which motors are constrained to rebind in a way that preserves their sequence. The agreement between the simulations results shown in Figure 2.17 and the analytical distributions with limited number of binding sites (Eq. 2.9) provides evidence that the mismatch between the analytical probability distribution and the simulation results in section 2.4.3 is due to including sequence preservation on motor rebinding in those simulations.

2.7.3 The mismatch between the approximate $P(n)$

The mismatch between the approximate $P(n)$ given by Eq. 8 and the simulations does not directly depend on the total number of motors, N, but it does depends on how the cluster is bound on the track. Eq. 8 with average M overestimates the number of motors bound compared to the simulations with binding

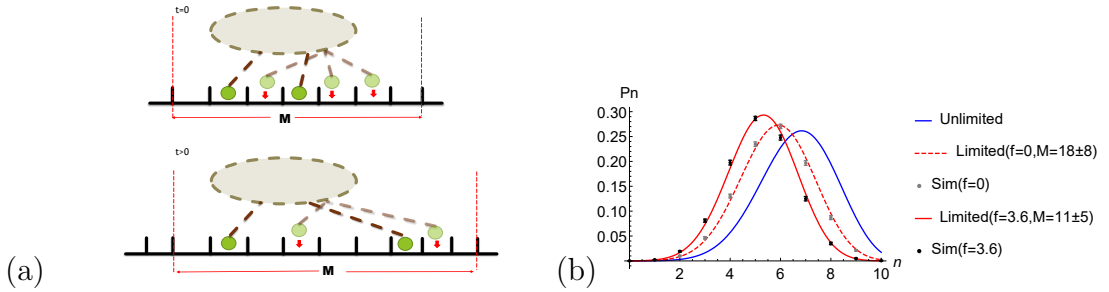

Fig. 2.17: (a) Cartoon showing scenario B variable number of binding sites but without sequence preservation i.e. motors can bind to any available site such that they may swap positions by unbinding and re-binding. (b) Probability distribution of $N = 10$ non-processive motors at $f = 0$ and $f = f_s = 3.6$ attached on the same cargo. Simulation results (grey and black points), analytical Eq. 2.7 (dark blue line) and Eq. 2.9 using the average M number of binding sites found in the simulations (dashed and solid red lines). The parameter values used are $k_{\text{on}} = 20\,\text{s}^{-1}$, $k_{\text{off}} = 10\,\text{s}^{-1}$, $p = 22\,\text{s}^{-1}$, $q = 2.2\,\text{s}^{-1}$ and $\delta = 0.5$.

restricted by sequence preservation. This increases with N since a larger proportion of the binding region M is affected by sequence preservation restrictions. As requested by the referee we provide here in Figure 1 a plot of a measure of the accuracy against N.

The plot shows the general trend of increasing mismatch with increasing N. However two of the $N = 3$ points have a larger magnitude mismatch than this trend would expect. These points correspond to $n = 1$ and $n = 3$. Figure 9(a2) in the main text shows that the analytical curve with binding sites limited to $M = 7$ is actually shifted to smaller numbers of motors bound compared to the simulations. This is due to the end effects of allowing binding one site in front and one site behind the first/last motor on the filament in the simulations giving more freedom than the analytical equivalent of $M = 7$ fixed sites. These end sites are a greater proportion of the total number of sites available for small number of motors (29% for $N = 3$) than for lager number of motors (17% for $N = 5$, 1% for $N = 100$). Hence the mismatch due to the effect is most prominent for the $N = 3$ case.

2.7.4 Stall force for large numbers of motors

In Figure 2.19 we show an extended version of Figure 2.11 of the stall force against number of motors N up to $N = 100$. This additional data shows that the numerical result for non-processive motors with unlimited number of binding sites

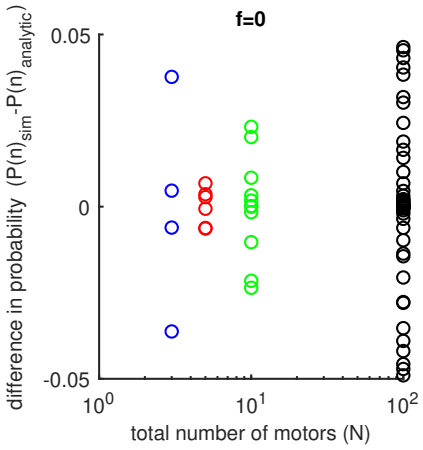

Fig. 2.18: Difference in the probability distribution of bound motors against the total number of non-processive motors N for zero load force, $f = 0$. The difference, $P(n)_{\text{sim}} - P(n)_{\text{analytic}}$, is defined as the difference between the mean value of $P(n)$ from 100 simulation runs and the analytically calculated value $P(n)$ from Eq.8 using the mean value of M taken from the corresponding simulations. In the figure, each circle represents the accuracy of the point on the probability distribution with n bound motors out of the total N motors.

increases linearly for large number of motors ($N > 10$) with the same gradient as that for processive motors. This is also the case for binding sites limited to the average found in simulations.

The black circles in Figure 2.19 show that for small number of motors the stall forces for non-processive Ncds extracted from our simulations correspond well with those those numerically calculated from the analytical solutions with the number of binding sites unlimited (green crosses) and limited (light blue crosses). However for $N > 3$ the results from our simulations are are lower than those obtained from the analytical expressions and remain lower for $N > 10$.

2.7.5 *Single motor approximation*

For $q \ll pe^{-f/2}$, we can approximate Eq. 2.1 by $V_N \approx pe^{-f/2} - qe^{f/2}(q/p)^{N-1}$ which is the single motor case with the backwards stepping rate modified by the factor $(q/p)^{N-1}$. This can reproduce an approximation to the curves seen in Figure 2.2 but has the disadvantage of only being valid for $q \ll pe^{-f/2}$ which is not well satisfied for our parameter values.

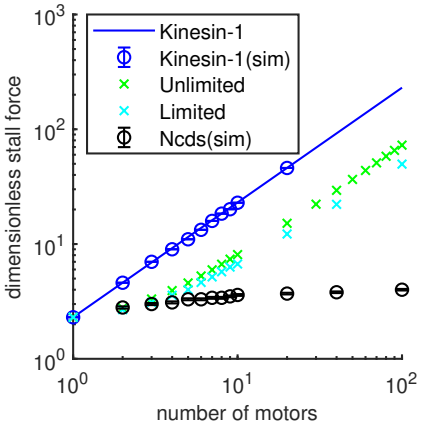

Fig. 2.19: Extended version of manuscript Figure 2.11 of dimensionless stall force against number of motors, N, including data for $10 \leq N \leq 100$ on a log-log plot. For processive kinesin-1 motors we calculate this analytically by setting Eq. (2.1) to zero (solid blue line). For non-processive Ncd motors we set Eq. (2.4) to zero and solve numerically using the distribution of bound motors with limited (Eq. 2.9, light blue crosses) and unlimited (Eq. 2.7 green crosses) binding sites. Simulation results are shown with circle symbols for parameter values $p = 100\,\mathrm{s}^{-1}$ and $q = 10\,\mathrm{s}^{-1}$ for kinesin-1 processive motors (blue circles) and $p = 22\,\mathrm{s}^{-1}$ $q = 2.2\,\mathrm{s}^{-1}$, $k_{\mathrm{on}} = 20\,\mathrm{s}^{-1}$ and $k_{\mathrm{off}} = 10\,\mathrm{s}^{-1}$ for Ncd non-processive motors (black circles).

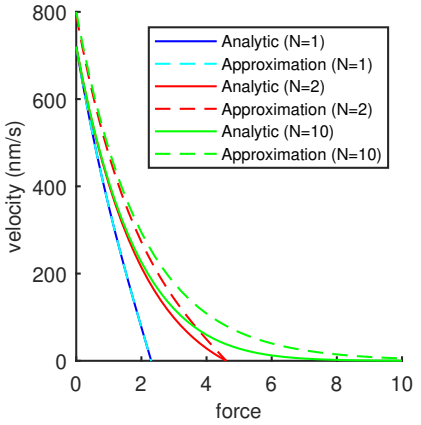

Fig. 2.20: Force-velocity curves of $N = 1$ (blue), 2 (red) and 10 (green) processive motors using the full analytical expression, Eq. 2.1 (solid lines) and an approximate analytical expression $V_N \approx pe^{-f/2} - qe^{f/2}(q/p)^{N-1}$ which corresponds to a single motor with backwards stepping rate modified by the factor $(q/p)^{N-1}$ (dashed lines). The equivalent simulation points are show on the main text Figure 2.2.

3. MANY-LANE MODEL

3.1 Abstract

Cargo transport mostly involves multiple molecular motors which move along cytoskeletal filaments. The motors have ability to detach and reattach on the filament and possibly switch onto another filaments. The cargo transport by multiple motors on a single filament has been widely studied, but cargo transport involving motors switching between filaments is still not well understood. Here, we use lattice based Monte Carlo simulation to investigate the properties of transport on multiple filaments such as velocity, run length and mean first passage time compared to transport on a single filament. The analytical expression of velocity for multiple lanes is an extension of that for a single lane with a limited number of binding sites, which is satisfactory for describing the force-velocity curves of the systems on multiple lanes. Our results show that cargoes being transported on multiple filaments move faster and further than those transported by a single filament. The time taken to deliver cargo to a set target is measured by mean first passage time, and these measurements showed a decrease in time taken for transport on multiple filaments. Moreover, we found that molecular motor's intrinsic properties in binding kinetics also relates to their transport. Molecular motors with high binding on and off rates transport slower and achieve shorter run lengths compared to the same number of motors with low rates. Consequently, motors with high binding rates require more time than motors with slow binding rates to reach the same target.

3.2 Introduction

Cargo transport of many organelles such as mitochondria and synaptic vesicles in cells requires molecular motor proteins which move along cytoskeletal filaments[82, 12]. Molecular motors play a role to deliver the cargo to its destination for example from the cell centre to the cell periphery by kinesin which is directed to the plus end of microtubules (MTs). In the reverse direction, cargo is carried by dynein to the minus end of MTs.

In general, transport in a cell is mediated by more than one motor proteins

which are simultaneously bound to a cargo [100, 48, 24, 8, 24]. This brings into a question that how many motors can attach to the same cargo and how they are organized on the cargo's surface. The typical number of motors present on the cargo from *in vivo* experiments between 1 and 10 [24]. The organization of motors binding on the cargo surface is also important for cargo transport. Most modeling work in this area assumes that the motors are aligned along the filament [48, 8, 13, 12, 51]. Some results have demonstrated that the motors are assumed to organize randomly on the cargo surface [24]. This supports the idea that the molecular motors are more likely to bind on many filaments. Also, that *in vivo* many filaments exist. Many filaments act as many lanes where the "lanes" terminology is an analogy to driving on a motorway with several lanes.

The motors' processivity is also crucial for cargo transport [82]. There are two different classes of molecular motors classified by their processivity which are processive and nonprocessive motors [12, 50]. In some modeling work, kinesin-1 is considered as a fully processive motor which never unbinds from the filaments[12]. Some theoretical work considers kinesin-1 as a slightly nonprocessive motor which can rarely unbind from the filament, although it still remains on the filament for long time [48]. *In vivo* experiments have shown that a single kinesin-1 motor can perform 100 steps on average before detaching from MTs [50]. Therefore, the cargo transported by multiple kinesin-1 can stay attached for longer steps and achieve longer run length. This obviously indicates that the distance traveled along the filament depends on the number of motors. Kinesin-14 (Ncd) is a kind of nonprcessive motor which often unbinds from the filaments but rebinds to them rather fast [33, 79, 74, 48]. It is difficult to measure the collective transport by identifying the number of motors *in vivo* experiment. However, important work has been done constructing the collective transport of kinesin-1 and Ncds by defining a number of motors in vitro and showing that the velocity and run length increases with the number of motors [33] .

Past studies [7] show that the distance of a cargo transport is longer than the length of a single MT which is about 10-40 μm. This supports the idea that the transport occurs on more than one filament. Which means that the molecular motors attached to the cargo can move along several filaments at the same time and can switch lanes in the case of nonprocessive motors[7, 82, 48]. The mechanism underlying this process is obviously unknown because molecular motors switching lanes are of the size and time scales that are very difficult to observe even with modern super resolution microscopy techniques. Most of *in vivo* studies of transport by multiple motors investigate this behaviour using cargo tracking and it is still a challenge to track the dynamics of individual motors and lane-switching in real time [82]. Therefore, simulations are necessary investigating this process.

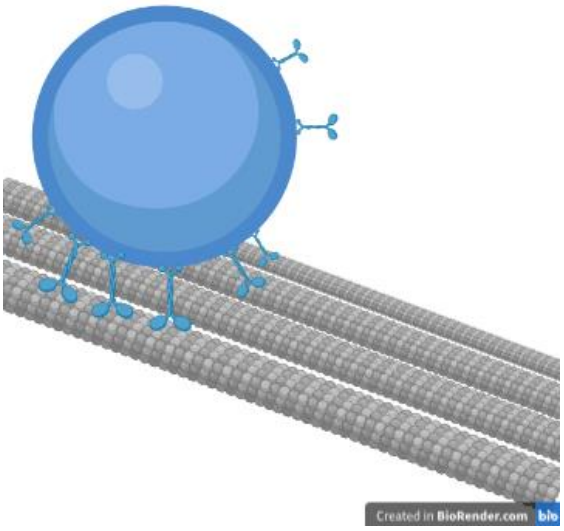

Fig. 3.1: Sketch of multiple molecular motors randomly distributed on organelle surface transporting along several microtubules. The random organization of motors on cargo surface is supported by [24].

This chapter is mainly focus on cargo transport pulled by several motors with the ability to switch between several microtubules. We aim to investigate the efficiency of the transport of molecular motors switching between several filaments. The molecular motors are studied in two different classes of microtubule binding kinetics which are classified by slow and fast of detachment and reattachment rates. Kinesin-1 attachment is intrinsically slow because the motors can roughly bind to microtubules in a small area which relates to the area of one tubulin dimer [46] whereas kinesin-14 (Ncd) has inherently high binding on and off rates. The intrinsically different properties of molecular motors' binding kinetics are then compared to study the effect of transport with switching filaments.

3.3 Mathematical models: extending the one-lane to many-lane model

Cargo transport by multiple molecular motors with the ability of attachment and detachment on a single filament has been explored through the comparison of analytical calculations with simulations in Chapter 2. The analytic expressions for non-processive motors in the case of finite binding sites along a single lane is validated by simulations of the corresponding system in section 2.4.1. Now, we extend the system into multiple lanes, so the motors are allowed to switch between

lanes. The analytic expression in the case of multiple lanes based on the leading motor model is discussed in this section.

3.3.1 Distribution of number of bound motors

We first calculated the distribution of the number of bound motors (n) which can be actively bound, which ranges from 0 to maximum number of motors N on a single lane within a number of binding sites (M) determined by the cargo width. $P_n(N, M)$ is the probability distribution of bound motors (n) out of total number of motors (N) within M binding sites. This probability can be obtained by the following master equation (see more details in section 2.4.1).

$$\begin{aligned}\frac{\partial P_n(N,M)}{\partial t} =&(N-n+1)(M-n+1)k_{on}^s P_{n-1} + (n+1)k_{off}P_{n+1} \\ &- (N-m)(M-n)k_{on}^s P_n - nk_{off}P_n\end{aligned} \tag{3.1}$$

where $k_{on} = (M-n)k_{on}^s$ for an unbound motor

At steady state, $\frac{\partial P_n(N,M)}{\partial t} = 0$, we obtain

$$\begin{aligned}P_n(N,M) =&\frac{1}{n!}(\frac{k_{on}^s}{k_{off}})^n \frac{N!}{(N-n)!}\frac{M!}{(M-n)!}P_0 \\ P_0 =&\left(\sum_{n=0}^{N}\frac{N!M!}{n!(N-n)!(M-n)!}\left(\frac{k_{on}^s}{k_{off}}\right)^n\right)^{-1}\end{aligned} \tag{3.2}$$

3.3.2 Average velocity

The velocity of a cargo pulled by several nonprocessive motors along a single filament is given by

$$\bar{V} = \sum_{n=1}^{N}\frac{P_n V_n}{1-P_0} \tag{3.3}$$

where P_n is the probability of number of bound motors and V_n is the velocity when there are n bound motors [48]. We assume that the velocity of n bound motors, including Simple Exclusion Process (SEP) in which the motors cannot overtake each other, is limited by the velocity of the leading motor [12]. Their velocity is equal to

$$V_n = p\frac{(1-e^f(q/p)^n)(1-q/p)}{e^{f\delta}(1-q/p)+e^f(q/p-(q/p)^n)}. \tag{3.4}$$

Thus, the velocity of N nonprocessive motors moving along a single filament with limited number of binding sites M can be obtained by substituting Eq. 3.4 and Eq. 3.2 into Eq. 3.3.

$$\bar{V} = \sum_{n=1}^{N} \frac{N!}{n!(N-n)!} \frac{M!}{(M-n)!} \frac{P_0}{1-P_0} \left(\frac{k_{\text{on}}^s}{k_{\text{off}}}\right)^n \left(\frac{p(1-e^f(\frac{q}{p})^n)(1-\frac{q}{p})}{e^{f\delta}(1-\frac{q}{p}) + e^f(\frac{q}{p} - (\frac{q}{p})^n)}\right). \tag{3.5}$$

In case of multiple lanes, each leading motor shares force with leading motors on other lanes, so the leading motors' rates are $p_1 = pe^{\frac{-f\delta}{L}}$ and $q_1 = qe^{\frac{f(1-\delta)}{L}}$ where L is number of lanes occupied by motors. The following motors' rates are unchanged, p and q. We assumed that it makes no difference to the probability of binding, and the cargo velocity in this case is determined by the forwardmost leading motor's velocity. Thus, the analytic solution for multiple lanes is

$$\bar{V} = \sum_{n=1}^{N} \frac{N!}{n!(N-n)!} \frac{M!}{(M-n)!} \frac{P_0}{1-P_0} \left(\frac{k_{\text{on}}^s}{k_{\text{off}}}\right)^n \left(\frac{p(1-e^{\frac{f}{L}}(\frac{q}{p})^n)(1-\frac{q}{p})}{e^{\frac{f\delta}{L}}(1-\frac{q}{p}) + e^{\frac{f}{L}}(\frac{q}{p} - (\frac{q}{p})^n)}\right). \tag{3.6}$$

where L is the number of bound lanes which can be taken as an average value $\langle L \rangle$ from simulations.

3.4 Multiple-lanes model

The system is sketched in Figure 3.1 and our model is shown in Figure 3.2. We have developed a model of transport by multiple molecular motors along multiple lanes including motor's ability to switch between lanes. It is performed using discrete lattice based models in Fixed Time Step Monte Carlo simulations. Motors transporting a cargo move on a square lattice keeping the sequence in the same lane with the hopping rates (forward (p) and backward q stepping rates) and can also switch to the other lanes with binding (k_{on}) and unbinding (k_{off}) rates. The lanes are aligned in parallel. Along the lane, the motor performs asymmetric random walks. It hops with different rates to the neighbouring sites. It makes a forward step with rate p and a backward step with rate q as shown in 3.2. It makes no step if it would involve moving to an occupied lattice site, thus the motors cannot overtake each other while stepping on the same lane according to Simple Exclusion Process. In the model, the leading motor and the following motors perform stepping with different rates. The leading motor's stepping rates (p_1 and q_1) depends on force transmitted from the cargo whereas the following motors do not experience to the force and step with constant rates p and q. It is important to

note for this model that the leading motors on each lane share the force equally, so each leading motor experiences to $f_L = \frac{f}{L}$ where f is the total force is transmitted from the cargo and L is the number of bound lanes. Therefore, the rates of leading motors can be written as $p_1 = pe^{-f_L\delta}$ and $q_1 = qe^{f_L(1-\delta)}$. While performing steps along the lane, the motor can unbind from the filaments with rate k_{off} and rebind it again or bind to the other lanes with rate k_{on}. Also, the motor is allowed to bind on an empty lattice site within a limited number of sites (M). At each time, the M binding sites are determined by the sites between the position of the forwardmost leading motor and last motor plus one more site in front and behind. Binding is rejected if the site is occupied. We have performed a simulation of 1×10^8 steps for kinesin-1 and 1×10^7 steps for Ncd in which all motors can possibly unbind off the filament. This is important in calculating run length. The simulation time step is 0.001 s and the simulating procedures are as follows.

1. Initially, we have N motors which are not bound to the lane but attached on a cargo with random positions within a length given by M lattice sites.

2. Then, at subsequent time steps, we visit each of the N motors to consider their possible states and positions by generating a random number. Each motor is allowed to either bind to and unbind from the lane according to the relevant probability, $P_{\text{on}} = k_{\text{on}}\,\mathrm{d}t$ or $P_{\text{off}} = k_{\text{off}}\,\mathrm{d}t$, respectively.

3. If it is determined that the motor will bind, then a second random number is generated to choose which lane it will bind to.

4. In each step, the number of bound lanes can be changed by motors switching lane. This is related to the leading motors' stepping rates in which f_L depends on the number of bound lanes which will be used in the next step.

5. After binding, the bound motors are allowed to move along the chosen lane by calculating their tentative steps forward and backward. The forward and backward stepping probabilities are $p_1\,\mathrm{d}t$ and $q_1\,\mathrm{d}t$ for leading motors which relate to f_L, and $p\,\mathrm{d}t$ and $q\,\mathrm{d}t$ for following motors. The step is not allowed if the site is occupied, so the motor stays the same site.

6. We calculate velocity, run length and mean first passage time for transporting along multi-lanes from simulation results.

In this work, we study the transport on multiple filaments with two types of molecular motors which are slow and fast microtubule binding kinetic motors. They are kinesin-1 and kinesin-14 (Ncds) which have low and high on and off rates. The parameters of the two motors used in this study are described in 3.1. Our main purpose is to investigate the efficiency of transport by several molecular motors on multiple filaments compared to a single filament by calculating the velocity, run length and mean first passage time of the transport. Moreover, we also show how the different kinetics of molecular motors' attachment on microtubules affect cargo transport. We have used kinesin-1 and Ncds as the representatives of slow

Tab. 3.1: Parameters of kinesin-1 and Ncds

Parameters	Kinesin-1 (s^{-1})	Ncd (s^{-1})
forward rates (p)	100 [14, 33]	22 [33]
backward rate (q)	10 [12]	2.2 [12]
binding rate (k_{on})	5 [48, 26]	20
unbinding rate (k_{off})	1 [48]	10 [77, 86]

and fast binding motors on microtubules, respectively.

3.5 Results

Intracellular cargo transport controlled by molecular motors along cytoskeletal filaments is active transport [65]. Molecular motor proteins facilitate the transport along the cytoskeletal filaments which are a complex network in the cells. Individual filaments have a polarity sorting the direction of motor movements, so the molecular motors have directed motion, such as from cell body to cell periphery by kinesin motors. In this chapter, the molecular motors are allowed to switch from one filament to another during transport. Hence, we assumed that multiple filaments can affect the transport of molecular motors by considering the result of velocity and run lengths. First passage time is also interesting for studying the time it takes to deliver a cargo to a target.

We perform kinesin-1 as a slightly nonprocessive motor. It is able to bind on and off with small rates of 5 and 1 s^{-1} , respectively, as revealed in some experiments [42, 98, 16]. This is different from the definition of most modelling work and our first work in Chapter 2 defined kinesin-1 as a fully processive motor. On the other hand, kinesin-14 or Ncd is very nonprocessive with higher attachment and detachment rates of 20 and 10 s^{-1} [77, 86].

Representative example of trajectories of bound kinesin-1 and Ncds (n) out of maximum 10 kinesin-1 and 10 Ncds attached on a cargo on multiple filaments are shown in Figure 3.3 (a) and (b), respectively. The trajectories of bound motors are plotted as the number of spatial steps against the number of time steps on each lane. We set a gap between lanes to show trajectories on each lane clearly as 500 spatial steps and 100 spatial steps for kinesin and Ncd, respectively. One step size represents 8 nm. As can be seen in these results, Ncd is more often unbound from the lane than kinesin-1.

At each time step, unbinding and rebinding events can happen to bound and unbound motors, respectively. In rebinding, the motor can either bind to the same lane or change to other lanes, so the number of bound lanes is changed at each step, as seen in Figure 3.4 (a). The figure shows an example of number of lanes

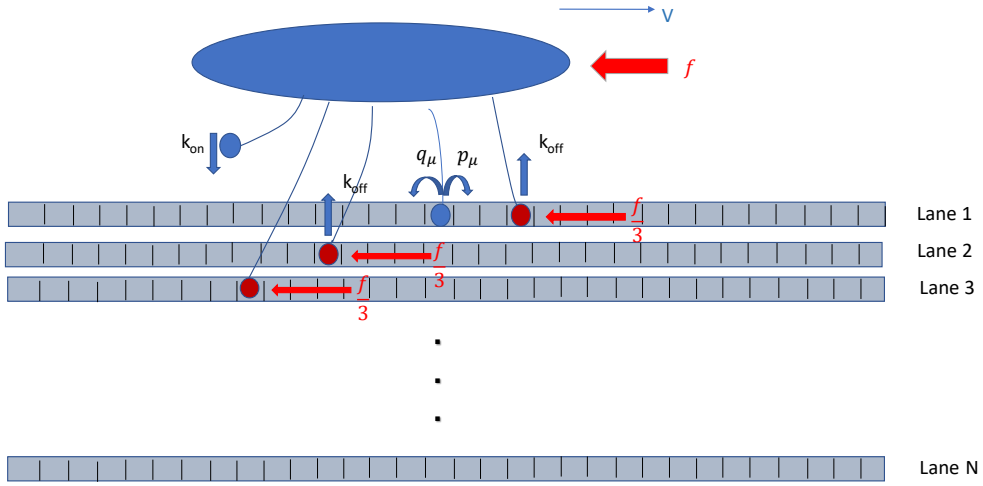

Fig. 3.2: Diagram of many-lane models: an example of five motors attached on the cargo surface switching lanes with (k_{on}) and off (k_{off}) rates and performing steps with a forward p_μ and backward q_μ rates where μ is the index of motors. The bound leading motors share the force equally $\frac{f}{L}$ where $L = 3$ in this diagram.

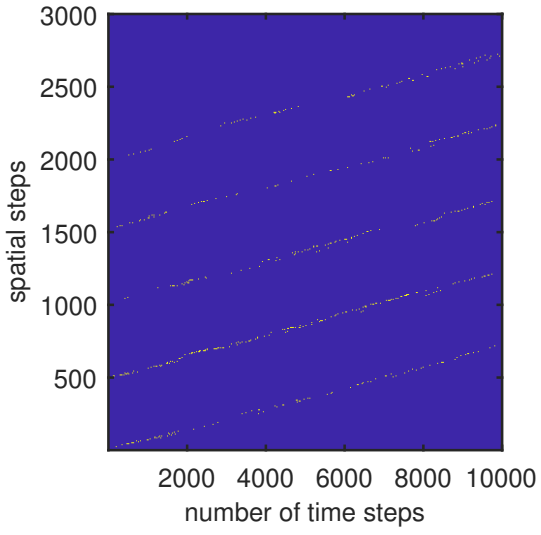

(a)

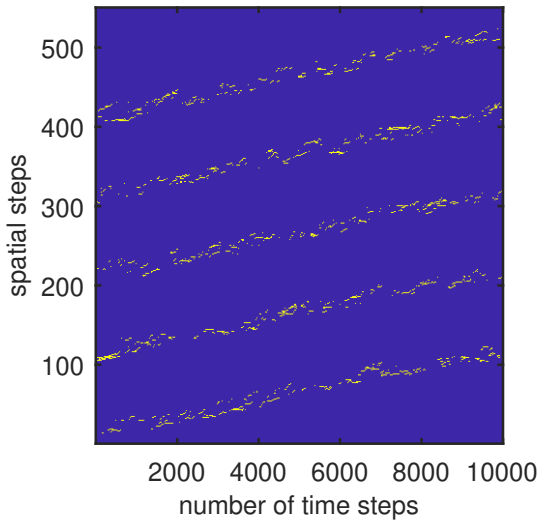

(b)

Fig. 3.3: (a) Trajectories of ten kinesin-1 motors on five lanes in 10^4 steps at $f = 2$ (b) Trajectories of ten Ncds on five lanes in 10^4 steps at $f = 2$. The parameters used are presented in Table 3.1.

bound by 10 kinesin-1 and 10 Ncds transporting along 5 lanes in a time of $500s$ at $F = 2$. From the results, Ncds switch lanes more often than kinesin-1 because of higher binding and unbinding rates. The probability for the number of bound lanes for 10 kinesin-1 and Ncds switching between five lanes for 100 runs are plotted in Figure 3.4 (b). The results show that Ncds and kinesin-1 bind on four lanes most of the time. However, there is less probability of Ncds occupying all lanes because

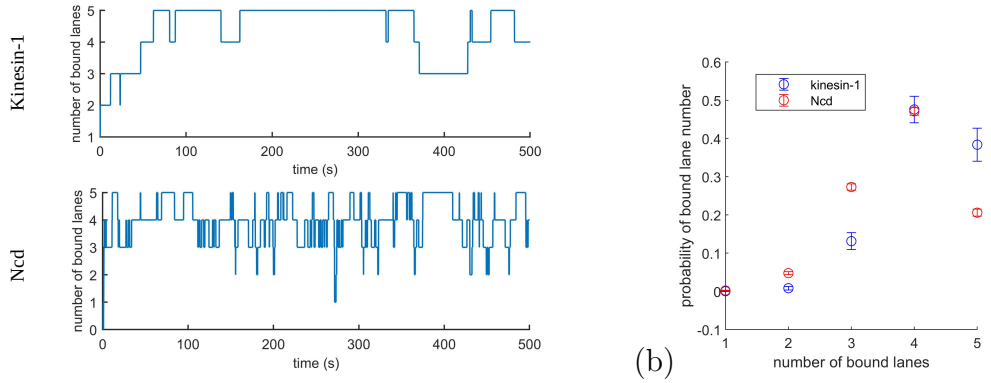

Fig. 3.4: (a) Time course of changing number of bound lanes for kinesin-1 (above) and Ncd (bottom) at $N = 10$ and $L = 5$ which are related to the trajectories in Figure 3.3 (a3) and (a4), respectively. (b) The probability of number of bound filaments of ten kinesin-1 (blue symbols) and ten Ncds (red symbols) distributed on five filaments.

of higher unbinding rates. Ncds mostly bind to a few filaments with higher density compared to kinesin-1.

3.5.1 Velocity of transport by several motors on multiple lanes

In simulation, we measured the velocity of a cargo transported by multiple motors along several lanes which is equal to the velocity of the forwardmost leading motor. The following motors' movement is limited by the leading motor because of simple exclusion process. As a single lane, the velocity of a cluster of N nonprocessive motors working against a force f, is equal to the leading motor velocity which can be analytically expressed by Eq. 3.5 in which the number of binding sites (M) is limited, but the sequence preservation is not included. The velocity of a cargo transported by ten kinesin-1 and ten Ncds along several filaments from simulations are shown in Figure 3.5 (a) and (b) respectively, compared to the velocity on a single filament. The transport of cargo by multiple motors on one lane is thoroughly demonstrated in chapter 2. In the absence of force, kinesins and Ncds move at velocities of 720 nm/s and 160 nm/s as displayed in Figure 3.5. In the simulation, we calculate the velocity of the transport by averaging the velocity of the leading motor for a single lane and the forwardmost leading motor for multiple lanes at different forces. In Figure 3.5, the simulation results correspond to our analytical models on a single lane ($L = 1$) and multiple lanes ($L = 2$ and $L = 3$) following Eq. 3.5 and Eq. 3.6, respectively. In case of multiple lanes, we substitute the averaged number of bound lanes $\langle L \rangle$ at each force from simulations into Eq. 3.6. From the results in Figure 3.5, the velocity of the transport carried by ten kinesins

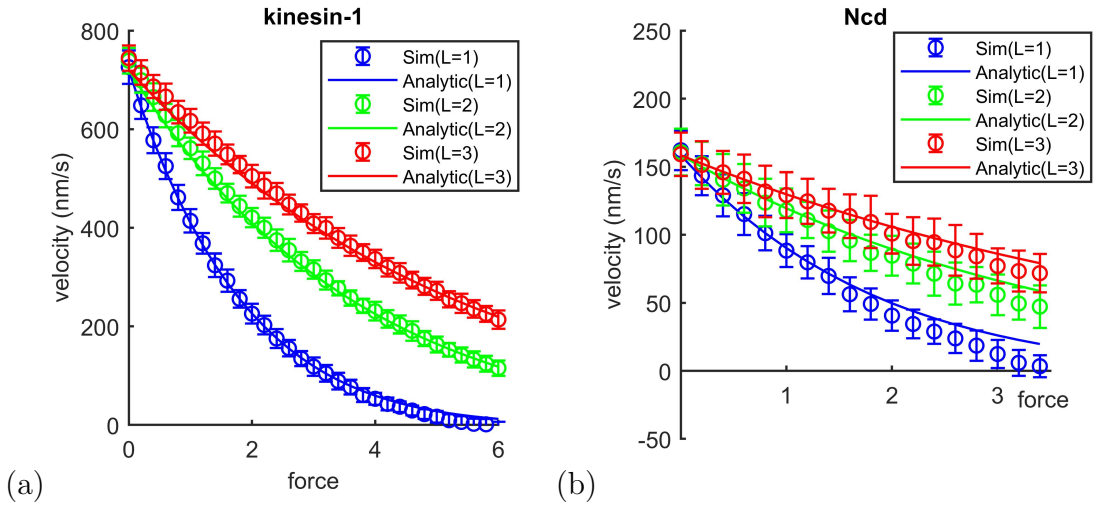

Fig. 3.5: (a) Force-Velocity relation of a cluster of 10 kinesin-1 on one (blue) and two (green) lanes. (b) Force-Velocity relation of a cluster of 10 Ncds on one (blue) and two lanes(green). The solid lines represent the analytic velocity using Eq. 3.5 for single lane and Eq. 3.6 for multiple lanes substituted by the mean value of $\langle L \rangle$ averaged throughout the simulation time of 100 runs at each force. For example, $\langle L \rangle$ is 2.9267±0.0157 for kinesin and 2.7742±0.0106 for Ncd on three lanes ($L = 3$) at stall force (f_s). The parameters of kinesin-1 and Ncds are mentioned in Table 3.1.

and Ncds on single and multiple lanes decreased rapidly with increasing force but the transport on two and three lanes are faster with the same total force compared to a single lane. This is because the transport on multiple lanes can have more than one leading motor which shares the force transmitted from the cargo. Each leading motor experiences a smaller force which is $f_{lane} = F/L$ where F is the total force is transferred from the cargo and L is the number of lanes. This implies that having more lanes facilitates the transport. Therefore, the cargoes transporting on multiple lanes move faster than on single lane with the same total number of motors and the same total force.

The velocity of a cluster of ten kinesin-1 and ten Ncd motors on different number of lanes are calculated by the velocity of forwardmost leading motor and shown in Figure 3.6. At a particular time, the motors can switch to different lanes. The velocity is calculated from the same forwardmost leading motor's movement in a period of time until it changes to the new forwardmost leading motor. From the results, we can see it clearly that the velocity increases with the number of lanes which corresponds with force-velocity relations in Figure 3.5.

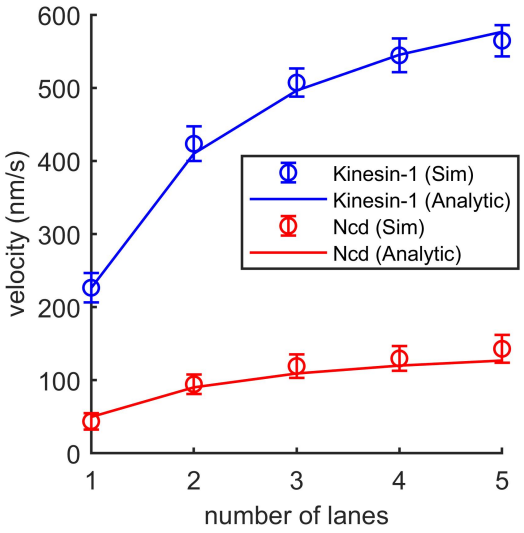

Fig. 3.6: Velocity of the forwardmost leading motors of ten kinesin-1 (blue symbols) and ten Ncds (red symbols) against number of lanes ($L = 1$ to 5). The solid lines represent the analytic velocity using Eq. 3.6 substituted by the mean value of $\langle L \rangle$. For example, at $L = 5$, $\langle L \rangle$ is 4.2338 ± 0.0619 and 3.8302 ± 0.0178 for kinesin-1 and Ncd, respectively.

3.5.2 Runlength of transport by several motors on multiple lanes

During stepping of motors along the lane, the motors have ability to unbind from the lane allowing them to then rebind the same or a different lanes. In order to obtain run lengths of the transport of a cargo by multiple nonprocessive motors on multiple lanes, we consider when there is at least one bound motor carrying the cargo until all motors detach from the lanes. The run length is then defined as the difference between the position of the first bound motor and the position where all motors unbind. In this section, we also chose to study fewer motors from ten to five motors because of compuational restrictions.

The averaged run length of five kinesin-1 and Ncds transporting at different forces on a single and two lanes are plotted in Figure 3.7 (a) and (b) respectively. The run length of transport by five kinesin-1 and five Ncds on a single and two lanes decreases monotonically with force. However, the run lengths of motor teams on two lanes are longer than a team transporting on a single lane. It importantly indicates that intracellular cargoes transported by a team of molecular motors along more than one filament can reach the further target cell. It corresponds with the past studies on a single filament that the run length of kinesin-1 decreases exponentially with the external load force [51, 69], but the run length of Ncd is

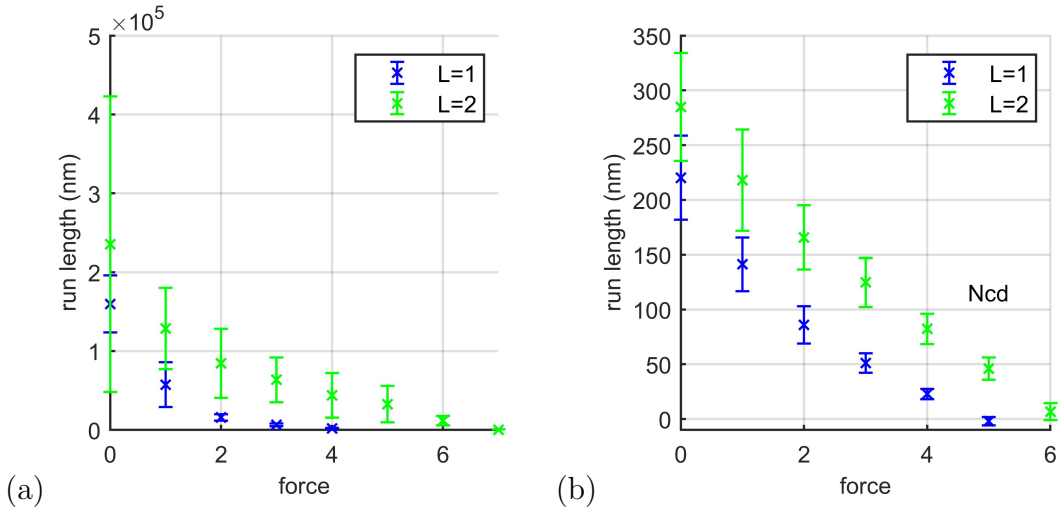

Fig. 3.7: (a) Run length of five kinesin-1 and (b) five Ncds transporting on a single (blue symbols) and two lanes (green symbols) against total force.

likely to decrease linearly with the force. In our simualtion, the run length of kinesin-1 and Ncd decrease with increasing forces in the same trend on one and two lanes.

We then show the effect of number of lanes on run length in Figure 3.8 for transport by five kinesin-1 and five Ncds on multiple by varying number of lanes from one to five. It is obvious that the run length of kinesin-1 is higher than that of Ncds because Ncds have higher rates of detachment and stay on the lane for shorter period of time. The transport is terminated quicker at which a run length is obtained. As the results, the run lengths of five kinesins increase from 10 μm to 100 μm on one and five lanes whereas the run lengths of five Ncds increase from 50 nm to 200 nm on one and five lanes. It is clear that the run length increases with the number of lanes. Although, it seems to saturate at a point with the determined maximum number of motors ($N = 5$) attached to the cargo. Our results correspond to the past studies that revealed that the distance of cargo transport is longer than typical lengths of microtubules ($50\mu m$) [7, 82, 48]. It is importantly noted that our simulation does not restrict the length of microtubules(lanes) but the simulation is limited with total simulation time or total number of steps, thus the run length in our results is an intrinsic properties of having five kinesin-1 and Ncds transporting a cargo with specific transition rates. Furthermore, the run length also depends on the number of motors attached on the cargo which is discussed in the previous chapter focusing on transporting by a team of motors on one lane (see more details in Chapter 2).

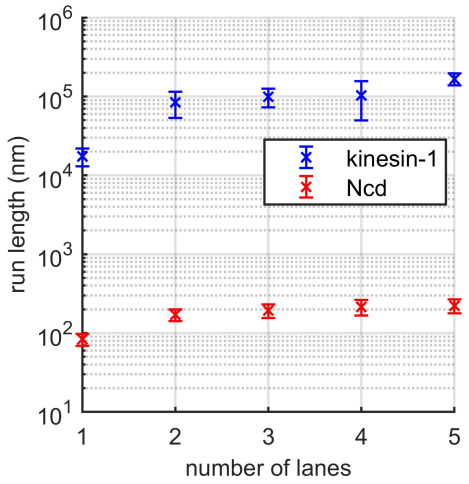

Fig. 3.8: Run Length of five kinesin-1 (blue symbols) and five Ncds (red symbols)on different number of lanes (L=1 to 5).

3.5.3 Mean First Passage Time (MFPT) of transport by several motors on multiple lanes

The first passage time (FPT) or the first hitting time is defined as the time taken by the first leading motor to reach a given distance. In the simulation, there are multiple motors transporting along the lanes with the ability to unbind and rebind the lane which provides a bound and unbound state at any particular time in their trajectories as shown in Figure 3.3. From these trajectories, the FPT is the amount of time that the first motor out of N motors reaches to the given distance. It is then averaged by many simulation runs and called Mean First Passage Time (MFPT). The MFPT is characterized and shown as a function of the number of lanes in Figure 3.9 (a) and (b) for kinesin-1 and Ncd, respectively, and the comparison of the delivery between kinesin-1 and Ncd towards the same destination in Figure 3.9 (c).

It is clearly shown that multiple lanes can enhance the efficiency of transport by decreasing the amount of time taken to reach to the targeting position. This is emphasizing that our results of MFPT are a function of the number of filaments. This is consistent with the results in [65] which characterized the MFPT as function of number and length of filament by simulating a network of cytoskeletal filament with different length of filaments. As we know that the kinesin-1 team stay longer than Ncds on the filaments, then the run length by the kinesin team is greater than that by the Ncd team. The set distance is also essential to be lower than the run lengths at which all motors detach from the lanes, as shown in section 3.5.2. It is reasonable to choose the destination length of kinesin about 10 - 40

μm whereas Ncd destination is given about 80-200 nm. At different distance with increasing the number of lanes, both kinesins and Ncds can reach to the point with less amount of time. Furthermore, we also show that the kinesin team require less time in reaching the same destination than the Ncd team at different number of lanes, as illustrated in Figure 3.9 (c) because kinesin-1 is more processive and faster than Ncd.

3.6 Conclusion

Over the past few decades, our understanding of cargo transport in the cell has been dramatically increased by experimental, simulation and theoretical studies. However, most studies involved with the cooperative behaviors and mechanisms of molecular motors are referred to as along a single filament. The finding still has a gap monitoring the transport performed on many filaments and the behaviors of switching filament. It is also difficult to elucidate the dynamics *in vivo*. Our simulation is a part addressing the gap and focuses on the efficiency of transport by molecular motors along multiple filaments. Our results obviously indicate that the number of filaments (lanes) can enhance the intracellular cargo transport. This is supported by the measurement of velocity, run length and mean first passage time in this work. The velocity and run length against force applied to molecular motors is faster and longer compared to the transport on single filament. Obviously, the velocity and run length of transport are increased with the number of filaments. Multi-lane transport is also characterized by the Mean First Passage Time (MFPT). Transport of multiple motors along several cytoskeletal filaments can substantially decrease time to deliver a cargo to the target point compared with single filament transport. Furthermore, our findings also show that the intrinsic properties of molecular motors can affect the transport. We compared kinesin-1 and Ncd which have significantly differences in microtubule binding and unbinding rates. Transport by several kinesin-1 moves faster and further than by Ncds with shorter time reaching targets. These findings help to further our understanding of cargo transport by molecular motors in complex cytoskeletal systems in crowded environment in cells[7, 54, 82, 36] and neuronal transport which is long-range transport evidencing for switching filaments [35, 85, 99].

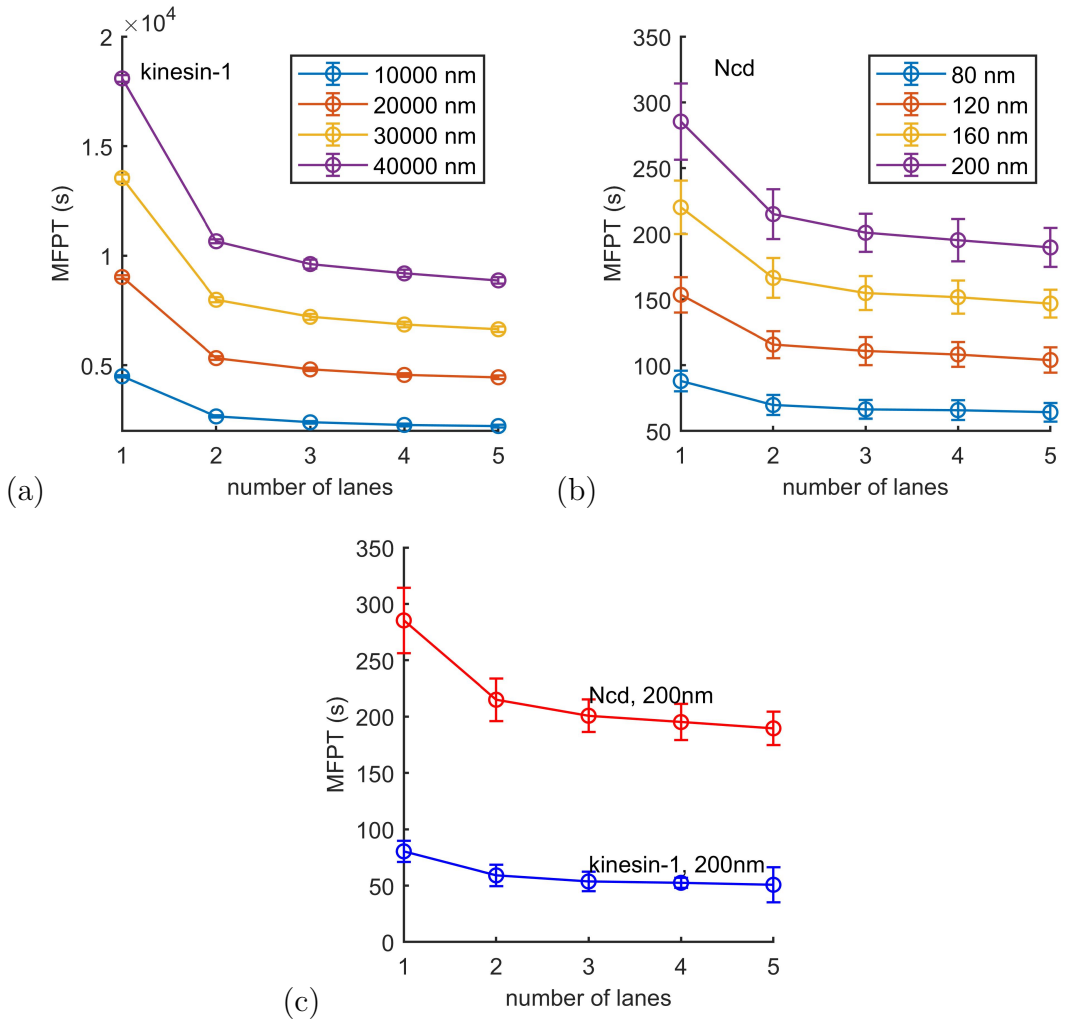

Fig. 3.9: (a) Mean First passage time (MFPT) of five kinesin-1 on different number of lanes reaching to $10, 20, 30$ and 40μm. (b) Mean First passage time (MFPT) of five kinesin-1 on different number of lanes reaching to $80, 120, 160$ and 200 nm. (c) At 200 nm, Mean First passage times (MFPT) of five kinesin-1 are compared to that of five Ncds at different number of lanes .

4. CARGO DEFORMATION

4.1 Abstract

An intracellular cargo can be simultaneously attached by different species of molecular motors which move in different directions resulted in bidirectional movement. The mechanism of bidirectional motion is generally explained by a tug-of-war between the two motor species. The motor tug-of-war can cause cargo deformation which is found during paused state in experiment. However, it has not been broadly studied. In this chapter, we assumed that the cargo can change shape and position. We apply the tug-of-war model to study the cargo properties as a results of force generated by kinesin motors' stepping on anti-parallel microtubules. Our model can be applied to the deformation and translocation of nucleus. Our results show that the nuclear deformation and displacement depend on the number of molecular motors and microtubules. The more number of microtubules is, the more deformation of nucleus is. The nucleus pulled by unbalanced teams displays non-zero displacement. The more differences in strength between the two pulling teams, the more displacement of nucleus is. Our simulation results correspond to experimental results by P. Monteiro and S.A. Godinho.

4.2 Introduction

4.2.1 Tug-of-war

Vesicles, organelles and any other intracellular cargoes are transported by molecular motor proteins such as kinesin and dyneins. Sometimes, different motor types can be simultaneously bound to the same cargo and moved in opposite direction following the polarity of microtubules. This leads to bidirectional transport described as tug-of-war model between the two species of motors in which kinesin is directed to plus-end of microtubules and dynein is directed to minus-end of microtubules, as proposed in many experimental and modelling studies [68, 41, 34]. Intracellular cargoes such as mitochondria and mRNA complexes are either directed to the preferred direction by competing between the two types of motors or paused. The pause state could be potentially caused by equally pulling force between the opposite teams of motors across the cargo. Interestingly, Gennerich

et al found deformed cargo (mitochondria) during paused state in experiments [34, 41]. However, vesicle elongation and cargo deformation have not been widely studied.

4.2.2 Cargo deformation

In previous chapters, we have assumed the cargo is rigid solid that cannot change shape. However, this assumption about the physical properties of a cargo has been changed in this chapter. We apply the tug-of-war model of opposite molecular motors resulting in size shape changes of the cargo influenced by motor pulling force. Over a past few decades, the behaviours of molecular motors in transporting a cargo have been significantly studied in simulation models and theoretical point of view. However, it has never been clearly studied how molecular motors' movement impacts on the cargo itself, especially in changing shape. Importantly, the previous models have not considered the properties of a cargo and the possibility that the cargo could be deformed. In this work, we therefore develop the model applying by tug-of-war of opposing teams of motors to study the effect of motors' stepping behaviour on cargo deformation as well as cargo displacement. However, in our model, it is focused on the same type of molecular motors which are microtubule based kinesins, a plus end-directed microtubule motors, moving on anti-parallel filaments. Our results are significantly interesting because it reveals how the cargo is changed in shape and position by molecular motor pulling force which has not been investigated yet.

4.2.3 Nucleus

One important example of organelle deformation in cell is nucleus because the nucleus needs to change shape to move through constrictions in metastasis and invasion of cancer cells. Metastasis is the spreading process of cancer onto a distant part of the body. The cancerous cells can leave from the main tumor then invade and form new tumors in new parts. The understanding of abnormal nuclear morphology is then crucial in identifying cancer. Therefore, understanding mechanical bases underlying cell and nuclear movement and deformation could potentially lead to improve treatment of cancer [93].

There are a number of ways to experimentally observe cell and nuclear movement and deformation to determine its mechanical properties. Nuclear mechanics were first measured by aspiration into micropipette (Figure 4.1 (a)) [40] which revealed the length of nuclei measured over time. This shows that it is deformable and suggests that the nucleus behaves like a viscoelastic solid [57, 40].

There is an interesting study that determined the magnitude of forces required for moving and deforming the nucleus by applying a direct force probe into nuclei

in cultured, living, adherent cells (Figure 4.1 (b)) [70]. They sealed a micropipette tip to the nuclear surface at one end then translated the pipette tip away from the nucleus. It reveals that a minimum force pulling a nucleus which can significantly displace and deform it is required a few nanonewtons ($2-3nN$) which is far greater than intracellular motor pulling forces [70]. Note that the stall force for a single kinesin-1 is 1.22 pN or $f = 2.3$ in dimensionless unit (see more details in section 2.4.3). This indicates that there are many intracellular forces acting on the nucleus to displace and deform.

Later, a key mechanical parameter which is important for describing nuclear deformation was measured by a technique of micropipettes by Stephens et al., 2018 [93] (Figure 4.1 (c)). They attached a micropipette at one end of an isolated nucleus and the other end is attached with a force reporting pipette. The force against the nuclear extension is then quantified. They calculated the nuclear spring constant from the slope of the force-extension plot, which is $0.52nN/\mu m$.

Understanding the mechanics of how the nucleus is moved and deformed is still complex. The sources and the magnitude of forces required for these changes are still in an open question. There are many competing hypotheses for generating forces acting on nuclear surface[71]. The source of forces which are generated in or transmitted through the cytoskeleton onto the nucleus are various such as actomyosin forces that push on and pull the nucleus and/or extracellular forces applied to adhesion receptors and transmitted through the cytoskeleton and/or microtubule motors (dynein and kinesin) [70, 57]. Generally, nuclear movement will occur when there is a net differential in mechanical forces across the nucleus, while nuclear deformation will occur when the mechanical forces overcome the resistance of the structure of the nucleus [57]. In stationary cells, the nuclear shape and position are maintained in homeostasis in which the forces are generated constantly or balanced on the nucleus [70]. It is interesting how the nucleus is moved and deformed. This is necessary to know the source and the magnitude of forces and how these forces change. Particularly, motor pulling force influencing to deform and/or move the nucleus has not yet been investigated.

4.3 Method

The tug of war model between the opposing teams of motors, which are directed by kinesin and dynein, is presented in Figure 4.2. We developed the model based on this paradigm to study cargo deformation. The specific example of the nucleus is an application we are interested in. Our tug-of-war model is competed between two teams of motors composing of the same type of motor which is kinesins. They attached on one and multiple microtubules which are anti-parallel, as illustrated in Figure 4.3 (a) and (b). This is different from the usual tug-of-war composing of

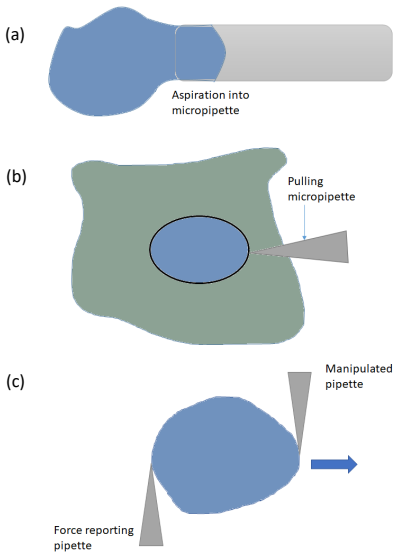

Fig. 4.1: Schematic showing methods to study nuclear mechanics. (a) An isolated nucleus is aspirated into a micropipette. (b) A micropipette is attached to the nuclear surface and then pulled away. (c) The micromanipulation technique in which one pipette pulls the isolated nucleus and the other pipette reports the force.

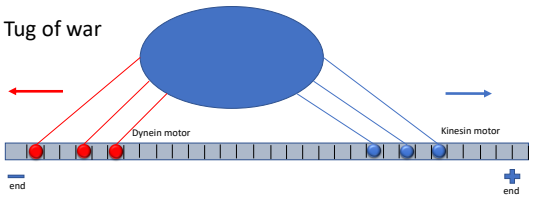

Fig. 4.2: Schematic of tug-of-war between oppositely directed molecular motors arising from a distinct polarity of microtubules which are plus-end-directed kinesin and minus end-directed dynein along the same microtubule.

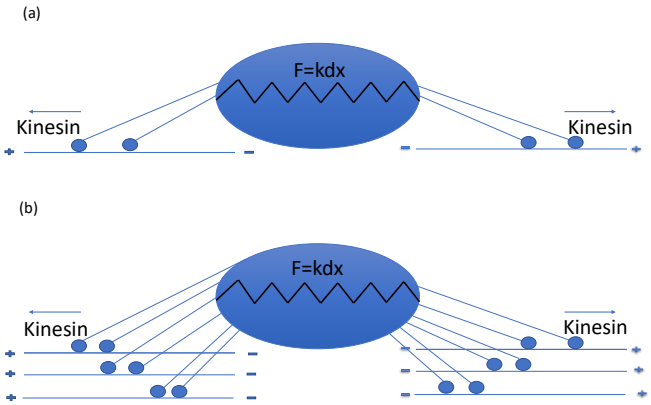

Fig. 4.3: Schematic of tug-of-war between two opposite teams of the same type of molecular motors which is kinesin along (a) one and (b) multiple microtubules in differently oriented direction of polarity. The nucleus acts as a spring with the nuclear spring constant, $k = 0.52nN/\mu m$ [92].

two types of differently directed molecular motors along the same microtubule. In our model, we have chosen the simplest model even though the nucleus mechanics is likely to be more complex. We assume that the nucleus is purely elastic and acts as a spring model. Note that this modeling method is general for any cargo for which the spring model is reasonable.

To determine how MT motor pulling forces can move and deform the nucleus, we assume that the nucleus's shape and position are changed following motors' stepping distance. The nucleus is then able to either extend or displace or both until motors stop moving when they reach stall force.

4.3.1 Model

We know that cytoskeletal motor force is one of the forces relating to nuclear shape and position [70]. Our model aims to estimate how much the nucleus is moved and deformed by force generated by kinesin motors stepping along microtubules based on the tug-of-war paradigm. The motor pulling force is generated when the motors move along the cytoskeletal filaments and this pulling force is transmitted into the the nucleus then result in changing its shape and position. We simplified the model that the cytoskeletal filaments are aligned. The molecular motor in this model is specified by kinesin-1 which moves from the cell centre to the cell edge. The motor force generated during stepping on microtubules are transmitted to nuclear envelope at the right and left edges. This provides the net

differential motor force between right and left ends of nucleus resulting in nuclear displacement and sum of the motor force across the nucleus resulting in nuclear deformation.

We assumed that the motors performing steps on the microtubules generate force to pull the nucleus resulting in its deformation and movement. We simulated the motors as biased random walkers on a one dimensional lattice [12] by using Gillespie algorithm as described below. Simple Exclusion process and the leading motor model are included into the dynamics of motors as describe in section 1.2.1 and section 1.3, respectively. For simplicity we initially assume that kinesin-1 are fully processive without detachment from microtubules at which nonprocessive motors like kinesin-14 (Ncd) does. The modelling dynamic of kinesin-1 is similar to the simulation of processive motors with short range repulsion as described in section 2.3.2 of chapter 2. For parameters of kinesin-1, the forward rate (p) is $100s^{-1}$ and the backward rate (q) is $10s^{-1}$ [14, 32, 12] whereas the leading motor's rates depend on force which is written as $p_1 = pe^{-f\delta}$ and $q_1 = qe^{f(1-\delta)}$. Due to simple exclusion process, the motors are not allowed to overtake each other. Following the results of [12, 25] and our simulation results of force-velocity relation in section 2.3, the analytic velocity of N processive motors moving on one lane is given by

$$V_N = p\frac{(1 - e^f(q/p)^N)(1 - q/p)}{e^{f\delta}(1 - q/p) + e^f(q/p - (q/p)^N)}. \tag{4.1}$$

where f is dimensionless force.

The mechanical properties of a cargo in our previous models have not considered the possibility that the cargo could be deformed. In this chapter, we then focus on the study of cargo behaviours which relate to the stepping mechanism of molecular motors. Our model can be generally applied to any cargo but we are interested in nucleus. The mechanical properties of the nucleus is assumed as a spring. There is experimental support that the rigidity of nucleus acts as a spring [59, 92, 93, 88] (see more details in section 1.6). In Figure 4.3, the kinesin motors stepping on anti-parallel microtubules are simultaneously bound on the right and left ends of a spring nucleus. The nucleus is pulled by different direction of motor pulling forces exerted onto right and left ends of the nuclear envelope. This generated force can deform and displace the nucleus. The extension of nucleus is calculated by the stepping distance of motors on the filaments. Here, it is important to note that it is counted by the movement of the forwardmost leading motor of right and left team. The force generated onto the nucleus is $f_{\text{spring}} = kdx$ where k is nuclear spring constant, $k = 0.52$ nN/μm [93] and dx is the extension of nucleus, $dx_{\text{extended}} = dx_r + dx_l$ where dx_r and dx_l are the moving distance of forwardmost leading motor of right and left team, respectively. The displacement

of nucleus is determined by difference in moving distances of right and left motor team, $dx_{\text{displaced}} = dx_r - dx_l$ in which sign shows the net direction of movement. For example, plus sign shows that the nucleus is moved towards plus ends of microtubules. The nucleus will stop deforming and displacing when motors of both teams stop moving at which the velocity vanished. The velocity of motor team of kinesin-1 on individual microtubule is calculated by Eq. 4.1. It is important noting that an initial nucleus size in our model can be arbitrary. Our model shows the results of how much the nucleus is deformed and displaced by the stepping behavior of molecular motors.

4.3.2 Simulation procedures

We study the extension and displacement of nucleus (cargo) pulled at both ends connected to microtubules on which molecular motors move and result in pulling force. We simulate the model by using gillespie method as described in section 4.3.3. Generally, the simulating procedures are followed by these steps.

1. Initialize motor's position on each lanes within a determined number of lattice sites.

2. Calculate nuclear spring force, $f_{\text{spring}} = kdx_{extended}$ where k is nuclear spring constant, $k = 0.52$ nN/μm [93] and $dx_{extended}$ is the extension of nucleus. At initial time, $dx_{extended} = 0$.

3. Calculate motor pulling force which is force experienced by each leading motor on each microtubule (lane), $f_L = \frac{f_{\text{spring}} \times 1.87}{L}$ where f_{spring} is nuclear spring force, L is the number of lanes at each side (right/left sides) and 1.87 is a fraction converting a spring force into a dimensionless unit of motor force which is calculated by $\frac{dx}{k_B T}$ where dx is a step size of kinesin-1 ($dx = 8nm$) and k_B is the Boltzmann's constant, $1.38 \times 10^{-23} J.K^{-1}$ and T is body's temperature ($T = 310K$).

4. Calculate the velocity of group of N motors transporting on each lane as given by Eq. 4.1 by substituting $f = f_L$. According to gillespie method, only one event happens at a particular time. This means that only one motor steps at a time. The nucleus would only be pulled if that motor happened to be the leading motor.

5. If the normalized velocity of motor cluster on each lane at a time point, $|\frac{V_t}{V_0}|$, is larger than the setting up threshold, then one of motors is allowed to perform a step as described the details in section 4.3.3. V_t and V_0 are velocity at any particular time and an initial time ($t = 0$), respectively. However, if the velocity is lower than the determined threshold, then the simulation stops. This means motors of both sides stopped moving and f_{spring} becomes the stall force of the system.

6. At any particular time, extension and displacement of nucleus are calculated by $dx_{\text{extended}} = dx_r + dx_l$ and $dx_{displaced} = dx_r - dx_l$, respectively. If the nucleus is

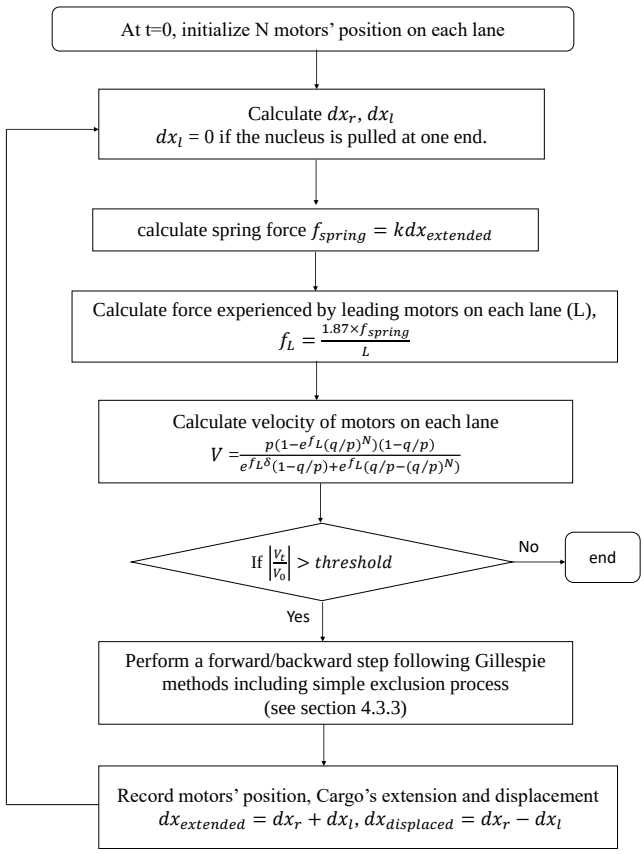

Fig. 4.4: Flow chart of our simulation procedures of cargo extension and displacement pulled by motor force at right and left ends.

pulled by only one end (right end), then $dx_l = 0$.

We summarize our procedures for simulating a nucleus (cargo) extended and displaced by MT motor forces in a schematic of Figure 4.4.

4.3.3 Gillespie Algorithms

We developed Gillespie algorithm to simulate our model of molecular motors' stepping in cells. We use our simulation to study the extension and displacement of nucleus (cargo) as a result of motors' movement. The gillespie algorithm is the method where the time until the next event dt is drawn from an exponential distribution with rate parameter given by the sum of the rates of all possible events from the current state. The main concept is that one event happens at each step and the duration of each time step is changed in every iteration because it is drawn

from a distribution according to a random number generated.

According to the model, the forces are generated by stepping activities of MT motors to pull across the nucleus at right and left ends. The motors of right and left teams hop to the neighboring sites with the rates of p_{1r}, q_{1r} and p_{1l}, q_{1l} for the leading motor and the rates of p_r, q_r and p_l, q_l for following motors. Therefore, there are eight possible events, however, due to the simple exclusion process, not all these events will be available in each time step. Only one event happens at a particular time. The time step (dt) is changed and calculated as $\tau = \frac{1}{\alpha_0} \ln \frac{1}{r_1}$ where α_0 is the total probability of all possible events in that time step and r_1 is a random number from a uniform distribution $(0, 1)$. The event happening in that time step is determined by a second random number, r_2, drawn from the uniform distribution. To simulate the model of the motor stepping then analyze to calculate the effect on the nucleus (cargo), we follow these steps.

(1) Generate two random numbers uniformly distributes in (0,1), r_1 to compute the time step and r_2 to choose which events happen.

(2) Compute α_0 for all the events,

$$\begin{aligned}
\alpha_1 &= a_1 \times p_{1r} \\
\alpha_2 &= a_2 \times q_{1r} \\
\alpha_3 &= a_3 \times p_r \\
\alpha_4 &= a_4 \times q_r \\
\alpha_5 &= a_5 \times p_{1l} \\
\alpha_6 &= a_6 \times q_{1l} \\
\alpha_7 &= a_7 \times p_l \\
\alpha_8 &= a_8 \times q_l \\
\alpha_0 &= \alpha_1 + \alpha_2 + \alpha_3 + \alpha_4 + \alpha_5 + \alpha_6 + \alpha_7 + \alpha_8
\end{aligned} \tag{4.2}$$

where $a_{1,\ldots,8}$ is the number of possible events depending on simple exclusion (SEP) for each condition and the $a_{1,\ldots,8}$ can be only interger values $\{0, 1, 2, ...\}$. For example, a_1 is the number of possible events that the leading motors on every lanes at right side can move forward. It is then multiplied by the rates $p_{1r} = pe^{-f_L \delta}$ where $f_L = \frac{f_{spring} \times 1.87}{L}$, L is the number of sharing lanes at each side and $f_{spring} = kdx_{extended}$ and defined as α_1. Note that the following motors' forward and backward rates are independent of force, $p_{r,l} = p$ and $q_{r,l} = q$ and the number of motors on each microtubule on the same side is the same but that between right and left sides can be different.

(3) Compute the time when the next event takes place as $t + \tau$ where

$$\tau = \frac{1}{\alpha_0} ln[\frac{1}{r_1}]. \tag{4.3}$$

(4) Compute one event happening at time $t+\tau$ by

$$
\begin{aligned}
&state1: x_{1r} = x_{1r} + 1 \quad \text{One of leading motors of right team moves forward.}\\
&\qquad if \quad r_2 \le \frac{\alpha_1}{\alpha_0}\\
&state2: x_{1r} = x_{1r} - 1 \quad \text{One of leading motors of right team moves backward.}\\
&\qquad if \quad \frac{\alpha_1}{\alpha_0} \le r_2 \le \frac{\alpha_1+\alpha_2}{\alpha_0}\\
&state3: x_{\mu r} = x_{\mu r} + 1 \quad \text{One of following motors of right team moves forward.}\\
&\qquad if \quad \frac{\alpha_1+\alpha_2}{\alpha_0} \le r_2 \le \frac{\alpha_1+\alpha_2+\alpha_3}{\alpha_0}\\
&state4: x_{\mu r} = x_{\mu r} - 1 \quad \text{One of following motors of right team moves backward.}\\
&\qquad if \quad \frac{\alpha_1+\alpha_2+\alpha_3}{\alpha_0} \le r_2 \le \frac{\alpha_1+\alpha_2+\alpha_3+\alpha_4}{\alpha_0}\\
&state5: x_{1l} = x_{1l} - 1 \quad \text{One of leading motors of left team moves forward.}\\
&\qquad if \quad \frac{\alpha_1+\alpha_2+\alpha_3+\alpha_4}{\alpha_0} \le r_2 \le \frac{\alpha_1+\alpha_2+\alpha_3+\alpha_4+\alpha_5}{\alpha_0}\\
&state6: x_{1l} = x_{1l} + 1 \quad \text{One of leading motors of left team moves backward.}\\
&\qquad if \quad \frac{\alpha_1+\alpha_2+\alpha_3+\alpha_4+\alpha_5}{\alpha_0} \le r_2 \le \frac{\alpha_1+\alpha_2+\alpha_3+\alpha_4+\alpha_5+\alpha_6}{\alpha_0}\\
&state7: x_{\mu l} = x_{\mu l} - 1 \quad \text{One of following motors of left team moves forward.}\\
&\qquad if \quad \frac{\alpha_1+\alpha_2+\alpha_3+\alpha_4+\alpha_5+\alpha_6}{\alpha_0} \le r_2 \le \frac{\alpha_1+\alpha_2+\alpha_3+\alpha_4+\alpha_5+\alpha_6+\alpha_7}{\alpha_0}\\
&state8: x_{\mu l} = x_{\mu l} + 1 \quad \text{One of following motors of left team moves backward.}\\
&\qquad if \quad \frac{\alpha_1+\alpha_2+\alpha_3+\alpha_4+\alpha_5+\alpha_6+\alpha_7}{\alpha_0} \le r_2 \le \frac{\alpha_1+\alpha_2+\alpha_3+\alpha_4+\alpha_5+\alpha_6+\alpha_7+\alpha_8}{\alpha_0}
\end{aligned}
\tag{4.4}
$$

where μ is the index of motor if $\mu = 1$ is the leading motor. In case of the nucleus pulled at one end, there will be four possible states which are state 1 to 4 of the right team and all state of left team (state 5 to 8) vanishes.

4.4 Results

We have performed Monte Carlo simulation using Gillespie algorithm to study the extension and displacement of nucleus (cargo) caused by pulling force generated by motors stepping along cytoskeletal filaments. The extension is proportional to the force across the nucleus as Hookean spring which is corresponded with the distance of molecular motors moving along microtubules. Each microtubule is all

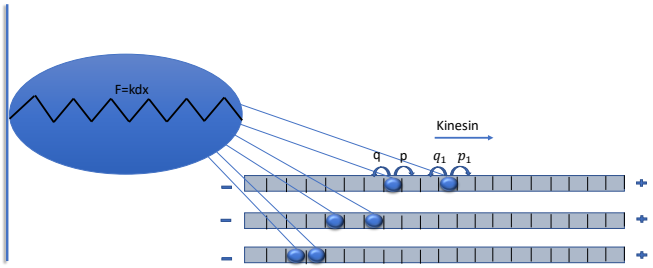

Fig. 4.5: Diagram of nucleus connected with three filaments (lanes, $L = 3$) at one end on which molecular motors move with forward (p) and backward (q) rates. The parameters for kinesin-1 are $p = 100\ s^{-1}$, $q = 10\ s^{-1}$ and $\delta = 0.5$ [14, 32, 12] and the nuclear spring constant is $k = 0.52$ nN/μm [93].

occupied by N kinesins. If it is no motors bound to MTs, then it is no generating force. We simply assume that individual microtuble in this model is all bound by N kinesins which are not included the ability of detachment as fully processive. All microtubules either on right or left sides are parallel alignment. We begin with the model of nucleus (cargo) pulled at one end as illustrated in Figure 4.5, then follow by that pulled at both ends as illustrated in Figure 4.8.

4.4.1 Nucleus is pulled at one end

The first model is a nucleus connected with a team of motors on a single and multiple lanes on the right as shown in Figure 4.5. In this case, the force is pulled in one direction toward the plus end of microtubule and the other end is fixed. N kinesin-1 motors are bound to each microtubule. The force pulling and deforming the nucleus is generated by steps of leading motor for a single MT and the forward most leading motor for multiple MTs.

We study the effect of number of motors (N, kinesins) and lanes (L, microtubules) to the extension of nucleus by varying N and L. The nucleus is extended according to the numbers of steps of the (forward most) leading motor. When the motors step further, the nucleus is more stretched. Meanwhile, the team of motors moves with less speed when the force is larger. Finally, the motors stop moving when the velocity reaches zero. However, the velocity of cluster of processive motors does not clearly reach zero as shown in the relation of force-velocity in Figure2.2 in chapter 2, so we set up the different threshold reaching zero from 10^{-4} to 10^{-10}. The threshold is defined by the fraction of velocity at a time and initial velocity, $|\frac{V_t}{V_0}|$. We found that the simulation results are dependent of threshold. However, we choose the threshold of 10^{-5} in our study because it provides the same accuracy as the experiemtnal results *in vitro* [32] and *in vivo* [78].

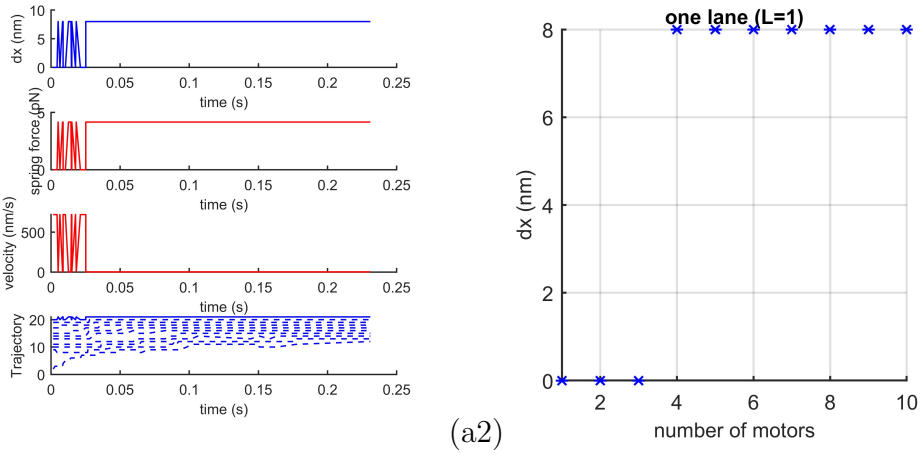

(a1) (a2)

Fig. 4.6: (a1) An example of time course of extension (dx), force ($f = kdx$), velocity and trajectories of motors in number of lattice (Blue solid line for the leading motor and dashed blue line for the following motors) of ten kinesin-1 ($N = 10$) stepping along one lane ($L = 1$) for a single run. (a2) Nuclear extension (dx) pulled by one lane ($L = 1$) with varying number of motors (N).

Henceforth, we study the effect of motor number (N) and lane number (L) using the threshold of 10^{-5}. We begin the first case of a nucleus connected with a single lane ($L = 1$) having a number of motors from $N = 1$ to 10 as shown in Figure 4.6 (a2). An example of the time course of results of ten kinesin-1 ($N = 10$) on $L = 1$ is shown in Figure 4.6 (a1). First, the nuclear extension (dx) is calculated by the difference of the leading motors' current and initial position ($dx = 0$ at $t = 0$). From the trajectories of ten kinesin-1 motors, we can see that the initial position of the leading motor (solid blue) is at 20 on lattice and its final position is at 21. The extension of the nucleus (dx) is finally 8 nm which is one step of kinesin-1 as can be seen in the plot of dx (nm). Second, the nuclear spring force is generated, $f_{spring} = k \times dx$. Third, the velocity of motor is calculate by Eq. 4.1. If the calculated $|\frac{V_t}{V_0}|$ is larger than the threshold of 10^{-5} then the motor is allowed to perform a step. After that the position of motor is updated and recorded. The simulations stop when reached the chosen threshold. At final time, the extension of nucleus is $8nm$ which is the result of one forward step of the leading kinesin. The larger force reduces the velocity of motor team. When the calculated velocity is below the threshold then the motors stop moving. The final extension of nucleus is recorded and averaged for 100 runs and plotted in Figure 4.6 (a2). In Figure 4.6 (a2), it shows that there is no extension ($dx = 0$ nm) for $N = 1$ to 3 and an extension of $8nm$ at $N = 4$ to $N = 10$. This implies that a few motors on a single MT are too weak to deform the nucleus because the force ($f_{spring} = 4.16pN$)

Tab. 4.1: The number of motors (N) and lanes (L) in Figure 4.7 (a) in which the total number of motors (N_T) is 100.

$L = 1$	$N = 100$
$L = 2$	$N = 50$
$L = 4$	$N = 25$
$L = 5$	$N = 20$
$L = 10$	$N = 10$
$L = 20$	$N = 5$
$L = 25$	$N = 4$
$L = 50$	$N = 2$
$L = 100$	$N = 1$

generated by a single step of kinesin (8 nm) is lager than their stall force.

We then study the effect of number of lanes (L) on the extension by having N number of motors on each lane. In Figure 4.7, we fix the total number of motors as $N_T = 100$ and vary the number of lanes (L) as shown in table 4.1. When we increase the number of lanes ($L > 1$), leading motors on each lane help sharing force equally. The leading motors on several lanes experience smaller force compared to only on a single lane. This allows motors to perform more steps. The nucleus can then be more stretched. Therefore, the results clearly show that more numbers of lanes shows more extension. This implies that the nucleus is more stretched with more microtubules. However, the result also show that it becomes plateau for the final four points in Figure 4.7 in which there are $N \leq 5$ on each lane. This implies that the number of motors on each microtubule is also involved. If we increase the number of lanes (L), but the number of motor on each lane is small ($N \leq 5$), then it becomes a weak team which cannot perform more extension. This implies that it would be powerful in pulling the nucleus when a cluster of motors have at least five motors on each microtubule.

In fact, the nucleus in living cells is not static. It is movable, so the other end of nucleus is not fixed and can also be pulled by an opposite team. Then this allows displacement of nucleus and show the results in the next section.

4.4.2 Nucleus is pulled at both ends

Now, we are considering the model of nucleus pulled by motor force in opposite direction between right and left ends resulting in its extension and displacement. At right and left ends, each side of nucleus can be connected with either a single or several microtubules on which N kinesins are bound. Individual microtubules of both sides are simulated in parallel orientation. In this case, we study the nucleus pulled by balanced and unbalanced teams at both ends in section 4.4.3 and section

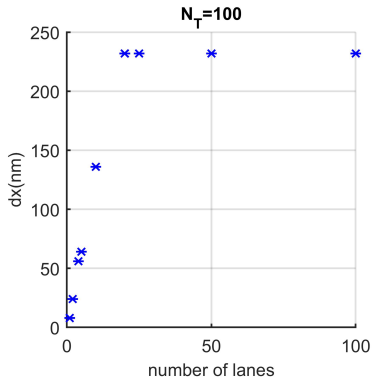

Fig. 4.7: Nuclear extension (dx) pulled at one end with increasing number of microtubules (lanes) and the total of 100 motors ($N_T = 100$). All possible cases having $N_T = 100$ are shown in Table 4.1.

4.4.4, respectively. The balanced teams are defined by the same number of motors ($N_r = N_l$) and lanes ($L_r = L_l$) at both ends whereas there are differences in either motor ($N_r \neq N_l$) or lane numbers ($L_r \neq L_l$) for the case of unbalanced teams.

4.4.3 Balanced pulling teams

According to Figure 4.8, we simulate the model of the nucleus pulled by balanced teams between both ends ($N_r = N_l, L_r = L_l$). An example of extension and displacement resulted by pulling force of four motors bound on a single right and left lane ($L_r = L_l = 1$,$N_r = N_l = 4$) in one simulation run is shown in Figure 4.9 (a1). It displayed time course of nuclear spring force, velocity of right and left motor teams and trajectories of individual motors of both sides until they stop moving when reach the threshold. From the trajectories of four motors on each team, it shows that the initial and final position of the leading motor of right team (blue solid line) are the same at 20 on lattice whereas those of the leading motor of left team (red solid line) are at -20 and -21 at initial and final time, respectively. This provides $dx_r = 0$ and $dx_l = 8$ nm which is one step from the leading motor of left team. The extension ($dx_r + dx_l$) is then 8 nm and the displacement ($dx_r - dx_l$) is -8 nm in which the minus sign is the movement direction towards the minus end of microtubule but that on average it is zero as shown in the case of ($L_r = L_l = 1$,$N_r = N_l = 4$) in Figure 4.9 (a2). The extension and displacement of nucleus pulled by the balanced teams of motors on one ($L_r = L_l = 1$), two ($L_r = L_l = 2$), three ($L_r = L_l = 3$) and ten ($L_r = L_l = 10$) lanes at final time are averaged for 100 runs and plotted in Figure 4.9 (a2). It shows that the results of nuclear extension approach a plateau when $N \geq 5$ for one and multiple lanes at the chosen threshold. The nucleus pulled by the balanced team show no translocation

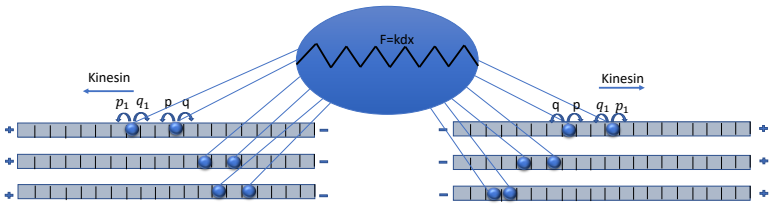

Fig. 4.8: Diagram of nucleus connected with three filaments ($L_r = L_l = 3$) at both ends with two kinesin-1 motors move on each filament ($N_r = N_l = 2$). The total number of motor on each side ($N_T = 6$) is the same. Note that teams of kinesin-1 stepping along filaments connected at both ends of nucleus generate force in opposite direction across the nucleus resulting in displacement and extension of nucleus. The parameters for kinesin-1 are $p = 100\ s^{-1}$, $q = 10\ s^{-1}$ and $\delta = 0.5$ [14, 32, 12] and the nuclear spring constant is $k = 0.52$ nN/μm [93].

(zero displacement on average). This is reasonable that they are pulled by force which is generated by the balanced teams of motors and lanes ($N_r = N_l, L_r = L_l$).

4.4.4 Unbalanced pulling teams

In this section, we focus on the nuclear extension and the nuclear displacement pulled by unbalanced teams between right and left sides of the nucleus. We first study the effect of difference in motor number ($N_r \neq N_l$) on a fixed single lane on each side ($L_r = L_l = 1$). We then consider the effect of difference in lane number. In this case, the number of lanes between both sides is different but the total number of motors on each side is fixed ($N_r = N_l$, $L_r \neq L_l$).

The effect of different number of motors

Modelling examples of nucleus pulled by the different number of motors between one lane on the right and one lane on the left are illustrated in Figure 4.10 (a). We made the stronger team on the right and the smaller team on the left, so $N_r > N_l$. In the simulation, we fix N_l, then increase N_r with the differences in motor numbers ($\Delta N = N_r - N_l$) from 1 to 10. For example, $N_l = 1$ then N_r can be 2 and up to 11. The nuclear extension and displacement pulled by smaller left team and larger right team are shown in Figure 4.10 (b1) and (b2), respectively in which N_l is varied from 1 to 10. The results show that the nucleus pulled by teams unbalancing in the number of motors show small deformation and a non-zero averaged displacement. However, it is interesting if the number of motors on the left team is at least five ($N_l \geq 5$) and the number of motors on the right team

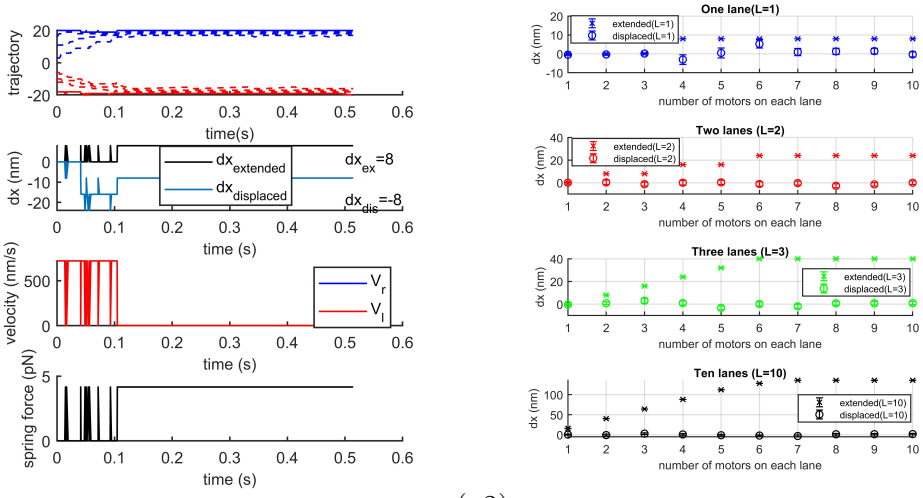

(a1) (a2)

Fig. 4.9: (a1) An example of trajectories in number of lattice of four motors ($N_r = N_l = 4$) stepping along one lane on the left and one lane on the right ($L_r = L_l = 1$). Blue and red solid lines represent the position in number of steps of the leading motor on the right and left lane, respectively. Blue and red dashed lines represent the position in number of steps of the following motors on the right and left lanes, respectively. The nucleus is extended and displaced which are calculated by $dx_{extended} = dx_r + dx_l$ and $dx_{displaced} = dx_r - dx_l$. Note that dx_r and dx_l are counted by the forward most leading motor's distance stepping from initial position. (a2) Nuclear extension ($dx_{extended}$) and displacement ($dx_{displaced}$) pulled by balanced right and left teams of motors stepping along one, two and three filaments ($L = 1, 2, 3$ and 10) against the number of motors from 1 to 10 on each lane. In this plot, the error bar is calculated by $SE = \frac{\sigma}{\sqrt{n}}$ where σ is sample standard deviation and n is number of runs.

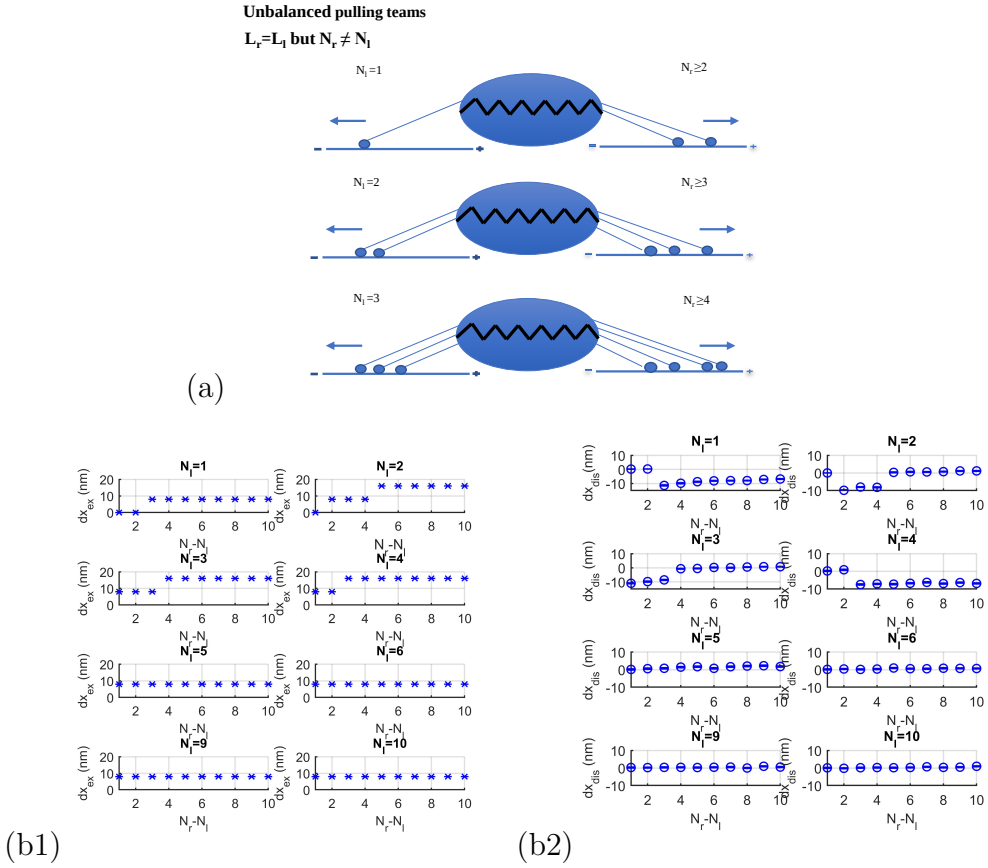

Fig. 4.10: (a) Diagram shows the nucleus pulled between smaller left team and larger right team on one lane ($L_r = L_l = 1, N_r > N_l$). (b1) The extension and (b2) displacement of the nucleus pulled by the unbalanced teams with varying $\Delta N = N_r - N_l$ from 1 to 10.

is larger than that then they act like a balanced team as results of zero averaged displacement. This corresponds to the results of Figure 2.3 in which the velocity of processive motors when ($N_l \geq 5$) is indistinguishable.

The effect of different number of lanes

We simulate the model of nucleus pulled by the different number of lanes on the right and the left sides in which the total number of motors on each side (N_T) is 12 as illustrated in Figure 4.11 (a1). We compare for two cases. The first case is $L_l = 2, N_l = 6$ and $L_r = 3, N_r = 4$ and the second case is $L_l = 3, N_l = 4$ and $L_r = 4, N_r = 3$. Both cases show the same extension but different displacement which are averaged for 100 runs. The first case show more displacement than the

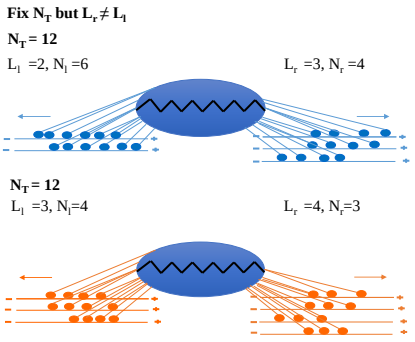

(a1)

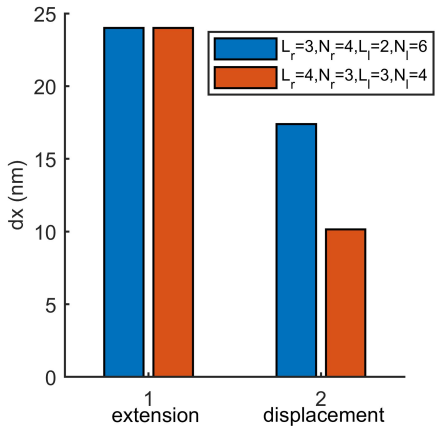

(a2)

Fig. 4.11: (a1) Diagram shows the nucleus pulled by the unbalanced teams between right and left sides in which the total number of motors on each side is equal ($N_T = 12$). The first case is $N_r = 4, L_r = 3, N_l = 6, L_l = 2$ and the second case is $N_r = 3, L_r = 4, N_l = 4, L_l = 3$. (a2) The bar graph shows the extension and displacement of the nucleus pulled by 12 total number of motors on each side.

second case because the strength between right and left teams in the first case is more different than the second case which is related to the shared force between two sides. The ratio of shared force between right and left teams of the first case is more different than that of the second case.

From our results showing the effect of number of motors, the unbalance teams can act like the balanced teams when $N \geq 5$ on each side. By this reason, we vary the number of left and right lanes with ten motors ($N = 10$) on each lane. We simply simulate by having one-lane ($\triangle L = 1$) and two-lane ($\triangle L = 2$) differences between right and left ends, $\triangle L = L_r - L_l$. The extension and displacement of the nucleus are plotted against the number of left lanes varying from $L_l = 1$ to 10 with $\triangle L = L_r - L_l = 1$ and $\triangle L = L_r - L_l = 2$ in Figure 4.12 (a1) and (a2), respectively. The results show that the extension of the nucleus increases linearly with the increasing number of lanes in both cases.

Interestingly, the nucleus is more displaced for the case of $\triangle L = 2$ than the case of $\triangle L = 1$ because there are more different strength between two sides. This also corresponds with the results in Figure 4.11. Consequently, if the number of microtubules at each side of the nucleus increases, then it is resulting in more extension. If the nucleus is pulled by balanced teams then it provides zero displacement. However, when the teams pulling across the nucleus are unbalanced, this drives the nuclear translocation and provides non-zero displacement. We can conclude that the more number of microtubules are, the more nucleus is extended and the more differences of pulling teams between right and left sides of the nucleus

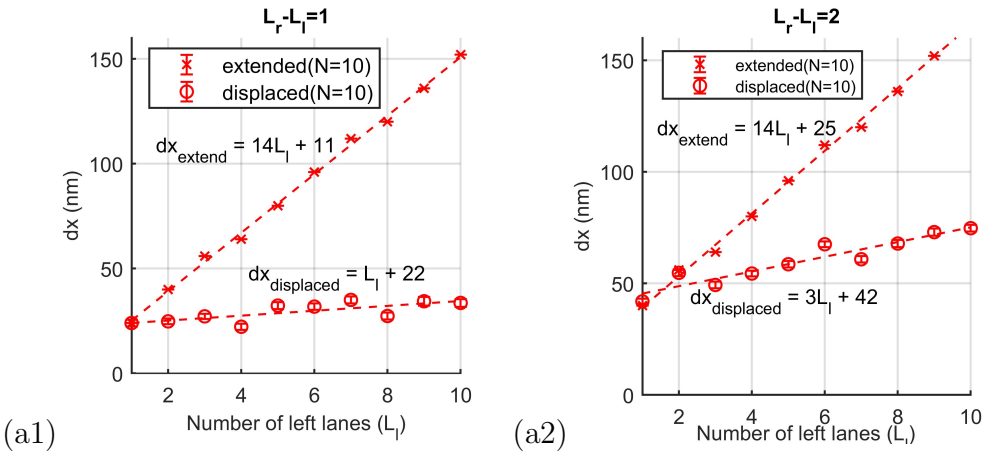

Fig. 4.12: Nuclear extension and displacement pulled by different number of lanes between right and left ends with ten motors on each lane ($N_r = N_l = 10$) is plotted against the number of left lanes (L_l). The number of left lanes (L_l) increases from 1 to 10, so the total number of motors on each side (N_T) increases as L_l. (a1) There is one more lanes on the right, $\triangle L = L_r - L_l = 1$, so the number of lanes on the right (L_r) is from 2 to 11 in this case. (a2) There are two more lanes on the right, $\triangle L = L_r - L_l = 2$, so the number of right lanes is from 3 to 12 in this case.

are, the more displacement is.

4.4.5 Experimental support

We received experimental results by Susana Godinho's group from Barts Cancer Institute, Queen Mary University of London, UK. Some of the experimental results was published in [3].

In this experiment, they found interesting results that will be useful in regulating nuclear translocation and deformation during cell invasion. In many types of cancer cells, a common feature seen during the development of cancer is centrosome amplification. The centrosomes influence nuclear and cell structure through the nucleation and the organization of microtubules. The mechanism underlying cell invasion involving centrosome amplification is interesting. They hypothesised that the increase of cell invasion and the nucleus translocation of cancer are affected by microtubules (MTs) because microtubules are increased by centrosome amplification.

The results are clearly shown that cells carrying extra centrosomes exhibit higher nuclear deformation and translocation. It can be seen in Figure 4.13 (a1) that cells containing extra centrosomes which are induced by doxycycline treat-

ment (+Dox) showed more protrusive cells with nucleus and reduced the nuclear circularity ($\frac{\text{Width}}{\text{Length}}$) on 2D environments compared to (-Dox) cells. Also, cells with extra centrosomes (+Dox) have an increased nuclear deformation which extended in the length of $1.205\mu m$ measured by ImageJ and observed by a reduced nuclear circularity on 3D environments in Figure 4.13 (a2). However, at this points, there are two factors involving in nuclear extension which are the increasing number of centrosomes and microtubules.

Monterio et al. performed an experiment to work out whether extra centrosomes or just extra microtubules affect nuclear deformation. This is to examine the contribution of microtubules on nuclear deformation by reducing them but remaining extra centrosomes. The MTs and centrosomes were increased by +Dox treatment then the MTs were reduced by knockdown of CEP192 which kept the centrosomes, as illustrated in Figure 4.14. The results show that cells with centrosome amplification and reduced MTs nucleation do not affect nuclear circularity which showed the same shape as control condition. This suggests that MTs play an important role in nuclear deformation and also imply that centrosome amplification is not a crucial factor to deform the nucleus. Therefore, this can be concluded that increased microtubules induced more deformation of the nucleus. This corresponds with our simulation results that the nucleus is more deformed by increasing number of microtubules and their associated motors generating more force applied onto the nucleus. Moreover, our model shows that it also enhances the nuclear translocation by increased number of MTs in unbalanced pulling teams.

4.5 Conclusion

This chapter aims to study the effect of force generated by stepping behaviour of molecular motors along cytoskeletal filaments on cargo extension and displacement. The study can be applied to understand nucleus deformed and displaced by the motor transport force which has not been widely studied. The tug-of-war model which describes the mechanical competition model between two opposing teams of motors has been used in this study. In general, the two opposing teams consist of two different species of molecular motors moving in different directions simultaneously bound to a cargo. However, our model focuses on the same type of motor proteins stepping on antiparallel microtubules and generate pulling force onto the cargo or nuclear surface. Gillespie algorithm based on Monte Carlo simulation obeying simple exclusion process has been used to simulate this model. Our study assesses the role of molecular motors and microtubules in this mechanism. We found that if the cargo (nucleus) is pulled by balanced teams consisting of the same number of motors and microtubules between both ends, then it is deformed but not displaced. On the other hand, if it is pulled by unbalancing teams then it is

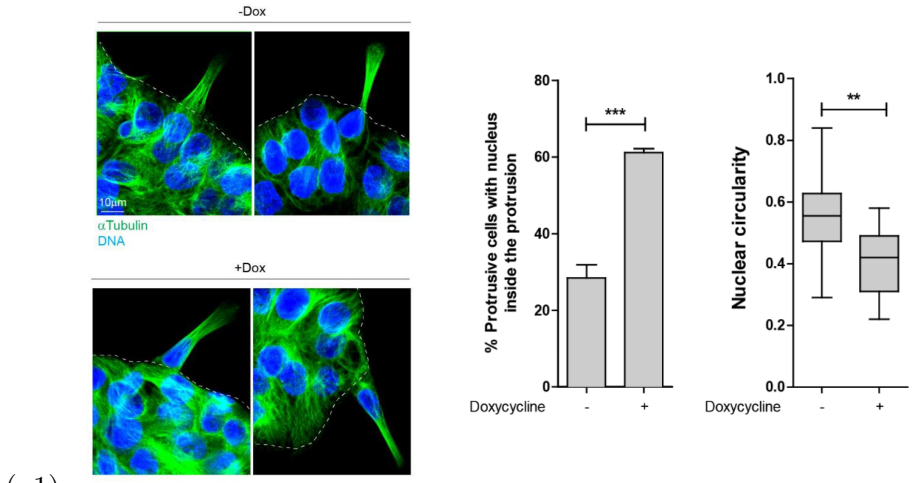

(a1)

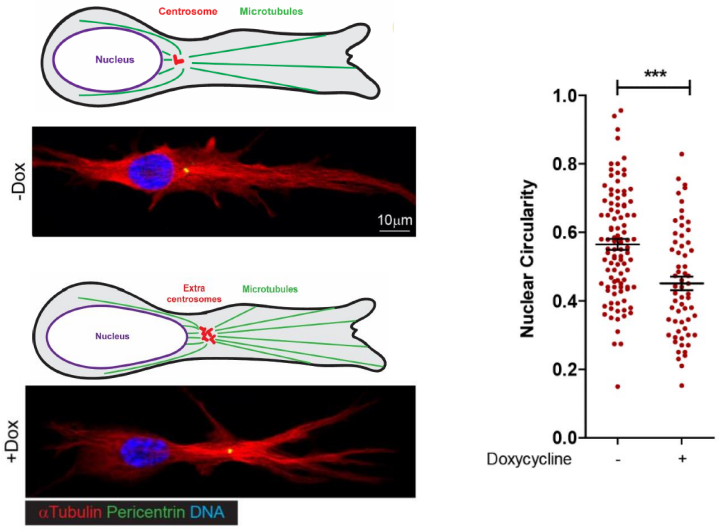

(a2)

Fig. 4.13: Nucleus containing DNA is labelled in blue and microtubules (α Tubulin) increased by extra centrosome (+Dox) are labelled in green on 2D substrate. (a1) The number of protrusive cells with nucleus inside the protrusion and nuclear circularity ($\frac{\text{Width}}{\text{Length}}$) of +Dox cells are compared to -Dox cells. (a2) The nucleus is blue and microtubules are red in 3D environment. The nuclear circularity is compared between +Dox and -Dox cells. The results are from P. Monteiro and S. Godinho.

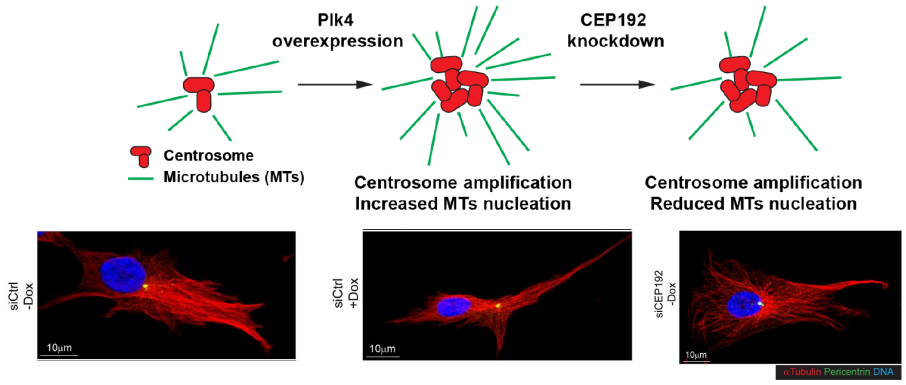

Fig. 4.14: This shows the protocol which decreases centrosomal MTs nucleation without affecting centrosome number compared to the control condition. Images of nucleus (blue) and microtubules (red) in 3D environment are also shown. The results are from P. Monteiro and S.A. Godinho.

both deformed and displaced. Our simulation results also show that a few motors on a single microtubule are not strong enough to change the nucleus's shape and position, but the increasing number of microtubules on which molecular motors step can perform more deformation. The nuclear translocation can be induced by the unbalance of pulling teams. Furthermore, our results are corresponded with experiment results by P. Monteiro and S.A. Godinho. The experiment revealed that the increasing number of microtubules exhibit higher nuclear deformation and nuclear translocation in 2D and 3D environments. However, our model is limited for processive motors. We believe that if the model is developed for nonprocessive motors then it can provide significant results and more understanding this mechanism in cells.

5. CONCLUSION

Molecular motors are responsible for intracellular transport of a variety of biological cargo. They can be classified by their processivity. In our work, processive motors never unbind from cytoskeletal filaments on which they are moving. Nonprocessive motors can unbind from the filaments. We proposed theoretical investigation of cargo transport by multiple motors based on a leading motor model in which external force is experienced by the leading motors We extend this analytical work on processive motors to the case of non-processive motors, which is capable to bind on and off a single filament. We consider the collective behaviour in transport of a finite number of non-processive motors in a spacial confinement in binding on the filament. We analytically study the distribution and the velocity of a cluster of non-processive motors and perform Monte Carlo latticed based stochastic simulations. In our simulation, the attachment and reattachment of non-processive motors are included sequence preservation and their stepping behaviors are obeyed on a simple exclusion process. We found that the sequence preservation and limited binding sites on the filament reduce the binding probability of non-processive motors but has a small effect on the velocity of the cluster. Our results can be compared well by *in vivo* and *in vitro* experimental results.

Later, we extend the analytic expression of velocity of non-processive motors and the simulation model on limited binding sites along a single filament into multiple filaments. The non-processive motors are assumed to bind randomly on the cargo surface and can attach simultaneously to many parallel filaments. They are allowed to switch between filaments. The switching mechanism provides more than one leading motor sharing the external force. Our results show that the switching mechanism can enhance the transport. The transport by multiple non-processive motors along many filaments is faster because the motors can avoid blocking each other during stepping on the same lane as the effect of simple exclusion process. The averaged run length is longer compared to the transport on one lane. Time in transporting a cargo along many lanes decreases.

Our previous work has studied the transport properties of non-processive motors on a single and multiple filaments limiting the number of binding sites. However, we have not yet studied the cargo behavior affected by the motor transport. We then simulate the model of motor transport on cytoskeletal filaments attaching to the edge of cargo. For simplicity, the molecular motors are simulated by

processive motors, so the number of motors on each filament is fixed. Force generated by motor steps exerts to the cargo which acts as a spring and cause the extension of cargo. Our model can apply to any cargo for which the spring model is reasonable, but nucleus is the specific example of cargo that we are interested in. It is worth to note that nobody has studied the nuclear deformation and displacement affected by motor pulling force. In fact, there are different types of forces pulling the nucleus resulting in changing its shape and position. The both ends of nucleus can attach to either a single or multiple filaments which are anti-parallel as a tug-of-war model. The force generating onto the nuclear envelope in this case can cause displacement. We obviously found that the nuclear extension and displacement depends on the number of cytoskeletal filaments and the number of molecular motors moving on them. Increasing number of filaments provides more cargo (nucleus) deformation and displacement.

Therefore, we explore a leading motor model for processive and non-proessive molecular motors. It does so through the comparison of analytic calculations with simulations. The novel result is the extension of the analytic expressions for the non-processive motors to the case of finite binding sites, which is then validated by simulations of the corresponding system. We discuss the effects of motor sequence preservation which never been introduced in the modeling of motor transport. The general conclusion is that the use of analytic models is satisfactory for describing the number of bound motors and force-velocity curves of the systems on a single filament. The one-lane model is then developed in analytical study and simulation models for the case of transport on multiple filaments including the switching ability of motors. Many filaments can obviously enhance the transport. Furthermore, we provide new insights on cargo behavior affected by processive motor pulling forces. The tug-of-war model has been used to simulate deformable and movable cargo which are applicable to the case of nuclear deformation and displacement by the motor pulling force.

Potential future work is an extension of this model simulating non-processive motors pulling a deformable cargo. We strongly believe that this future work would provide a novel result of nuclear deformation by non-processive motors.

BIBLIOGRAPHY

[1] R. Ait-Haddou and W. Herzog. Brownian ratchet models of molecular motors. *Cell biochemistry and biophysics*, 38(2):191–213, 2003.

[2] C. Appert-Rolland, M. Ebbinghaus, and L. Santen. Intracellular transport driven by cytoskeletal motors: General mechanisms and defects. *Physics Reports*, 593:1–59, 2015.

[3] T. Arnandis, P. Monteiro, S. D. Adams, V. L. Bridgeman, V. Rajeeve, E. Gadaleta, J. Marzec, C. Chelala, I. Malanchi, P. R. Cutillas, et al. Oxidative stress in cells with extra centrosomes drives non-cell-autonomous invasion. *Developmental cell*, 47(4):409–424, 2018.

[4] A. Ashkin, K. Schütze, J. Dziedzic, U. Euteneuer, and M. Schliwa. Force generation of organelle transport measured in vivo by an infrared laser trap. *Nature*, 348(6299):346, 1990.

[5] F. Berger, C. Keller, M. J. Mueller, S. Klumpp, and R. Lipowsky. Cooperative transport by molecular motors, 2011.

[6] S. M. Block. Kinesin motor mechanics: binding, stepping, tracking, gating, and limping. *Biophysical journal*, 92(9):2986–2995, 2007.

[7] K. J. Böhm, R. Stracke, P. Mühlig, and E. Unger. Motor protein-driven unidirectional transport of micrometer-sized cargoes across isopolar microtubule arrays. *Nanotechnology*, 12(3):238, 2001.

[8] S. Bouzat. Models for microtubule cargo transport coupling the langevin equation to stochastic stepping motor dynamics: caring about fluctuations. *Physical Review E*, 93(1):012401, 2016.

[9] S. Bouzat and F. Falo. The influence of direct motor–motor interaction in models for cargo transport by a single team of motors. *Physical biology*, 7(4):046009, 2010.

[10] S. Bouzat and F. Falo. The influence of direct motor–motor interaction in models for cargo transport by a single team of motors. *Physical biology*, 7(4):046009, 2010.

[11] P. C. Bressloff and J. M. Newby. Stochastic models of intracellular transport. *Reviews of Modern Physics*, 85(1):135, 2013.

[12] O. Campas, Y. Kafri, K. Zeldovich, J. Casademunt, and J.-F. Joanny. Collective dynamics of interacting molecular motors. *Physical review letters*, 97(3):038101, 2006.

[13] O. Campàs, C. Leduc, P. Bassereau, J. Casademunt, J.-F. Joanny, and J. Prost. Coordination of kinesin motors pulling on fluid membranes. *Biophysical journal*, 94(12):5009–5017, 2008.

[14] N. J. Carter and R. Cross. Mechanics of the kinesin step. *Nature*, 435(7040):308, 2005.

[15] L. Ciandrini, M. C. Romano, and A. Parmeggiani. Stepping and crowding of molecular motors: statistical kinetics from an exclusion process perspective. *Biophysical journal*, 107(5):1176–1184, 2014.

[16] R. A. Cross. The kinetic mechanism of kinesin. *Trends in biochemical sciences*, 29(6):301–309, 2004.

[17] K. N. Dahl, S. M. Kahn, K. L. Wilson, and D. E. Discher. The nuclear envelope lamina network has elasticity and a compressibility limit suggestive of a molecular shock absorber. *Journal of cell science*, 117(20):4779–4786, 2004.

[18] P. M. Davidson and J. Lammerding. Broken nuclei–lamins, nuclear mechanics, and disease. *Trends in cell biology*, 24(4):247–256, 2014.

[19] B. Derrida, M. R. Evans, V. Hakim, and V. Pasquier. Exact solution of a 1d asymmetric exclusion model using a matrix formulation. *Journal of Physics A: Mathematical and General*, 26(7):1493, 1993.

[20] M. Ebbinghaus and L. Santen. A model for bidirectional traffic of cytoskeletal motors. *Journal of Statistical Mechanics: Theory and Experiment*, 2009(03):P03030, 2009.

[21] S. E. Encalada, L. Szpankowski, C.-h. Xia, and L. S. Goldstein. Stable kinesin and dynein assemblies drive the axonal transport of mammalian prion protein vesicles. *Cell*, 144(4):551–565, 2011.

[22] R. Erban, S. J. Chapman, Philip, and K. Maini. A practical guide to stochastic simulations of reactiondiffusion processes, 35 pages, available as http://arxiv.org/abs/0704.1908, 2007.

[23] R. P. Erickson, S. P. Gross, and C. Y. Clare. Filament-filament switching can be regulated by separation between filaments together with cargo motor number. *PLoS One*, 8(2), 2013.

[24] R. P. Erickson, Z. Jia, S. P. Gross, and C. C. Yu. How molecular motors are arranged on a cargo is important for vesicular transport. *PLoS computational biology*, 7(5), 2011.

[25] M. Evans. Bose-einstein condensation in disordered exclusion models and relation to traffic flow. *EPL (Europhysics Letters)*, 36(1):13, 1996.

[26] Q. Feng, K. J. Mickolajczyk, G.-Y. Chen, and W. O. Hancock. Motor reattachment kinetics play a dominant role in multimotor-driven cargo transport. *Biophysical journal*, 114(2):400–409, 2018.

[27] D. A. Fletcher and R. D. Mullins. Cell mechanics and the cytoskeleton. *Nature*, 463(7280):485–492, 2010.

[28] D. Frenkel and B. Smit. *Understanding molecular simulation: from algorithms to applications*, volume 1. Academic press, 2001.

[29] A. Fruleux and R. J. Hawkins. Physical role for the nucleus in cell migration. *Journal of Physics: Condensed Matter*, 28(36):363002, 2016.

[30] M.-m. Fu and E. L. Holzbaur. Jip1 regulates the directionality of app axonal transport by coordinating kinesin and dynein motors. *Journal of Cell Biology*, 202(3):495–508, 2013.

[31] Y.-B. Fu, S.-K. Guo, P.-Y. Wang, and P. Xie. Dynamics of cooperative cargo transport by two elastically coupled kinesin motors. *The European Physical Journal E*, 42(4):41, 2019.

[32] K. Furuta, A. Furuta, Y. Y. Toyoshima, M. Amino, K. Oiwa, and H. Kojima. Measuring collective transport by defined numbers of processive and nonprocessive kinesin motors. *Proceedings of the National Academy of Sciences*, 110(2):501–506, 2013.

[33] K. Furuta, A. Furuta, Y. Y. Toyoshima, M. Amino, K. Oiwa, and H. Kojima. Measuring collective transport by defined numbers of processive and nonprocessive kinesin motors. *Proceedings of the National Academy of Sciences*, 110(2):501–506, 2013.

[34] A. Gennerich and D. Schild. Finite-particle tracking reveals submicroscopic-size changes of mitochondria during transport in mitral cell dendrites. *Physical biology*, 3(1):45, 2006.

[35] V. K. Godena, N. Brookes-Hocking, A. Moller, G. Shaw, M. Oswald, R. M. Sancho, C. C. Miller, A. J. Whitworth, and K. J. De Vos. Increasing microtubule acetylation rescues axonal transport and locomotor deficits caused by lrrk2 roc-cor domain mutations. *Nature communications*, 5(1):1–11, 2014.

[36] C. Goldman. A hopping mechanism for cargo transport by molecular motors on crowded microtubules. *Journal of Statistical Physics*, 140(6):1167–1181, 2010.

[37] C. Goldman and E. T. Sena. The dynamics of cargo driven by molecular motors in the context of asymmetric simple exclusion processes. *Physica A: Statistical Mechanics and its Applications*, 388(17):3455–3464, 2009.

[38] Y. Gruenbaum and R. Foisner. Lamins: nuclear intermediate filament proteins with fundamental functions in nuclear mechanics and genome regulation. *Annual review of biochemistry*, 84:131–164, 2015.

[39] H. Grzeschik, R. Harris, and L. Santen. Traffic of cytoskeletal motors with disordered attachment rates. *Physical Review E*, 81(3):031929, 2010.

[40] F. Guilak, J. R. Tedrow, and R. Burgkart. Viscoelastic properties of the cell nucleus. *Biochemical and biophysical research communications*, 269(3):781–786, 2000.

[41] W. O. Hancock. Bidirectional cargo transport: moving beyond tug of war. *Nature reviews Molecular cell biology*, 15(9):615–628, 2014.

[42] W. O. Hancock and J. Howard. Kinesin's processivity results from mechanical and chemical coordination between the atp hydrolysis cycles of the two motor domains. *Proceedings of the National Academy of Sciences*, 96(23):13147–13152, 1999.

[43] T. Harada, J. Swift, J. Irianto, J.-W. Shin, K. R. Spinler, A. Athirasala, R. Diegmiller, P. D. P. Dingal, I. L. Ivanovska, and D. E. Discher. Nuclear lamin stiffness is a barrier to 3d migration, but softness can limit survival. *Journal of Cell Biology*, 204(5):669–682, 2014.

[44] A. G. Hendricks, E. Perlson, J. L. Ross, H. W. Schroeder III, M. Tokito, and E. L. Holzbaur. Motor coordination via a tug-of-war mechanism drives bidirectional vesicle transport. *Current Biology*, 20(8):697–702, 2010.

[45] J. Howard et al. Mechanics of motor proteins and the cytoskeleton. 2001.

[46] R. Jiang, S. Vandal, S. Park, S. Majd, E. Tüzel, and W. O. Hancock. Microtubule binding kinetics of membrane-bound kinesin-1 predicts motor copy numbers on intracellular cargo. *Proceedings of the National Academy of Sciences*, 116(52):26564–26570, 2019.

[47] E. Karsenti, F. Nédélec, and T. Surrey. Modelling microtubule patterns. *Nature cell biology*, 8(11):1204–1211, 2006.

[48] S. Klumpp and R. Lipowsky. Cooperative cargo transport by several molecular motors. *Proceedings of the National Academy of Sciences*, 102(48):17284–17289, 2005.

[49] A. B. Kolomeisky and M. E. Fisher. Molecular motors: a theorist's perspective. *Annu. Rev. Phys. Chem.*, 58:675–695, 2007.

[50] C. B. Korn, S. Klumpp, R. Lipowsky, and U. S. Schwarz. Stochastic simulations of cargo transport by processive molecular motors. *The Journal of chemical physics*, 131(24):12B624, 2009.

[51] A. Kunwar and A. Mogilner. Robust transport by multiple motors with nonlinear force–velocity relations and stochastic load sharing. *Physical biology*, 7(1):016012, 2010.

[52] A. Kunwar, S. K. Tripathy, J. Xu, M. K. Mattson, P. Anand, R. Sigua, M. Vershinin, R. J. McKenney, C. Y. Clare, A. Mogilner, et al. Mechanical stochastic tug-of-war models cannot explain bidirectional lipid-droplet transport. *Proceedings of the National Academy of Sciences*, 108(47):18960–18965, 2011.

[53] A. Kunwar, M. Vershinin, J. Xu, and S. P. Gross. Stepping, strain gating, and an unexpected force-velocity curve for multiple-motor-based transport. *Current biology*, 18(16):1173–1183, 2008.

[54] M. Lakadamyali. Navigating the cell: how motors overcome roadblocks and traffic jams to efficiently transport cargo. *Physical Chemistry Chemical Physics*, 16(13):5907–5916, 2014.

[55] C. Leduc, K. Padberg-Gehle, V. Varga, D. Helbing, S. Diez, and J. Howard. Molecular crowding creates traffic jams of kinesin motors on microtubules. *Proceedings of the National Academy of Sciences*, 109(16):6100–6105, 2012.

[56] C. Leduc, F. Ruhnow, J. Howard, and S. Diez. Detection of fractional steps in cargo movement by the collective operation of kinesin-1 motors. *Proceedings of the National Academy of Sciences*, 104(26):10847–10852, 2007.

[57] T. P. Lele, R. B. Dickinson, and G. G. Gundersen. Mechanical principles of nuclear shaping and positioning. *Journal of Cell Biology*, 217(10):3330–3342, 2018.

[58] R. Lipowsky, J. Beeg, R. Dimova, S. Klumpp, and M. J. Müller. Cooperative behavior of molecular motors: cargo transport and traffic phenomena. *Physica E: Low-dimensional Systems and Nanostructures*, 42(3):649–661, 2010.

[59] K. Maeshima, S. Tamura, and Y. Shimamoto. Chromatin as a nuclear spring. *Biophysics and physicobiology*, 15:189–195, 2018.

[60] R. Mallik and S. P. Gross. Intracellular transport: how do motors work together? *Current Biology*, 19(10):R416–R418, 2009.

[61] R. Mallik, A. K. Rai, P. Barak, A. Rai, and A. Kunwar. Teamwork in microtubule motors. *Trends in cell biology*, 23(11):575–582, 2013.

[62] D. Marples, T. A. Schroer, N. Ahrens, A. Taylor, M. A. Knepper, and S. Nielsen. Dynein and dynactin colocalize with aqp2 water channels in intracellular vesicles from kidney collecting duct. *American Journal of Physiology-Renal Physiology*, 274(2):F384–F394, 1998.

[63] N. Metropolis, A. W. Rosenbluth, M. N. Rosenbluth, A. H. Teller, and E. Teller. Equation of state calculations by fast computing machines. *The journal of chemical physics*, 21(6):1087–1092, 1953.

[64] S. V. Mikhailenko, Y. Oguchi, and S. Ishiwata. Insights into the mechanisms of myosin and kinesin molecular motors from the single-molecule unbinding force measurements. *Journal of The Royal Society Interface*, 7(suppl_3):S295–S306, 2010.

[65] P. J. Mlynarczyk and S. M. Abel. First passage of molecular motors on networks of cytoskeletal filaments. *Physical Review E*, 99(2):022406, 2019.

[66] G. A. Monzon, L. Scharrel, L. Santen, and S. Diez. Activation of mammalian cytoplasmic dynein in multimotor motility assays. *J Cell Sci*, 132(4):jcs220079, 2019.

[67] M. J. Müller, S. Klumpp, and R. Lipowsky. Motility states of molecular motors engaged in a stochastic tug-of-war. *Journal of Statistical Physics*, 133(6):1059, 2008.

[68] M. J. Müller, S. Klumpp, and R. Lipowsky. Tug-of-war as a cooperative mechanism for bidirectional cargo transport by molecular motors. *Proceedings of the National Academy of Sciences*, 105(12):4609–4614, 2008.

[69] W. Nam and B. I. Epureanu. Highly loaded behavior of kinesins increases the robustness of transport under high resisting loads. *PLoS computational biology*, 11(3), 2015.

[70] S. Neelam, T. Chancellor, Y. Li, J. A. Nickerson, K. J. Roux, R. B. Dickinson, and T. P. Lele. Direct force probe reveals the mechanics of nuclear homeostasis in the mammalian cell. *Proceedings of the National Academy of Sciences*, 112(18):5720–5725, 2015.

[71] S. Neelam, R. B. Dickinson, and T. P. Lele. New approaches for understanding the nuclear force balance in living, adherent cells. *Methods*, 94:27–32, 2016.

[72] J. Newby and P. C. Bressloff. Local synaptic signaling enhances the stochastic transport of motor-driven cargo in neurons. *Physical biology*, 7(3):036004, 2010.

[73] K. Nishinari, Y. Okada, A. Schadschneider, and D. Chowdhury. Intracellular transport of single-headed molecular motors kif1a. *Physical review letters*, 95(11):118101, 2005.

[74] B. Nitzsche, E. Dudek, L. Hajdo, A. A. Kasprzak, A. Vilfan, and S. Diez. Working stroke of the kinesin-14, ncd, comprises two substeps of different direction. *Proceedings of the National Academy of Sciences*, 113(43):E6582–E6589, 2016.

[75] D. Oriola and J. Casademunt. Cooperative force generation of kif1a brownian motors. *Physical review letters*, 111(4):048103, 2013.

[76] A. Parmeggiani, T. Franosch, and E. Frey. Phase coexistence in driven one-dimensional transport. *Physical review letters*, 90(8):086601, 2003.

[77] E. Pechatnikova and E. Taylor. Kinetics processivity and the direction of motion of ncd. *Biophysical journal*, 77(2):1003–1016, 1999.

[78] A. D. Pilling, D. Horiuchi, C. M. Lively, and W. M. Saxton. Kinesin-1 and dynein are the primary motors for fast transport of mitochondria in drosophila motor axons. *Molecular biology of the cell*, 17(4):2057–2068, 2006.

[79] A. R. Popchock, K.-F. Tseng, P. Wang, P. A. Karplus, X. Xiang, and W. Qiu. The mitotic kinesin-14 klpa contains a context-dependent directionality switch. *Nature communications*, 8(1):1–9, 2017.

[80] M. Rief, R. S. Rock, A. D. Mehta, M. S. Mooseker, R. E. Cheney, and J. A. Spudich. Myosin-v stepping kinetics: a molecular model for processivity. *Proceedings of the National Academy of Sciences*, 97(17):9482–9486, 2000.

[81] W. H. Roos, O. Campas, F. Montel, G. Woehlke, J. P. Spatz, P. Bassereau, and G. Cappello. Dynamic kinesin-1 clustering on microtubules due to mutually attractive interactions. *Physical biology*, 5(4):046004, 2008.

[82] J. L. Ross, M. Y. Ali, and D. M. Warshaw. Cargo transport: molecular motors navigate a complex cytoskeleton. *Current opinion in cell biology*, 20(1):41–47, 2008.

[83] H. W. Schroeder III, A. G. Hendricks, K. Ikeda, H. Shuman, V. Rodionov, M. Ikebe, Y. E. Goldman, and E. L. Holzbaur. Force-dependent detachment of kinesin-2 biases track switching at cytoskeletal filament intersections. *Biophysical journal*, 103(1):48–58, 2012.

[84] H. W. Schroeder III, C. Mitchell, H. Shuman, E. L. Holzbaur, and Y. E. Goldman. Motor number controls cargo switching at actin-microtubule intersections in vitro. *Current biology*, 20(8):687–696, 2010.

[85] J. V. Shah and D. W. Cleveland. Slow axonal transport: fast motors in the slow lane. *Current opinion in cell biology*, 14(1):58–62, 2002.

[86] P. M. Shaklee, L. Bourel-Bonnet, M. Dogterom, and T. Schmidt. Nonprocessive motor dynamics at the microtubule membrane tube interface. *Biophysical journal*, 98(1):93–100, 2010.

[87] Y.-L. Shih and L. Rothfield. The bacterial cytoskeleton. *Microbiol. Mol. Biol. Rev.*, 70(3):729–754, 2006.

[88] Y. Shimamoto, S. Tamura, H. Masumoto, and K. Maeshima. Nucleosome–nucleosome interactions via histone tails and linker dna regulate nuclear rigidity. *Molecular biology of the cell*, 28(11):1580–1589, 2017.

[89] V. Soppina, A. K. Rai, A. J. Ramaiya, P. Barak, and R. Mallik. Tug-of-war between dissimilar teams of microtubule motors regulates transport and fission of endosomes. *Proceedings of the National Academy of Sciences*, 106(46):19381–19386, 2009.

[90] F. Spitzer. Interaction of markov processes. *Advances in Mathematics*, 5(2):246–290, 1970.

[91] F. Spitzer. Interaction of markov processes. *Advances in Mathematics*, 5(2):246–290, 1970.

[92] A. D. Stephens, E. J. Banigan, S. A. Adam, R. D. Goldman, and J. F. Marko. Chromatin and lamin a determine two different mechanical response regimes of the cell nucleus. *Molecular biology of the cell*, 28(14):1984–1996, 2017.

[93] A. D. Stephens, P. Z. Liu, E. J. Banigan, L. M. Almassalha, V. Backman, S. A. Adam, R. D. Goldman, and J. F. Marko. Chromatin histone modifications and rigidity affect nuclear morphology independent of lamins. *Molecular biology of the cell*, 29(2):220–233, 2018.

[94] K. Sugden and M. Evans. A dynamically extending exclusion process. *Journal of Statistical Mechanics: Theory and Experiment*, 2007(11):P11013, 2007.

[95] M. Sun, M. Wartel, E. Cascales, J. W. Shaevitz, and T. Mignot. Motor-driven intracellular transport powers bacterial gliding motility. *Proceedings of the National Academy of Sciences*, 108(18):7559–7564, 2011.

[96] T. Szekely and K. Burrage. Stochastic simulation in systems biology. *Computational and structural biotechnology journal*, 12(20):14–25, 2014.

[97] M. C. Ucar and R. Lipowsky. Collective force generation by molecular motors is determined by strain-induced unbinding. *Nano Letters*, 20(1):669–676, 2019.

[98] R. D. Vale, T. Funatsu, D. W. Pierce, L. Romberg, Y. Harada, and T. Yanagida. Direct observation of single kinesin molecules moving along microtubules. *Nature*, 380(6573):451–453, 1996.

[99] R. D. Vale, B. J. Schnapp, T. S. Reese, and M. P. Sheetz. Movement of organelles along filaments dissociated from the axoplasm of the squid giant axon. *Cell*, 40(2):449–454, 1985.

[100] M. Vershinin, B. C. Carter, D. S. Razafsky, S. J. King, and S. P. Gross. Multiple-motor based transport and its regulation by tau. *Proceedings of the National Academy of Sciences*, 104(1):87–92, 2007.

[101] K. Visscher, M. J. Schnitzer, and S. M. Block. Single kinesin molecules studied with a molecular force clamp. *Nature*, 400(6740):184, 1999.

[102] Q. Wang and A. B. Kolomeisky. Theoretical analysis of run length distributions for coupled motor proteins. *The Journal of Physical Chemistry B*, 123(27):5805–5813, 2019.

[103] Z. Wang, S. Khan, and M. P. Sheetz. Single cytoplasmic dynein molecule movements: characterization and comparison with kinesin. *Biophysical Journal*, 69(5):2011–2023, 1995.

[104] M. Welte and S. Gross. Molecular motors: a traffic cop within? 2008.

[105] M. A. Welte, S. P. Gross, M. Postner, S. M. Block, and E. F. Wieschaus. Developmental regulation of vesicle transport in drosophila embryos: forces and kinetics. *Cell*, 92(4):547–557, 1998.

[106] J. O. Wilson, D. A. Quint, A. Gopinathan, and J. Xu. Cargo diffusion shortens single-kinesin runs at low viscous drag. *Scientific reports*, 9(1):1–12, 2019.